

## Copyright Warning & Restrictions

The copyright law of the United States (Title 17, United States Code) governs the making of photocopies or other reproductions of copyrighted material.

Under certain conditions specified in the law, libraries and archives are authorized to furnish a photocopy or other reproduction. One of these specified conditions is that the photocopy or reproduction is not to be “used for any purpose other than private study, scholarship, or research.” If a user makes a request for, or later uses, a photocopy or reproduction for purposes in excess of “fair use” that user may be liable for copyright infringement,

This institution reserves the right to refuse to accept a copying order if, in its judgment, fulfillment of the order would involve violation of copyright law.

**Please Note: The author retains the copyright while the New Jersey Institute of Technology reserves the right to distribute this thesis or dissertation**

Printing note: If you do not wish to print this page, then select “Pages from: first page # to: last page #” on the print dialog screen



The Van Houten library has removed some of the personal information and all signatures from the approval page and biographical sketches of theses and dissertations in order to protect the identity of NJIT graduates and faculty.

## ABSTRACT

### APPLICATIONS OF ROOM TEMPERATURE IONIC LIQUIDS IN INTERFACIAL POLYMERIZATION

by  
Lining Zhu

Room temperature ionic liquids (ILs), with their unique physical and chemical properties, have been of great interest in various areas of chemical science and engineering during the last decade. In this dissertation, polyurea and polyamide films with surface nanostructures were synthesized by interfacial polymerization (IP) with ILs without stirring. Both polymers were prepared at the interface between n-hexane and a series of 1-alkyl-3-methylimidazolium ILs.

Nanoporous or nanofibrous polymer morphologies with various sizes ranging from 50 to 500 nm and geometries, depending on the ILs used, were observed by scanning electron microscopy (SEM). A correlation length of ~20nm and a suppression of three-dimensional (3-D) crystalline structure of the polyurea were found by small angle X-ray scattering (SAXS) and X-ray diffraction (XRD), respectively. FTIR spectra showed no significant changes in the chemical composition of the polymer by the employment of ILs. The peculiar nanostructure of the polymer could be ascribed to the intermolecular interactions between the ILs and the polymer, which affected the development of the polymer morphology.

The polyamides prepared with ILs showed larger intrinsic viscosities, and consequently higher molecular weights, compared to the one prepared without ILs; this could be due to the prevention of the side reaction between sebacoyl chloride and water. The enhancement of the molecular weight renders a better thermal stability to the

polyamide film, as revealed by thermogravimetric analysis (TGA) which showed a higher decomposition temperature.

Coating of fine particulates with polyurea by IP has been developed. With increasing stirring speed in the coating process, a decreased mean particle size and a narrower particle size distribution, as well as a lower coating weight percentage were found by particle size analysis and TGA, respectively. A Porous coating layer was formed in the IP coating in the presence of ILs.

The reaction kinetics of Nylon 610 film formation with ILs were studied by measuring the product mass at different reaction times. The polymer film ceased to grow in the late stage of the reaction due to the diffusion barrier formed by the film. The characteristic time marking the cessation of the film growth was found to be dependent on the initial reactant concentrations. The evolution of the polymer molecular weight with reaction time was monitored by intrinsic viscosity measurements. It is found that the molecular weight leveled off faster than the film growth under the same reactant concentrations. Based on our experimental studies, a simplified diffusion-controlled mathematical model of IP with ILs was developed, in which the effective diffusivity in the polymer film decayed with the square of time. The model was used to fit the measured growth rate of the polymer film and the fitting results showed a conspicuously good agreement between the model and the experimental data.

Physical properties of ILs relevant to the biphasic systems were also studied in this work. The interfacial tensions between organic solvents and ILs were found to decrease with ascending alkyl chain length attached to the imidazolium cations. In general, the interfacial tensions between ILs and aromatic solvents are lower than the ones with

aliphatic solvents; this is attributed to the  $\pi$ - $\pi$  interactions between ILs and the aromatic solvent. Self-aggregation of IL molecules in aqueous solutions and self-aggregation of ethanol in ILs are suggested based on the interfacial tension measurements. These properties are important in multi-phase chemical processes.

Our study has demonstrated the potential application of ionic liquids in the interfacial polymerization of polymers with nanoscale structures.

**APPLICATIONS OF ROOM TEMPERATURE IONIC LIQUIDS IN  
INTERFACIAL POLYMERIZATION**

**by  
Lining Zhu**

**A Dissertation  
Submitted to the Faculty of  
New Jersey Institute of Technology  
in Partial Fulfillment of the Requirements for the Degree of  
Doctor of Philosophy in Chemical Engineering**

**Otto H. York Department of Chemical Engineering**

**May 2006**

Copyright © 2006 by Lining Zhu

ALL RIGHTS RESERVED

**APPROVAL PAGE**

**APPLICATIONS OF ROOM TEMPERATURE IONIC LIQUIDS IN  
INTERFACIAL POLYMERIZATION**

**Lining Zhu**

---

Dr. Chien-Yueh Huang, Dissertation Advisor Date  
Assistant Professor of Chemical Engineering, NJIT

---

Dr. Sanjay V. Malhotra, Dissertation Co-Advisor Date  
Assistant Professor of Chemistry and Environmental Science, NJIT

---

Dr. Costas Gogos, Committee Member Date  
Distinguished Research Professor of Chemical Engineering, NJIT

---

Dr. Marino Xanthos, Committee Member Date  
Professor of Chemical Engineering, NJIT

---

Dr. Jing Wu, Committee Member Date  
Assistant Professor of Chemical Engineering, NJIT

---

Dr. Tae Hoon Kwalk, Committee Member Date  
Product Development Leader, Univation Technology,  
c/o Dow Chemical Company, Piscataway, NJ



## BIOGRAPHICAL SKETCH

**Author:** Lining Zhu  
**Degree:** Doctor of Philosophy  
**Date:** May 2006

### Undergraduate and Graduate Education:

- Doctor of Philosophy in Chemical Engineering,  
New Jersey Institute of Technology, Newark, NJ, 2006
- Bachelor of Science in Polymer Science and Engineering,  
East China University of Science and Technology, Shanghai, P. R. China, 1998

**Major:** Chemical Engineering

### Presentations and Publications:

Chien-Yueh Huang, Lining Zhu, Jenny Jun, S-T. Lee,  
“Analysis of Solubility and Spinodal Decomposition For Thermoplastic Foams”, SPE ANTEC 2004, 62<sup>nd</sup> (Vol.2), 2653-2657.

Sanjay V.Malhotra, Lining Zhu, Chien-Yueh Huang,  
“Interfacial Polymerization with Ionic Liquids”, 228<sup>th</sup> ACS National Meeting, Philadelphia, PA, August 22-26, 2004.

Lining Zhu, Chien-Yueh Huang, Sanjay V.Malhotra,  
“Nano-Structures in Interfacial Polymerization with Room Temperature Ionic Liquids”, AICHE 2004 Annual Meeting, Austin, TX, November 7-12, 2004.

Chien-Yueh Huang, Lining Zhu, Nai-Shang Liu, Tae Hoon Kwak, Yuen-Yuen D. Chiu,  
“Comparative Studies Between Charpy Impact Test and Dynatup Impact Test”, SPE ANTEC 2005, 63<sup>nd</sup>, 3917.

Lining Zhu, , Sanjay V.Malhotra, Jing Wu, Yamini Patel, Chien-Yueh Huang “Synthesis of Polymeric Nanostructures via Interfacial Polymerization in Room Temperature Ionic Liquids”, submitted to Macromolecular Rapid Communications.

Lining Zhu, , Sanjay V.Malhotra, Jing Wu, Jing Zhang, Chien-Yueh Huang, “Interfacial Polymerization of Polyurea with Nanostructures in Room Temperature Ionic Liquids”, in preparation.

Lining Zhu, , Sanjay V.Malhotra, Chien-Yueh Huang “Interfacial Polymerization in Aqueous Solutions of Room Temperature Ionic Liquids”, in preparation.

Lining Zhu, Chien-Yueh Huang, Marino Xanthos, Sanjay V. Malhotra, “Coating of Fine Particulates with Room Temperature Ionic Liquids”, in preparation.

To my beloved parents, my dear brother Jeff and sister-in-law Cathy and my lovely nephew  
Tiger

## ACKNOWLEDGMENT

I would like to express my deepest appreciation to Dr. Michael Chien-Yueh Huang, who served as my dissertation supervisor over the past five years, showing me different ways to approach and resolve the challenging research problems, and continuously giving me encouragements and advises in my research work. With his broad knowledge, diligent working attitude, optimistic and kind spirit in daily life, Michael acted not only as an academic mentor, but also as a good friend who will impact me in my future career. My appreciation to my dissertation co-advisor Dr. Sanjay Malhotra, who guided me into the world of ionic liquids, is also beyond my expression. I deeply appreciate Dr. Marino Xanthos for his consistent and insightful advises to my dissertation work. My special thanks also go to Dr. Costas Gogos, Dr. Jing Wu and Dr. Tae Hoon Kwalk for actively participating in my committee.

I would like to acknowledge the Otto H. York Department of Chemical Engineering for the financial support of my research over the past four years. I also deeply appreciate Professor Michael Huang and Professor Marino Xanthos, for their financial supports in Fall 2005 and Spring 2006, respectively. My great thanks are given to Dr. Jing Zhang and Dr. Jing Wu, who helped me in X-ray scattering study; Ms. Yamini Patel, for her help in the FTIR analysis; Dr. Dongguang Wei and Dr. Jun Yang, for their assistance and patience during my training in SEM; Dr. Victor Tan and Dr. Michael Jaffe, for providing DSC and TGA instruments; Dr. Wei-Kuo Lee, for his insightful inputs in the experimental design; Mr. Thomas Boland, for his help in providing lab equipment and accessories; and all those people who kindly gave me assistance in my research work. It would have been impossible to complete this work without their efforts. Finally, I am indebted to my fellow graduate students, Mr. Hongta Yang and Dr. BaoHua Yue, who always helped me in the lab.

## TABLE OF CONTENTS

<b>Chapter</b>	<b>Page</b>
1 INTRODUCTION .....	1
2 LITERATURE REVIEW .....	6
2.1 Introduction of Ionic Liquids (ILs) and Their Physical Properties .....	6
2.1.1 Composition of ILs .....	6
2.1.2 Volatility and Thermophysical Properties of ILs .....	6
2.1.3 Solvent Property of ILs .....	9
2.1.4 Viscosity of ILs .....	10
2.1.5 Molecular Structures in ILs .....	11
2.2 Applications of Ionic Liquids in Polymer Science and Engineering .....	15
2.3 Ionic Liquids in Formation of Nano-structured materials .....	18
2.4 Interfacial Polymerization (IP) .....	20
2.4.1 Principles of Interfacial Polymerization .....	20
2.4.2 Applications of Interfacial Polymerization .....	21
2.4.3 Kinetics Study of IP.....	22
3 THEORY .....	25
3.1 Polymerization Induced Phase Separation (PIPS).....	25
3.2 Phase Separation Kinetics .....	29
3.2.1 Nucleation and Growth (NG).....	29
3.2.2 Spinodal Decomposition (SD).....	30
4 EXPERIMENTAL SECTION .....	33

**TABLE OF CONTENTS**  
**(Continued)**

<b>Chapter</b>	<b>Page</b>
4.1 Materials .....	33
4.1.1 Room Temperature Ionic Liquids .....	33
4.1.2 Monomers for Interfacial Polymerization .....	35
4.1.3 Other Materials .....	35
4.2 Interfacial Tension Measurement .....	36
4.3 Interfacial Polymerization .....	39
4.3.1 Synthesis of Polyurea with ILs .....	39
4.3.2 Synthesis of Polyurea with IL Aqueous Solutions .....	42
4.3.3 Synthesis of Polyamides with ILs and Kinetics Study .....	42
4.3.4 Fine Particle Coating by IP .....	44
4.4 Material Characterization Methods .....	46
5 RESULTS AND DISCUSSION .....	51
5.1 Study of the Physical Properties of Ionic Liquids .....	51
5.1.1 Interfacial Tension between ILs and Organic Solvents .....	51
5.1.2 Self-aggregations of ILs in Aqueous Solution/Organic Solvent Systems .....	53
5.1.3 Self-aggregation of Ethanol in IL Solutions .....	55
5.1.4 Thermal Behavior of ILs .....	57
5.1.5 WAXS Study of the Structures of ILs .....	59
5.2 Synthesis of Polyurea at IL/n-hexane Interface .....	60
5.2.1 Reaction Conversion .....	60
5.2.2 FTIR Analysis .....	62

**TABLE OF CONTENTS**  
**(Continued)**

<b>Chapter</b>	<b>Page</b>
5.2.3 Thermal Analysis .....	64
5.2.4 Surface Morphology .....	65
5.2.5 Results by Small Angle X-ray Scattering (SAXS) .....	72
5.2.6 X-ray Diffraction Measurement .....	74
5.2.7 Molecular Interactions and the Formation of Polymeric Nanostructures in Various ILs.....	77
5.3 Interfacial Polymerization with Aqueous Solution of ILs .....	83
5.3.1 FTIR Analysis of Polyurea Synthesized with Aqueous Solutions of ILs..	83
5.3.2 Surface Morphology of Polyurea Synthesized in Aqueous Solutions of ILs .....	85
5.4 Synthesis of Polyamide Film with ILs .....	89
5.4.1 FTIR Analysis of Polyamide Films by IP in ILs .....	89
5.4.2 Effect of Ionic Liquids on Molecular Weight of Polyamides .....	90
5.4.3 Thermal Stability of Polyamide Films .....	92
5.4.4 Surface Morphology of Polyamide films Synthesized by IP in ILs .....	94
5.5 Fine Particulates Coating by Interfacial Polymerization .....	96
5.5.1 Surface Morphology.....	96
5.5.2 Particle Size Analysis .....	97
5.5.3 Coating Weight Percentage .....	102
5.5.4 Application of Ionic Liquids in Particle Coating by IP.....	104
5.6 Kinetics Study of Interfacial Polymerization in ILs .....	106
5.6.1 Mathematical Model of IP with ILs.....	106

**TABLE OF CONTENTS**  
(Continued)

<b>Chapter</b>	<b>Page</b>
5.6.2 Experimental Results .....	113
5.6.3 Comparison of Theoretical Prediction and Experimental Data.....	116
5.6.4 Molecular Weight versus Reaction Time .....	123
<b>6 CONCLUSIONS AND RECOMMENDATIONS FOR FUTURE WORK .....</b>	<b>125</b>
6.1 Conclusions .....	125
6.2 Recommendations for Future Work .....	127
 APPENDIX A INTERFACIAL TENSION BETWEEN IONIC LIQUIDS AND ORGANIC SOLVENTS.....	 129
 APPENDIX B INTERFACIAL TENSION BETWEEN N-HEXANE AND IONIC LIQUID AQUEOUS SOLUTIONS .....	 130
 APPENDIX C PARTICLE MEAN SIZE OF POLYUREA-COATED DCR UNDER VARIOUS STIRRING CONDITIONS.....	 131
 APPENDIX D PARTICLE MEAN SIZES OF POLYUREA-COATED DCR UNDER VARIOUS DIAMINE CONCENTRATIONS .....	 132
 APPENDIX E COATING WEIGHT PERCENTAGE OF POLYUREA-COATED DCR UNDER VARIOUS STIRRING SPEEDS.....	 133
 APPENDIX F REACTION CONVERSION OF NYLON 610 SYNTHESIZED BY IP IN ILS AS A FUNCTION OF TIME AT VARIOUS HDA/SEBACOYL CHLORIDE CONCENTRATION RATIOS.....	 134
 APPENDIX G PRODUCT MASS OF NYLON 610 SYNTHESIZED BY IP IN ILS AS A FUNCTION OF TIME AT VARIOUS HDA/SEBACOYL CHLORIDE CONCENTRATION RATIOS.....	 135
 REFERENCES .....	 136



## LIST OF TABLES

Table	Page
2.1 Well-known Classes of Ionic Liquids.....	7
2.2 Melting ( $T_m$ ), Freezing ( $T_f$ ), and glass transition ( $T_g$ ) temperatures of imidazolium-based ionic liquids as determined by DSC.....	8
2.3 Thermal decomposition temperatures of several imidazolium-based ionic liquids as determined by TGA.....	8
2.4 Surface tension and polarity of ionic liquid and common solvents.....	9
3.1 Comparison of the features of Phase separation mechanism.....	32
4.1 Material data of the ionic liquids used in this work.....	35
4.2 Miscibility observance results of ionic liquids in common solvents (1:1 volume ratio) based on visual observation.....	38
4.3 Reaction media of polyurea prepared from ethylene diamine in 1-alkyl-3-methylimidazolium tetrafluoroborates (Group 1).....	41
4.4 Reaction media of polyurea prepared from 1,4-diaminobutane in 1-alkyl-3-methylimidazolium tetrafluoroborates (Group 2).....	41
4.5 Reaction media of polyurea prepared in 1-alkyl-3-methylimidazolium hexafluorophosphates (Group 3).....	41
4.6 Reaction media of polyurea samples synthesized in IL aqueous solutions.....	42
4.7 Reaction Systems of Polyamide Films by IP in ILs.....	43
5.1 Reaction conversion of the polyureas synthesized with ILs.....	62
5.2 Summary of Surface Morphology of polyurea synthesized in ionic liquids.....	72
5.3 Surface morphology of polyureas synthesized in various aqueous solutions.....	85
5.4 Intrinsic viscosity of polyamides prepared by IP in different ILs.....	91

**LIST OF TABLES**  
**(Continued)**

<b>Table</b>	<b>Page</b>
5.5 Parameters used in the model described by Eq.(5.15).....	117
5.6 Final conversions and product mass of Nylon 610 and the characteristic times for various reactant concentrations .....	119
5.7 Intrinsic viscosity ( $[\eta]$ ) of the synthesized PA-HB8 ( $[HDA]:[SC] = 1.25M:0.42M$ ) as a function of reaction time .....	124

## LIST OF FIGURES

<b>Figure</b>	<b>Page</b>
3.1 Scheme of Polymerization Induced Phase Separation (PIPS).....	28
3.2 Plot of growing mode vs. wavelength of fluctuation in spinodal decomposition..	31
4.1 Structure of 1-alkyl-3-methylimidazolium-based room temperature ionic liquids used in this work.(For tetrafluoroborates, n=2,4,6,8, X=BF <sub>4</sub> ; for hexafluorophosphates, n=4,6, X=PF <sub>6</sub> ).....	34
4.2 Structure of 1-butyl-4-methylpyridinium room temperature ionic liquids. (X=BF <sub>4</sub> , PF <sub>6</sub> ).....	34
4.3 Chemical Structure of Dechlorane 515 Plus (C <sub>18</sub> H <sub>12</sub> Cl <sub>12</sub> ).....	36
4.4 Reaction Scheme of polyurea synthesis.....	39
4.5 Scheme of particle coating process by interfacial polymerization.....	45
5.1 Interfacial tensions between organic solvents and two series of ionic liquids: 1-alkyl-3-methylimidazolium hexafluorophosphates (a) and 1-alkyl-3-methylimidazolium tetrafluoroborates (b). The carbon number is pertaining to the one on the N-alkyl group.....	53
5.2 IL aqueous solutions/n-hexane interfacial tensions under various concentrations.....	54
5.3 Surface Tension vs. ethanol concentration in ethanol/IL inverse phase solution.....	56
5.4 DSC study results of ionic liquids: (a) [bmpm][PF <sub>6</sub> ]; (b) [hmim][PF <sub>6</sub> ]. (Test performed by heating-cooling-heating cycle, heating rate is 10°C/min, cooling rate is 5°C/min).....	58
5.5 WAXS data of [hmim][PF <sub>6</sub> ] at 20°C (Left) and [bmpm][PF <sub>6</sub> ] at 50°C (Right).....	60
5.6 FTIR spectra of neat ionic liquid and typical polyurea samples by interfacial polymerization: (a) [bmim][BF <sub>4</sub> ]; (b) PUA-0; (c)PUA-B4E; (d) PUA-B8E.....	63
5.7 DSC study results of PUA-B4B (left) and PUA-B8B (right) under the heating rate of 5°C/min.....	65
5.8 Scanning Electron Microscopy (SEM) images of the polyureas synthesized from ethylene diamine in [C <sub>n</sub> mim][BF <sub>4</sub> ] ionic liquids.....	66

**LIST OF FIGURES**  
**(Continued)**

<b>Figure</b>	<b>Page</b>
5.9 SEM images of regular polyurea synthesized at water/n-hexane interface: (a) 10,000X; (b) 50,000X.....	67
5.10 Scanning Electron Microscopy (SEM) images of the polyureas synthesized from 1,4-diaminobutane in [C <sub>n</sub> mim][BF <sub>4</sub> ] ionic liquids.....	69
5.11 Scanning Electron Microscopy (SEM) images of the polyureas synthesized in [C <sub>n</sub> mim][PF <sub>6</sub> ] ionic liquids: (a) PUA-P4E (10,000X); (b) PUA-P4E (50,000X); (c) PUA-P6E (10,000X); (d) PUA-P6E (50,000X).....	71
5.12 SAXS results of the polyurea synthesized by IP in ILs: (a) PUA-B2E; (b) PUA-B4E; (c) PUA-B8E; (d) PUA-B8B.....	73
5.13 XRD patterns of the polyureas synthesized by IP in ILs: (a) PUA-0 (regular polyurea); (b) PUA-B2E; (c) PUA-B4E; (d) PUA-B8E.....	74
5.14 Molecular structure of polyurea schemed by Cerius II <sup>®</sup> . ....	76
5.15 FTIR spectra of neat [bmim][BF <sub>4</sub> ] (a), unwashed PUA-B4E with residual [bmim][BF <sub>4</sub> ] (b), and PUA-B4E after repeated washes (c).....	80
5.16 FTIR spectra of neat [omim][BF <sub>4</sub> ] (a), unwashed PUA-B8E with residual [omim][BF <sub>4</sub> ] (b), and PUA-B8E after repeated washes (c).....	81
5.17 Standard FTIR absorbance spectra of (a) Ethylene Diamine and (b) TDI. (From Sigma-Aldrich Technical data).....	82
5.18 FTIR spectra of the polyurea samples by interfacial polymerization in various reaction media: (a) water/n-hexane; (b) n-hexane and aqueous solutions of three different ILs and aqueous solution of SDS.....	84
5.19 SEM micrographs of the polyureas synthesized with ionic liquid aqueous solutions: (a) PUA-0; (b) PUA-Bi; (c) PUA-Ei; (d) PUA-Bp; (e) PUA-SDS.....	86
5.20 Interfacial Tension between n-hexane and various aqueous-based solutions.....	87
5.21 Scheme of intermolecular network between [bmim][BF <sub>4</sub> ] and water: 1. Columbic Force; 2. Hydrogen bond.....	88
5.22 FTIR spectra of polyamides by interfacial polymerization at various conditions: (a) [bmim][BF <sub>4</sub> ]; (b) PA-B0; (c) PA-BB4.....	90
5.23 Intrinsic viscosities of polyamides prepared with various ILs.....	92

**LIST OF FIGURES**  
(Continued)

<b>Figure</b>	<b>Page</b>
5.24 TGA curves of Nylon 610 films by IP with different reaction media.( PA-H0: water/n-hexane interface; PA-HB8: [omim][BF <sub>4</sub> ]/n-hexane interface.).....	93
5.25 SEM pictures of Nylon films synthesized by IP in various reaction media: (a) PA-B0; (b) PA-H0; (c) PA-BB4; (d) PA-HB4; (e) PA-BB8; (f) PA-HB8. (Magnification for the pictures is 10,000X, except 5,000X for PA-H0).....	95
5.26 SEM Photographs of (a): bare DCR particles and (b): polyurea-coated DCR particles.....	97
5.27 SEM Photographs of polyurea-coated DCR under initial ethylene diamine volume concentrations of: 30% (a) and 50% (b).....	97
5.28 Effect of stirring on coated-particle agglomerate size.....	98
5.29 Particle Size Distribution of Polyurea-Coated DCR under various stirring speeds: DCR/TDI=5g/2.5ml, Volume ratio of Diamine and water is 30:70in (a) and 50:50 in (b).....	99
5.30 Particle mean size of polyurea-coated DCR under various stirring conditions (DCR/TDI=5g/2.5ml).....	100
5.31 Particle Size Distribution (top) and particle mean sizes (bottom) of polyurea-coated DCR under various diamine concentrations. (DCR/TDI=5g/2.5ml, 900 rpm).....	101
5.32 Thermo-Gravimetric Analysis (TGA) spectra of pure DCR: Temperature range from 50°C to 400°C, Heating rate=10°C/min.....	102
5.33 Comparison of TGA spectra of pure DCR, polyurea-coated DCR and pure polyurea.....	103
5.34 Coating weight percentage of polyurea-coated DCR under various stirring speeds. (DCR/TDI=5g/2.5ml, Volume concentration of ethylene diamine is 30%).....	104
5.35 SEM pictures for evaluation of DCR coating by IP of polyurea with ionic liquids: (a) bare DCR; (b) polyurea-coated DCR without IL; (c) polyurea-coated DCR with [bmpm][BF <sub>4</sub> ]; (d) polyurea-coated DCR with [bmpm][PF <sub>6</sub> ].....	105
5.36 Schematic illustration of interfacial polymerization model at the n-hexane/IL interface.....	107

**LIST OF FIGURES**  
(Continued)

<b>Figure</b>	<b>Page</b>
5.37 Conceptual illustration of simplified IP model at the n-hexane/IL interface.....	111
5.38 Conversion of polymer products vs. time of nylon 610 synthesized at the [omim][BF <sub>4</sub> ]/n-hexane interface with a constant concentration of HDA (1.25M) but different concentrations of sebacoyl chloride (0.42, 0.84, and 1.25M).....	115
5.39 Conversion of polymer products vs. time of nylon 610 synthesized by IP at the [omim][BF <sub>4</sub> ]/n-hexane interface with a constant concentration of SC (0.42M) but different concentrations of HDA (0.42, 0.84, and 1.25M).....	116
5.40 Comparison of the prediction (solid line) and the experimental data (symbols) for the conversion of PA-HB8 as a function of reaction time at various [HDA]/[SC] concentrations: (a) Samples A, B, and C; (b) Samples A, D, and E; (c) Samples C and F.....	118
5.41 Illustration of the relationship between morphology evolution and film growth of the nylon 610 film prepared with [omim][BF <sub>4</sub> ]( [HDA]/[SC]=1.25M:0.42M)..	121
5.42 SEM images of nylon 610 film prepared with [omim][BF <sub>4</sub> ] at different reaction times ([HDA]/[SC]=1.25M:0.42M): (a) 20min; (b) 40min; (c) 60min; (d) 180min; (e) 300min; (f) 24 hours.....	122
5.43 Intrinsic viscosity ( $[\eta]$ ) of the synthesized PA-HB8 ([HDA]:[SC] = 1.25M:0.42M) versus the reaction time.....	124

## LIST OF SYMBOLS

$A$	surface area of interface
$L$	film thickness
$M$	mobility
$N$	degree of polymerization
$Q$	inverse space (scattering vector), $\text{\AA}^{-1}$
$f$	local free energy
$D_i^{eff}$	effective diffusivity of species $i$
$k_B$	Boltzmann constant
$M_p$	product mass of polymer film, g
$\gamma$	surface/interfacial tension, dyne/cm
$\varepsilon$	porosity of polymer film
$[\eta]$	intrinsic viscosity, 100ml/g
$\kappa$	coefficient for the penalty in free energy
$\mu$	chemical potential
$\tau$	tortuosity of polymer film
$\chi$	Flory-Huggins interaction parameter
$\beta_1$	entropic contribution from the lattice constant
$\Delta F_m$	free energy of mixing
$\Delta G_b$	activation energy for nucleation
$\Delta g$	change of Gibbs energy density
$\delta_i$	solubility parameter of each species
$v_n$	nucleation rate
$\rho_p$	average density of polymer film

$\tau_c$

reaction characteristic time

$\phi_i$

volume fraction of the polymer species



## LIST OF ABBREVIATIONS

<i>B.C.</i>	boundary condition
BDA	1,4-diaminobutane
DCR	Dechlorane 515 Plus <sup>®</sup>
EDA	ethylene diamine
HDA	hexamethylene diamine
<i>I.C.</i>	initial condition
IL	ionic liquid
IP	interfacial polymerization
SC	sebacoyl chloride
SDS	sodium dodecyl sulfate
TDI	2,4-toluene diisocyanate
bmim	1-butyl-3-methyl imidazolium
bmprn	1-butyl-4-methyl pyridinium
emim	1-ethyl-3-methyl imidazolium
hmim	1-hexyl-3-methyl imidazolium
omim	1-octyl-3-methyl imidazolium

## CHAPTER 1

### INTRODUCTION

First developed between 1945 and 1960, interfacial polymerization (IP) has become a common technique to prepare condensation polymers. As two monomers dissolve in two immiscible phases, polymerization occurs at the interface with a rapid rate at low temperatures. IP can be used to prepare various types of polymers including polyamide, polyesters, polyurea, polyurethane, etc. (Mark et al., 1985)

In terms of industrial applications, IP has been well applied in membrane technology as well as microencapsulation. The major application in membranes is focused on reverse osmosis membrane, where a hydrogel layer is formed at the interface by IP (Baker, 2000). IP was also employed for microencapsulation of pesticides and fertilizers, in which monomers are made to polymerize at the interface of two immiscible substances under stirring (Yadav et al., 1993).

Room temperature ionic liquids (ILs) are organic salts with low melting temperature typically below 100°C. They are usually comprised of nitrogen-containing organic cations and anions such as halogens, tetrafluoroborates and hexafluorophosphates. ILs have excellent solvent properties featuring non-volatility, non-flammability, thermal stability, and a wide liquid temperature range. ILs also have unique physical and chemical properties including ionic conductivity, amphiphilicity and catalytic functions. All these characteristics project ILs as a potential alternative medium for many organic reactions (Welton, 1999; Rogers and Seddon, 2002; Zhao and Malhotra, 2002).

The low melting point of ionic liquids can be ascribed to the asymmetry in molecular structures, which largely lowers the packing efficiency and inhibits crystallization. Large sizes of anions can also contribute to the low melting point. The non-volatility and thermal stability of ILs result from the strong ionic interactions, hydrogen bonding, and sometimes relatively strong hetero-carbon interactions (Ngo et al., 2000).

The amphiphilicity of ILs originates from molecular structures typically consisting of two incompatible parts in one molecule, i.e. hydrophobic group and hydrophilic group. The amphiphilic properties of ionic liquids have also been revealed by their low surface tension (Law and Watson, 2001a), self-aggregation behavior in water (Bowers et al., 2004), and amphiphilic liquid crystal phase for ILs of long alkyl chains (Dietz et al., 2003).

Highly-correlated or even self-organized molecular structures are commonly observed in ILs. Long alkyl chain imidazolium-based ionic liquids are reported to present thermotropic liquid crystalline structures (Holbrey et al., 1999), while short alkyl chain isotropic ionic liquids present extended local orderness both in bulk and interface (Cammarata et al., 2001; Cang et al., 2003).

Due to the features mentioned above, ILs have found their applications in various types of organic reactions as reaction media or catalysts. Typical examples include Diels-Alder reaction (Earle et al., 1999; Xiao and Malhotra, 2004), Friedel-Crafts reaction (Earle et al., 1998), and polymerization (Zhang et al., 2002), etc. Other applications include nanostructured material fabrication (Zhou et al., 2004), separation and extraction (Bartsch et al., 2002), biotechnology (Park and Kazlauskas, 2003) and electrochemistry (Mazurkiewicz et al., 2003).

To our best knowledge, no systematic study was made towards the interfacial polymerization with ionic liquids. Based on the great solvent property and amphiphilicity of

ionic liquids, as well as their highly correlated structures, the following research objectives and approaches were implemented in this dissertation:

1) Study of relevant physical properties of ILs

Interfacial tension is a very important property in liquid-liquid chemical processes. The lower the interfacial tension is, the smaller the liquid droplets can be dispersed, leading to a larger specific surface area of the droplets and thus improving the mass and heat transfer rate between the immiscible liquids (Grace, 1982). Recently, ionic liquids have been studied to replace water in bi-phase catalytic reaction, when organometallic complexes and ligands are poorly soluble or unstable in water, but are found soluble in ILs. Current development of various ILs allows one to select IL from a broader spectrum of physical and chemical properties for different reaction systems. Typical examples include Diels-Alder reaction of cyclopentadiene with methylvinyl ketone in  $\text{BF}_4^-$  based ionic liquids and hydrogenation of olefins in IL media with rhodium complexes (Olivier, 1999). Law and Watson firstly reported systematic measurements of the surface tension of ILs by ring method (Law and Watson, 2001a) and the molecular orientations by direct recoil spectrometry (DRS) (Law and Watson, 2001b). The authors concluded that the surface tensions of 1-alkyl-3-methylimidazolium ionic liquids decrease as the alkyl chain is lengthened. The reduction of surface tension could be largely ascribed to the molecular orientations of ILs. To our knowledge, interfacial tension for the ILs/organic solvent systems, which may provide useful information in bi-phase reaction, separation, and other chemical processes, has not been systematically studied.

Due to the amphiphilic nature, IL molecules can self-aggregate similarly to common ionic surfactants. Bowers et al., 2004 reported the self aggregation behavior exhibited by

the ILs in aqueous solutions by measuring surface tension, conductivity, and by SANS. However, the information about the self aggregation behavior of ILs in the presence of other organic solvents is still lacking.

Ionic liquids are complex fluids compared to normal simple fluids, due to the strong Coloumbic interactions and other intermolecular interactions. These interactions result in extended correlations in IL, as well as slower translational and rotational mobility (Maggin et al., 2005). The strong interactions, complicated structures, and low mobility may easily lead to a glassy state after the temperature is lowered.

The interfacial tensions between ILs and common organic solvents will be measured by ring method and analyzed. The interfacial tension of IL aqueous solutions or other IL/solvent mixture system at various concentrations will also be studied to examine the behavior of self-aggregation. The local ordering of ionic liquids and their glassy state will be investigated by wide angle X-ray scattering (WAXS) and differential scanning calorimetry (DSC), respectively.

## 2) Synthesis and characterization of polymers with nanostructure by IP with ILs

Polyurea will be prepared by interfacial polymerization with selected ionic liquids or IL aqueous solutions as one of the reaction media to replace a more conventional water phase. Possible factors affecting the morphological features and other properties of polymers will be studied in detail.

Polyamides are a group of polymers typified by amide groups (-CO-NH-) and contain a range of materials named “nylons”. The different nomenclature for nylon is derived from the carbon numbers in the diamine and dibasic acid used to synthesize it. Nylons can be reinforced by inorganic fillers or blended with other engineering plastics

to improve their mechanical, thermal or processing performance. With their versatilities, nylons are widely utilized as fibers for textiles, films for food packaging and other industrial applications, such as automotive and electronic industries. (Mark et al., 1985b). Interfacial polymerization has been used to synthesize polyamides. In this work, polyamide films will be synthesized by IP with ILs as reaction media. The effect of ionic liquids on the morphology and the properties of the films will be investigated.

### 3) Develop applications of IP with ILs in particle coating

Fine particulates ( $\sim 10\mu\text{m}$ ) coating with polymers by interfacial polymerization will be developed and optimized through studying the effects of various operation parameters on coating performance. Surface morphology, particle size and coating weight percentage of the coated particles will be evaluated by SEM, particle size analysis and TGA, respectively. The incorporation of ionic liquids into the particle coating will be explored.

### 4) Kinetics study of Nylon film formation by IP with ILs

The production rate of nylon 610 by IP with ILs will be measured at different reaction time. The effect of monomer concentrations on the reaction kinetics will be studied by varying the initial monomer concentrations.

A simplified diffusion-controlled mathematical model will be developed to calculate the growth rate of the nylon films. The model will be examined by comparing the calculated results against the experimental data. The evolution of the molecular weight will be examined by measuring the intrinsic viscosity of the nylon at different reaction times.

## CHAPTER 2

### LITERATURE REVIEW

Some previous works including the composition and physical properties of ILs, the applications of ILs in polymer science and engineering and nanomaterials, as well as the interfacial polymerization technique relevant to this dissertation work will be introduced and summarized in this chapter.

#### 2.1 Introduction of Ionic Liquids and Their Physical Properties

##### 2.1.1 Composition of ILs

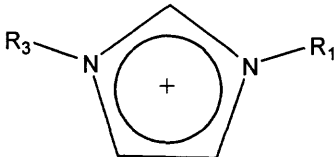
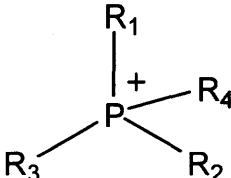
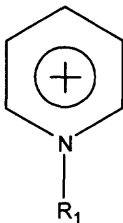
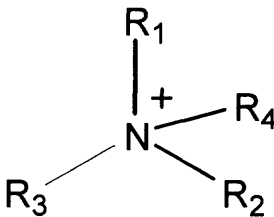
Room temperature ionic liquids (ILs) are organic salts with melting temperature normally below 100°C. The earliest ionic liquid, [EtNH<sub>3</sub>][NO<sub>3</sub>], was reported in 1914 with its melting point of 12°C (Walden, 1914). To date, many ILs have been synthesized. These compounds usually consist of an organic cation (such as N-alkyl-methylimidazolium or N-alkyl-methylpyridinium group, etc.) and an inorganic anion (such as halogen anion, tetrafluoroborate, hexafluorophosphate, etc.). A high degree of asymmetry in these organic salts frustrates the molecular packing thus inhibiting crystallization, and rendering a broad liquidus temperature range (Ngo et al., 2000). Cations and anions that are commonly found in ionic liquids are summarized in Table 2.1 (Brennecke and Maginn, 2001).

##### 2.1.2 Volatility and Thermophysical Properties of ILs

The potential of ionic liquids as an environmentally benign alternative solvent lies in their low vapor pressure, which can reduce the VOC emission as well as avoid the azeotrope formation

during the solvent-product distillation process. Most common ionic liquids, such as tetrafluoroborates and hexafluorophosphates, have high stability in both air and water. This low volatility feature, which comes from the strong columbic forces among ions, offers ILs a good opportunity for green chemistry applications.

**Table 2.1** Well-known classes of ionic liquids

Cations		Anions
imidazolium:	tetra alkylphosphonium:	[Cl <sup>-</sup> ], [Br <sup>-</sup> ], [BF <sub>4</sub> <sup>-</sup> ], [PF <sub>6</sub> <sup>-</sup> ], [CF <sub>3</sub> SO <sub>3</sub> <sup>-</sup> ], [NO <sub>3</sub> <sup>-</sup> ], [AlCl <sub>4</sub> <sup>-</sup> ], [AlBr <sub>4</sub> <sup>-</sup> ], [(CF <sub>3</sub> SO <sub>2</sub> ) <sub>2</sub> N <sup>-</sup> ], etc.
		
pyridinium:	quaternary ammonium:	
		

Holbrey et al., 2003 has reported on the thermal behavior of ILs including both heat capacity study and thermal stability. TGA shows that many ILs display decomposition temperature above 400°C. The specific heat capacity for the tested ILs, ranging from 1.17~1.80 J g<sup>-1</sup> K<sup>-1</sup> at 100°C, can be determined by DSC. The good thermal stability and wide liquidus range provided ILs a good potential as heat-transfer fluids.



Most recently, Fredlake et al., 2004 has updated the thermophysical data by presenting melting, freezing, cold crystallization, glass transition and thermal decomposition temperatures of 13 commonly used imidazolium-based ionic liquids as displayed by Table 2.2 and Table 2.3.

**Table 2.2** Melting ( $T_m$ ), Freezing ( $T_f$ ), and glass transition ( $T_g$ ) temperatures of imidazolium-based ionic liquids as determined by DSC

Compound	$T_m/^\circ\text{C}$	$T_f/^\circ\text{C}$	$T_g/^\circ\text{C}$
[emim][Tf <sub>2</sub> N]	-17	-50	-61
[emmim][Tf <sub>2</sub> N]	25	-25	
[pmmim][Tf <sub>2</sub> N]	15		
[bmim][Cl]	41		
[bmim][PF <sub>6</sub> ]	11		-37
[bmim][Tf <sub>2</sub> N]	-2		-44
[bmim][triflate]	13	-19	
[bmim][dca]	-6		-29
[bmmim][BF <sub>4</sub> ]	37		-3

Table source: Fredlake, C.P., Crosthwaite, J.M., Hert, D.G., Aki, S.D.V.K. and Brennecke, J.F. (2004). Thermophysical Properties of Imidazolium-Based Ionic Liquids. *Journal of Chemical Engineering Data*, 49, 961.

**Table 2.3** Thermal decomposition temperatures of several imidazolium-based ionic liquids as determined by TGA

Compound	$T_{\text{onset}}/^\circ\text{C}$	$T_{\text{start}}/^\circ\text{C}$
[bmim][Cl]	264	150
[bmim][Br]	273	215
[bmim][dca]	300	240
[bmim][BF <sub>4</sub> ]	361	290
[bmim][methide]	413	360
[bmim][triflate]	392	340
[bmim][Tf <sub>2</sub> N]	422	330
[bmmim][PF <sub>6</sub> ]	373	235
[bmmim][BF <sub>4</sub> ]	380	285
[pmmim][Tf <sub>2</sub> N]	462	385

Table source: Fredlake, C.P., Crosthwaite, J.M., Hert, D.G., Aki, S.D.V.K. and Brennecke, J.F. (2004). Thermophysical Properties of Imidazolium-Based Ionic Liquids. *Journal of Chemical Engineering Data*, 49, 963.

The results revealed a very different thermal behavior from common solvents of ILs. Unlike simple liquids, most ILs only exhibit crystallization upon heating, but they supercool to

form glasses during the cooling process. Given the same cation part, the thermal stability of ILs increases with anion size, which is crucial for future design and application of ionic liquids.

### 2.1.3 Solvent Property of ILs

One of the commonly accepted solvent classifications is solvent polarity. Table 2.4 has tabulated the relative polarity and surface tension of 1-butyl-3-methylimidazolium tetrafluoroborate and several commonly used solvents. In general, ionic liquids can be regarded as a polar phase, however, unlike conventional solvents, ILs are complex solvents with many types of solvent-solute interactions including hydrogen bonding,  $\pi$ - $\pi$ , ionic, dipolar, etc. All of these affect the solvent strength of ILs and can not be correlated in a simple way. Even though many ILs have similar polarity as short alkyl chain alcohols, they can show remarkably different properties from those traditional solvents because of the complexities mentioned above.

**Table 2.4** Surface tension and polarity of ionic liquid and common solvents

Solvent	Water	n-hexane	Toluene	Ethanol	THF	[bmim][BF <sub>4</sub> ]
Surface Tension at 20°C (dynes/cm) <sup>a</sup>	72.8	18.43	28.40	22.10	26.40	57.6 <sup>b</sup>
Relative Polarity <sup>a</sup>	1.000	0.009	0.099	0.654	0.207	0.673 <sup>c</sup>

<sup>a</sup>Data source: Reichardt, C. (1988). *Solvents and Solvent Effects in Organic Chemistry*, 2nd ed., VCH Publishers.

<sup>b</sup>Data source: Law, G. and Watson, P.R. (2001a). Surface Tension Measurement of N-Alkylimidazolium Ionic Liquids. *Langmuir*, 17, 6138-6141.

<sup>c</sup>Data source: Wasserscheid, P., Welton., T. (Eds.) (2002). *Ionic Liquids in Synthesis*, WILEY-VCH.

Recently, Huddleston et al., 2002 has applied a Linear Solvent Energy Relationship (LSER) model to predict the partitioning of organic solutes between the IL phase and water phase by using Abraham's generalized solvent equation as shown below:

$$\text{Log } D = c + rR_2 + s\pi_2^H + a\Sigma\alpha_2^H + b\Sigma\beta_2^H + vV_x \quad (2.1)$$

where  $D$  is distribution ratio defined by  $D = [\text{solute}]_{\text{IL}}/[\text{solute}]_{\text{org}}$ ,  $R_2$  is the excess molar refraction,  $\pi_2^H$  is the dipolarity or polarizability,  $V_x$  is the McGowan characteristic volume of the solutes,  $\Sigma\alpha_2^H$  and  $\Sigma\beta_2^H$  are the effective hydrogen bonding acidity and basicity, respectively. The terms  $r$ ,  $s$ ,  $a$ ,  $b$ , and  $v$  are parameters extracted from multiple regression from the distribution ratio data of 23 small organic molecules between IL-water phases. The distribution ratios were determined from the neutral form of the solutes in each phase. The predicted values were in good agreement with the experimental results for the distribution ratio of the solutes in both [bmim][PF<sub>6</sub>]-water and [hmim][PF<sub>6</sub>] biphasic system. This approach allows ILs to be classified and utilized based on their interactions with different organic solutes.

#### 2.1.4 Viscosity of ILs

Okoturo and Vandernoot, 2004 have measured the absolute viscosity of 23 ILs at 14 temperatures between 10 and 70°C, by using rolling-ball viscometer. It has been found that the viscosity of ILs was largely affected by the structure of anions. For the ILs with 1-butyl-3-methylimidazolium cation, the measured viscosity values fall in a wide range from 33 to 243 mPa·s at 25°C. Depending on different anions, the viscosities increase in the following order:



It was suggested that the high viscosity might be attributed to the symmetry of the anions and symmetrical charge distribution, thus resulting in more interactions with surrounding ions.

The viscosity-temperature relationship of ILs was obtained either by Arrhenius model fitting or Vogel-Tammann-Fulcher (VTF) equation. It was concluded that Arrhenius model was able to accurately describe the ILs containing less symmetrical cations without functional group in the alkyl chain; while VTF equation was sufficient to fit the viscosity-temperature dependence of those ILs containing small, symmetrical cations with low molar mass. However, there are still other types of ILs, which could not be modeled by either, indicating that further study on this complicated behavior is needed.

### **2.1.5 Molecular Structures in ILs**

In this subsection, some fundamental studies on structural characteristics of ionic liquids both in bulk and in mixture systems will be briefly reviewed. ILs exhibit a highly structured nature compared to simple liquid. The structures of ionic liquids have been studied by both experimental and computational methods.

**2.1.5.1 Structure of Isotropic ILs** Hardacre et al., 2003 have used neutron diffraction to probe the liquid structure of dimethylimidazolium chloride ([dmim][Cl]). A structural model was derived by Empirical Potential Structure Refinement (ESPR) based on the diffraction data. The results show the fact that, though an isotropic liquid, [dmim][Cl] has a strong local ordering structure resembling its crystal structure at solid state. It is indicated that the ionic liquid can retain short-range order in the isotropic liquid phase, as well as the expanded mesophase order compared to its crystal state. Simulation work also indicated that anion tends to form hydrogen bonding with the imidazolium ring hydrogen in the ring plane.

Both experimental work by Cang et al., 2003 and simulation work by Del Popolo et al., 2004 on orientation dynamics of 1-ethyl-3-methylimidazolium nitrate suggested that ionic

liquids exhibit longer spatial orders than other van der Waals organic solvents due to its strong long-range Coulombic force. The so-called “charge-ordering” effect was revealed by the three-dimensional charge distribution around cations with localization of anions, which leads to a highly local-ordering fluid structure.

Systematic simulation on 1-alkyl-3-methylimidazolium ionic liquids has been reported by Urahata and Ribeiro, 2004 using molecular dynamics. The resulted equilibrium structures were in good agreement with previous experimental static structure factors. It is also shown that large anions such as butyl and octyl derivatives prefer the regions above and below the imidazolium ring. Low wave vector peak from the correlation function for the long alkyl chain ionic liquids indicated the occurrence of intermediate range spatial correlation. Simulation works have also been done to investigate the local structure and interaction of ionic liquids with other solvents. Hanke et al., 2003 has reported the molecular dynamics simulation of benzene in dimethylimidazolium chloride and dimethylimidazolium hexafluorophosphate. The simulation result accounts for the solubility difference between the aromatic compounds and aliphatic compounds in ILs. The calculated local structure pattern in three-dimensional probability function also indicated that the local structure of the vicinity area is perturbed by solutes, while the ion charge oscillation can propagate in a longer distance.

**2.1.5.2 Liquids Crystals of ILs** It is well known that amphiphilic liquid crystals (LC) are formed via microphase separation induced by two incompatible parts in one molecule, i.e. hydrophilic group and hydrophobic group. Such liquid crystals can provide well-defined thermotropic or lyotropic mesophase behavior, which can be widely used in surfactants, membrane and other applications to improve the system performance. The potential of existence of LC phase in ionic liquids were disclosed by their chemical structures. Gordon et

al., 1998 and Holbrey and Seddon, 1999 first characterized the liquid crystalline phase of hexafluorophosphate salts with alkyl chain length longer than C<sub>12</sub>. The smectic A (S<sub>A</sub>) phase above the melting point was found in most of the tested salts, by using DSC and polarized optical microscopy (POM). The pyridinium salts also displayed the solid phase transition below the melting point, which requires further study. De Roche et al., 2003 applied small-angle and wide-angle X-ray diffraction (S-WAXS) on long-alkyl chain ionic liquids together with quasielastic neutron scattering (QENS) and Raman spectroscopy. The experimental data of the S-WAXS and Raman spectra results confirmed the S<sub>A</sub> phase, by identifying the two phase transitions at 348K and 398K for [C<sub>16</sub>mim][PF<sub>6</sub>], which are assigned to crystalline to S<sub>A</sub> and S<sub>A</sub> to isotropic liquid, respectively.

**2.1.5.3 Surface Ordering of ILs** Recently, Bowers and Vergara-Gutierrez, 2004 has reported the surface ordering of short alkyl-chain ionic liquids at liquid state probed by neutron reflection (NR). The NR study on the free surfaces of two ILs, [bmim][BF<sub>4</sub>] and [omim][BF<sub>4</sub>], has revealed a surface segregation with inhomogeneity extending to 40Å. The result has been interpreted by a proposed multi-layer ordering model, which is stacked with alternating alkyl-rich layer and a region of cation and anion groups.

Cammarata et al., 2001 employed attenuated total reflectance and transmission IR (ATR-IR) spectroscopy to investigate interactions between water and a series of 1-alkyl-3-imidazolium based ionic liquids. It was concluded that water molecules form H-bonded complex to anions in a symmetric fashion as anion<sup>⋯</sup>HOH<sup>⋯</sup>anion, and the energy of the H-bonding was estimated to be in the range of 8-13kJ/mol. It is implied that such hydrogen bond network may greatly affect the solvent properties of ILs, such as solubility, viscosity and diffusivity.

A recent SAXS study on 1-decyl-3-methylimidazolium bromide ( $[\text{C}_{10}\text{mim}][\text{Br}]$ ) demonstrated that  $[\text{C}_{10}\text{mim}][\text{Br}]$  assembles in the presence of water, eventually forming lamellar layers of lattice spacing 5~40Å, depending on the water concentration. (Dietz et al., 2003)

Surface tension of ILs was first measured by Law and Watson, 2001a by ring method. It was concluded that surface tension and surface excess energy of 1-alkyl-3-methylimidazolium ionic liquids decrease as the alkyl chain is lengthened. The results were verified via the direct recoil spectrometry (DRS) data, which were reported by the same authors later on. (Law and Watson, 2001b) The short alkyl chain hexafluorophosphates appeared to have favored vertical orientation with the N-atom uppermost, while long chain ILs or tetrafluoroborates exhibited a different orientation with more exposed methyl group, which are responsible for the drop in surface tension.

Aggregation behavior of aqueous solutions of three ionic liquids, 1-butyl-3-methylimidazolium tetrafluoroborate ( $[\text{bmim}][\text{BF}_4]$ ), 1-octyl-3-methylimidazolium chloride ( $[\text{omim}][\text{Cl}]$ ) and 1-octyl-3-methylimidazolium iodide ( $[\text{omim}][\text{I}]$ ), has been investigated by Bowers et al., 2004 using surface tension measurement, conductivity study, and small angle neutron scattering (SANS) measurements. Critical aggregation concentration was found for each system. Core-shell model with a Hayter-Penfold charge-sphere structure factor has been proposed based on the SANS data. However, further detailed studies are still needed to clarify the nature of the aggregates.

In brief, pure ionic liquids or their solution with other molecules can be regarded as supramolecular hydrogen-bonded structures with strong electrostatic interactions. The

well-defined self-organized liquid structure of ILs and their mixture systems can be employed as building template for nanoscale patterned materials.

## 2.2 Applications of Ionic Liquids in Polymer Science and Engineering

Hurley and Wier, 1951 first tested alkyl pyridinium halides as solvents in the 1950s. However, the intensive research in ionic liquids was not fully driven until the discovery of 1-ethyl-3-methylimidazolium chloroaluminate in 1982. (Wilkes et al., 1982) The study of ionic liquids has undergone a rapid growth in the past few decades not only because of the non-volatile nature of ILs, which offers a promising alternative for green solvents (Rogers et al., 2002), but also because of the unique physical and chemical properties of ionic liquids, which can be employed in many applications such as organic synthesis (Brennecke and Maginn, 2001; Oliver-Bourbigou, 2002), catalysis (Zhao et al., 2002), separation and extraction (Bartsch et al., 2002), electrochemistry (Mazurkiewicz et al., 2003), and polymerization (Kubisa, 2004), etc.

The earliest approach of application of ionic liquids in polymer science was the oxidative electropolymerization of pyrrole (Pickup and Osteryoung, 1984). The polypyrrole film was prepared in the 1:1 mole  $\text{AlCl}_3$  : N-1-butylpyridinium chloride at  $40^\circ\text{C}$ . The films are conductive when oxidized and are potential electrode materials. Over the last decade, ionic liquids in polymer electrolytes were intensively studied. Some typical examples include IL-polymer gel electrolytes (Ogihara et al., 2003), ionic liquid-polymer complexes (Watanabe and Mizumura, 1996), incorporation of IL into lithium-metal-polymer batteries (Shin et al., 2003), and solid-state actuator based on IL-polymer electrolytes (Zhou et al., 2003a), etc.



One of the important applications of ionic liquids in polymerization is free radical polymerization. It is justified not only because of the non-volatile feature of ILs, by which ILs can become a promising replacement for the volatile solvents; but also because the ionic liquids bring about a rapid polymerization rate and high molecular weight of the resulted polymer. Zhang et al., 2002 reported the homopolymerization of PMMA, PS, and PAA with 1-butyl-3-methylimidazolium hexafluorophosphate and 1-hexyl-3-methylimidazolium hexafluorophosphate using conventional initiators. It was found that the reaction rates of these systems were faster than the one with common organic solvent, and the molecular weight of PMMA and PS prepared in ILs was much higher than the one synthesized in benzene. Atom transfer radical polymerization (ATRP) is a powerful tool used to synthesize polymers with tailored molecular weight, molecular weight distribution and molecular architectures. Carmichael et al., 2000 first reported ATRP of MMA in ionic liquid. The polymerization process turned out to be more rapid and required lower temperature than those in bulk or other regular solvents. Recently, Ma et al., 2003 have reported the reverse ATRP (rATRP) of MMA in 1-butyl-3-methylimidazolium tetrafluoroborate and 1-dodecyl-3-methylimidazolium tetrafluoroborate. The resultant polymer can be easily separated and the ionic liquids can be reused for the reaction, based on the kinetics study data.

Up till now, the work on the polycondensation and polyaddition was really limited. With a series of ionic liquids as reaction media, Vygodskii et al., 2002 synthesized aromatic amides with high molecular weight. A more detailed work of direct polycondensation in ionic liquids was reported by the same group later on, presenting a successful practice of polycondensation of various polymers such as polyamides, polyamide imides, and polyhydrazides with

appreciable high yields. The high molecular weight of the polymers was characterized by the measurement of inherent viscosity. (Lozinskaya et al., 2004)

There are only few studies on coordination polymerization in ionic liquids. Mastrorilli et al., 2002 reported a polymerization of phenylacetylene in 1-butyl pyridinium tetrafluoroborate and 1-butyl-3-methylimidazolium tetrafluoroborate, in the presence of Rh(I) catalyst. The molecular weight of the resultant polymer was ranging from 55,000 to 200,000 as obtained from GPC. Both ionic liquids and catalysts are found to be recyclable in coordination polymerization.

Ionic liquids have also been attempted as solvents in other polymerization processes, including ionic polymerization (Biedron and Kubisa, 2004), enzymatic polymerization (Uyama et al., 2002), etc.

All the studies of polymerization with ionic liquids show that ionic liquids can be utilized in various polymerization processes, thus improving some of the properties of the resultant polymers (Kubisa, 2004). However, in-depth studies were only carried out in free radical polymerization; more systematic studies on incorporation of ILs in polymerization and their specific applications are still under way.

Recently, rather than reaction solvent, ionic liquids have been first incorporated into PMMA as low-volatility plasticizers. (Scott et al., 2003) The  $T_g$  of IL-plasticized PMMA could be controlled of over a wide temperature range. The material also exhibited low emissions at high temperature. Meanwhile, the elastic moduli of the PMMA plasticized with both ionic liquids and dioctyl phthalate (DOP) matched very well.

Another new area of ionic liquids application was opened in polymer blends. Snedden et al., 2003 reported the in-situ polymerization of crosslinked polymer-IL blend materials.

Copolymerizations of 4-vinylpyridine, divinylbenzene, or trimethylolpropane trimethacrylate in N,N-dialkylimidazolium ionic liquids were conducted, generating some blends with permanent porosity. The ionic liquid-polymer blends may find suitable use in membrane reactors or catalytic membranes.

### 2.3 Ionic Liquids in Formation of Nano-structured Materials

Recently, room temperature ionic liquids were employed as a novel solvent for the development of nano-structured materials. Nakashima et al., 2003 has synthesized hollow TiO<sub>2</sub> microspheres by using sol-gel reaction at oil droplet-[bmim][PF<sub>6</sub>] interface. The diameter of the microspheres varies from 3 to 50 μm, which could be controlled by temperature and stirring rate. The hollow titania gel can also be modified by coordinating carboxylic acids and other metal nanoparticles. Later on, the synthesis of 2~3 nm titania crystals in [bmim][BF<sub>4</sub>] and their assembly toward mesoporous titania spheres, which is called “nanosponge”, was reported by Zhou et al., 2003, who has also reported the preparation of wormlike mesoporous silica with assistance of [bmim][BF<sub>4</sub>] as template media. The pore size of 2.5 nm was identified by both transmission electron microscopy (TEM) and small angle X-ray scattering (SAXS) results. The H-bonding-co-π-π interaction was proposed as the mechanism of structure formation (Zhou et al., 2004). Li et al., 2005 fabricated LaCO<sub>3</sub>OH nanowires via solvothermal process at 150°C in a mixed solvent of water and ionic liquid. Wang and his coworkers recently reported the ZnO nanoflower or multipod structure achieved by microwave heating of Zn(OH)<sub>4</sub><sup>2-</sup> solution in [bmim][Cl] and [bmim][BF<sub>4</sub>] (Wang et al., 2005).

The mechanism of nanostructure formation in ionic liquids could be very complex. Some of the suggested possible causes are briefed as follows: (Dupont, 2004; Antonietti et al., 2004)

- 1) Low interfacial tension and interfacial energy of ILs can enhance nucleation rate, thus facilitate the generation of small-size structures, e.g. nanoparticles, nanopores, etc.
- 2) Good solvent properties to many other molecules enabled ionic liquids act as a ligand to coordinate nanostructures of dissolved chemical species.
- 3) Ionic liquids are self-organized liquids, which can form supramolecular hydrogen bond network. Strong ionic interaction and  $\pi$ - $\pi$  stacking interaction between neighboring imidazolium rings can also play an important role in mediating the nanostructures. Such highly structured systems can serve as template solvent media to develop well-defined nanoscale structures.

As mentioned above, most of the efforts of utilization of ionic liquids in nanostructure formation were focused on inorganic materials so far. The only work on fabrication of nanostructured organic materials was reported by Gao et al., 2004, who has reported the formation of polyaniline (PANI) nanoparticle at the water-ionic liquid interface. They synthesized PANI at aqueous/[bmim][PF<sub>6</sub>] interface by oxidizing aniline using potassium peroxydisulfate as oxidant, and particles with size from 30~80nm were observed by transmission electron microscopy (TEM). No special patterns were found by XRD, and thermal degradation temperature about 450°C was obtained via TGA measurement. The role of ILs in interfacial reactions is unclear at this point and systematic study of interfacial polymerization with room temperature ionic liquids is still lacking. Nanostructure synthesis of

polymeric materials using room temperature ionic liquids will be explored in this dissertation work.

## **2.4 Interfacial Polymerization (IP)**

### **2.4.1 Principles of Interfacial Polymerization**

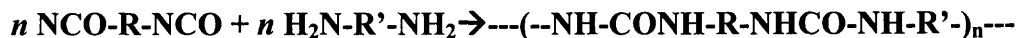
High molecular weight synthetic condensation polymers were first prepared by Carothers in 1929 at high temperature and pressure. One of the most typical examples is Nylon. Later on, low temperature techniques such as interfacial polymerization (IP) were developed gradually for preparation of condensation polymers (O dian, 2004).

In interfacial polymerization, the two fast-reacting reagents are dissolved in a pair of immiscible liquids, usually one of which is water. Polymer formation takes place at or near the liquid-liquid interface where the two solutions are brought together or stirred together.

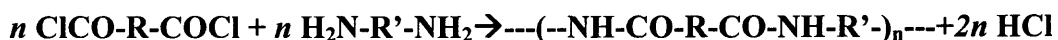
The mechanism of interfacial polymerization is described as follows using the formation of polyamide as an example: in polyamide preparation, the water phase acts as a solvent for diamine and as acid acceptor, extracting by-product acid from the reaction zone. In the course of interfacial polymerization, the monomers diffuse to the interfacial region and react with growing polymer chain ends only. Polymerization thus proceeds with an irreversible coupling of chain ends and a continuous diffusion of oligomers from the interface to the organic phase (Mark et al., 1985a).

### 2.4.2 Applications of Interfacial Polymerization

Interfacial polymerization has been extended to many different polymerization practices, including production of polyamides, polyesters, polyurethanes, polyureas, etc. A typical example reaction of synthesis of polyurea is depicted as follows:



A typical example reaction of synthesis of polyamide is depicted as follows:



The wide application of the technique can be attributed to its unique advantages as below:

(Odian, 2004)

- Rapid reaction rate;
- Exact stoichiometry is not needed;
- Impurity of the reactants is not important;
- Low temperature.

Major application of interfacial polymerization in membrane technology was focused on reverse osmosis. IP membranes offered lower salt permeability and higher water flux than those prepared by Loeb-Sourirajan process. A dense crosslinked polymer layer was formed on the surface of support membranes during the interfacial polymerization; while a more permeable hydrogel layer fills the pores of support membranes, this layer is fully hydrated and has little resistance to water flow, thus facilitates the reverse osmosis process (Baker, 2000).

Interfacial polymerization was also extensively used in the microencapsulation of pesticide, fertilizers, and controlled drug release. Microencapsulation by interfacial polymerization is a process whereby monomer is made to polymerize at the interface of two immiscible substances. (Yadav et al., 1993) One of the typical works is microencapsulation of insecticide by polyurea wall reported by Hirech et al., 2003. In his work, the hydrophobic

phase is composed of the insecticide and one monomer, hexamethylene diisocyanate (HDI), and the continuous phase of the liquid–liquid dispersion is an aqueous solution of polyvinyl alcohol. The second monomer, ethylene diamine, is added into the continuous phase after the dispersion in order to process the polyurea wall of the microcapsules. The microencapsulation is processed in a stirred batch reactor; the encapsulation yield determined by TGA is equal to 73%, and the microcapsules are characterized by a mean diameter of 30 $\mu$ m in order to ensure their suspension in the disinfectant solution.

### **2.4.3 Kinetics Study of IP**

Various theoretical models of interfacial polymerization between an organic and an aqueous phase have been studied in order to predict the growth of polymer films or microcapsules (Yadav et al., 1996; Ji et al., 2000; Kubo et al., 2001). Two common assumptions used in these models are: 1) The growing polymer film is uniform in thickness and density; 2) Monomers diffuse to a specific reaction zone for polymerization, and the reaction is diffusion-controlled. Recently, Yashin and Balazs, 2004 developed a theoretical model to describe the growth of polymer film at liquid-liquid interface that takes into account the influence of polydispersity. The model adopted a one-dimensional reaction-diffusion equation to describe interfacial polymerization of alternating copolymer AB at the interface. It has been found that the monomer/polymer composition profile in the film formation is similar in both reversible and irreversible reactions, indicating that the growth of film is controlled by the transport of monomers in the interfacial reaction zone. It was also suggested the spatial distributions of the copolymer volume fraction, the molecular weight, and the polydispersity of the polymer, is strongly dependent on the initial conditions.

Ji et al., 2001 reported a simplified steady-state diffusion-controlled model for interfacial polymerization with supporting membrane substrates. In their work, the concentration of monomer A in the supporting substrate phase was assumed to be constant, i.e.  $C_A(0,t) \approx C_A(0,0)$ . When the reaction constant is much larger than the effective diffusion constant, the polymer growth rate can be written as

$$L = \frac{1}{\phi_p} \sqrt{2D_M C(0,0)t} \quad , \quad (3.15)$$

where  $L$  is the thickness of the polymer film;  $\phi_p$  is the volume fraction of polymer in the film;  $t$  is the polymerization time;  $D_M$  is the effective diffusion coefficient, defined by  $D_M = D_p M_U / \rho_p$ , where  $D_p$  is the diffusion coefficient of monomer A in polymer,  $M_U$  is the molecular weight of the repeat unit,  $\rho_p$  is the density of the polymer. This model implicated that in the case of diffusion-controlled interfacial polymerization, the polymer film thickness is proportional to the square root of the reaction time, which was in agreement with the experimental results only within a short period of reaction time. Unfortunately, the prediction deviates from experimental data significantly when the reaction time continues to increase. The deviation is attributed to neglecting the diffusion barrier that evolves increasingly with time.

Karode et al., 1998 combined both spinodal decomposition and nucleation-and-growth (NG) mechanisms to predict the growth rate of nylon 610 film synthesized by interfacial polymerization. When NG is incorporated into the growth of the polymer film, a broader molecular weight distribution is expected. The measured polydispersity of the polymer films indicated that spinodal decomposition is the dominant mode for phase separation within a short period of reaction time, while both mechanisms become significant for phase separation after a



long period of reaction time. Unfortunately, the effect of film structure evolution on the change of effective diffusivity was not mentioned in this model. A mathematical model considering the decay of the monomer diffusivity with reaction time, resulting from the structural changes of the polymer film will be developed in this dissertation work in Chapter 5.

## CHAPTER 3

### THEORY

In this chapter, the theoretical background relevant to interfacial polymerization, including polymerization induced phase separation (PIPS), kinetics of phase separation, and diffusion-reaction models, is introduced. A simplified diffusion-control model is derived to describe the growth rate of the polymer films in the presence of ILs.

#### 3.1 Polymerization Induced Phase Separation (PIPS)

The development of polymer microstructures and morphology in interfacial polymerization is governed by the interplays between the polymerization reaction and the kinetics of polymer precipitation, i.e. phase separation of polymer from the solution. Phase separation in a non-reactive system occurs when the free energy density of the system becomes concave and the system favors coexisting polymer-rich and polymer-poor phases. This can be easily understood from the Flory-Huggins theory for a system consisting of a solvent (component 1) and a polymer (component 2) with the degree of polymerization  $N$ . The free energy of mixing per “lattice” for a binary polymer blend system can be described according to Flory-Huggins theory as

$$\frac{\Delta F_m}{k_B T n_0} = \frac{\phi_1}{N_1} \ln \phi_1 + \frac{\phi_2}{N_2} \ln \phi_2 + \chi \phi_1 \phi_2 \quad (3.1)$$

where  $\Delta F_m$  denotes the free energy of mixing,  $k_B$  is the Boltzmann constant,  $N_i$  and  $\phi_i$  denote the degree of polymerization and the volume fraction of the polymer species  $i$ , respectively.  $n_0$  is expressed as

$$n_0 = n_1 N_1 + n_2 N_2 \quad (3.2)$$

where  $n_i$  represents the number of chains of the  $i$ th component,  $N_i$  represents the number of lattices occupied by a chain,  $\chi$  is the Flory-Huggins interaction parameter, which can be correlated to temperature as

$$\chi = \beta_1 + \frac{V_1}{RT} (\delta_1 - \delta_2)^2 \quad (3.3)$$

where  $\beta_1$  denotes the entropic contribution from the lattice constant, normally  $\sim 0.35$ ;  $V_1$  is the molar volume;  $\delta_1$  and  $\delta_2$  represent the solubility parameters of each species. The equation indicates an increase of  $\chi$  with decreasing temperature, which results in a lower miscibility gap called “upper critical solution temperature” (UCST). Some polymer blends are exothermic and exhibit an upper miscibility gap called “lower critical solution temperature” (LCST). Possible explanations for such behavior may include: 1) Competition between attractive forces and repulsive forces with changing temperature; 2) Volume shrinkage effect. The free volume increases with temperature and overcompensates the dominating attractive forces. (Strobl, 1997)

For a polymer solution, the volume of solvent molecule can be scaled as unity, i.e.  $N_1=1$  (solvent, component 1) and  $N_2=N$  (polymer, component 2). The partial free energy of mixing of component 1 can be expressed as

$$\overline{\Delta G_1} = RT[\ln(1 - \phi_2) + (1 - 1/N)\phi_2 + \chi_1 \phi_2^2] \quad (3.4)$$

The critical point for the polymer solution can be obtained by solving the zeros simultaneously of both the first and second derivatives of  $\overline{\Delta G_1}$  with respect to  $\phi_2$  and can be written as

$$\begin{aligned}\phi_{2c} &= \frac{1}{1 + N^{1/2}} \\ \chi_c &= \frac{(1 + \sqrt{N})^2}{2N}\end{aligned}\tag{3.5}$$

The critical point denotes the lower bound of the physical conditions that phase separation can ever possibly occur. As the molecular weight of the polymer increases, the critical volume fraction of polymer  $\phi_c$  decreases and the critical interaction parameter  $\chi_c$  reaches 1/2. (Sperling, 2001a; Strobl, 1997)

For a reacting system, the molecular weight distribution of the polymer depends on the kinetics of polymerization. Neglecting the effect of chain length on the interaction parameter and the effect of polydispersity, the Flory-Huggins theory can be extended to describe the polymer solution as a pseudo binary system and the degree of polymerization is replaced with the average degree of polymerization  $\bar{N}$ . As the average molecular weight and the total volume fraction of the polymer increase with the extent of reaction, the critical point is eventually reached and phase separation occurs. Figure 3.1 depicts the mechanism of polymerization induced phase separation (PIPS) on a schematic plot of volume fraction of the polymer  $\phi_p$  vs. the temperature (Sperling, 2001a). Assuming the reaction is taking place isothermally,  $\phi_p$  follows a horizontal path as marked by 1 and the time-dependent phase diagram is moving from the lower right part on the plot towards the origin. The locus of the critical point, determined by the kinetics of the polymerization, is terminated between two end points:  $(\phi_c=1/2, \chi_c=2)$  and  $(\phi_c=0, \chi_c=1/2)$ . The former represents the stability limit of the monomer solution. The latter represents the stability limit of the polymer solution subject to infinite molecular weight. Note that the interaction parameter  $\chi$  must satisfy  $1/2 < \chi < 2$ ;

otherwise, the temperature is either too high for two-phase coexistence ( $\chi < 1/2$ ) or is too low that phase separation between the solvent and monomer occurs even before the reaction ( $\chi > 2$ ).

As the critical point of the virtual phase diagram evolves towards  $\chi_c = 1/2$ , the interception between the phase diagram (i.e. bimodal and spinodal curves) and the horizontal line denotes the change of thermodynamic stability for phase separation. Note that if the interception point is at the critical point, the phase separation is of the second order, and spinodal decomposition (SD) takes place. If the interception point falls on a bimodal curve, the system is under a metastable state (regime II in Figure 3.1) and phase separation follows the mechanism of nucleation and growth (NG). Nevertheless, it is possible that the arrow 1 rushes into an unstable regime (regime I in Figure 3.1) and induces spinodal decomposition forming interpenetrating morphology. More details about these two types of phase separation will be presented in Section 3.2.

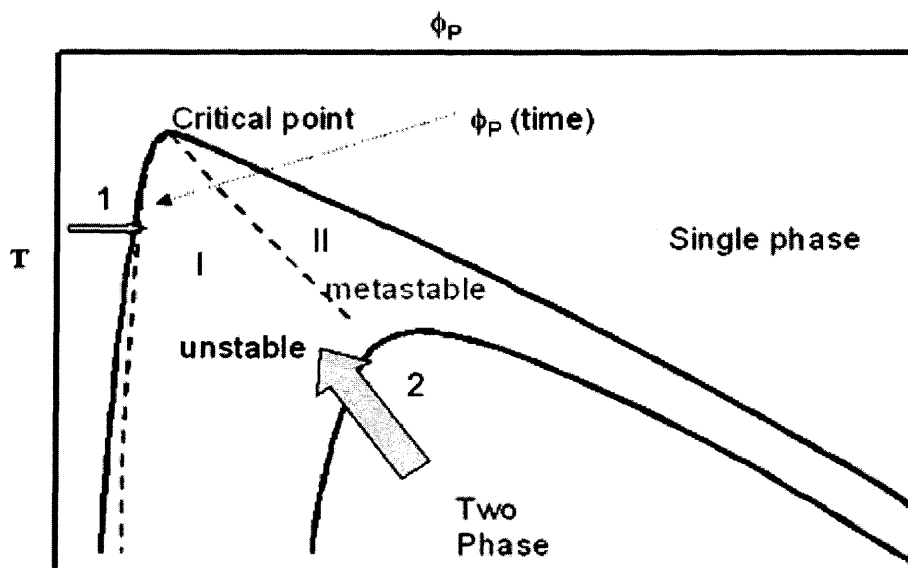


**Figure 3.1** Scheme of Polymerization Induced Phase Separation (PIPS).  $\phi_p$  represents volume fraction of the polymer,  $T$  represents the temperature.

The segregated polymer-rich phase may undergo a subsequent transition to solidification via crystallization or glass transition. Interventions from subsequent phase transitions are commonly observed in practice and may result in a drastic change in the reaction rate due to the reduction of chain mobility. It is also possible that there is no liquid-liquid phase separation at all; polymer chains precipitate directly and continuously from the solution. Again, the reaction rate will be reduced drastically once the live polymer chains become slow moving.

### 3.2 Phase Separation Kinetics

Normally, the kinetics of phase separation are governed by two types of mechanisms: nucleation and growth (NG) and spinodal decomposition (SD).

#### 3.2.1 Nucleation and Growth (NG)

The nucleation rate  $\nu_n$  of a spontaneous nucleation process can be expressed by an Arrhenius relationship as

$$\nu_n \sim \exp\left(-\frac{\Delta G_b}{kT}\right) \quad (3.6)$$

where  $\Delta G_b$  is the activation energy for nucleation. Following a spherical droplet model,  $\Delta G_b$  can be expressed as

$$\Delta G_b = \frac{16\pi}{3} \frac{\sigma^3}{(\Delta g)^2} \quad (3.7)$$

where  $\sigma$  is the interfacial energy per unit area,  $\Delta g$  is the change of Gibbs energy density with the concentration fluctuation,  $\Delta g = g(\phi_0) - g(\phi'')$ . Eq. (3.7) assumes that the nuclei are spherical, and the change of Gibbs free energy is related to the concentrations from the bulk

phase and the nuclei. A smaller interfacial energy  $\sigma$  or a larger  $\Delta g$  (i.e. deeper supercooling) results in a smaller energy barrier for nucleation and a larger nucleation rate. Once the nuclei are formed, Fickian diffusion dominates the transport of the solute from the bulk phase to the nuclei.

### 3.2.2 Spinodal Decomposition (SD)

SD in a binary system is induced by incessant concentration fluctuations amplified by thermodynamic instability. Assuming the composition of polymer is expressed as  $\phi(x,t)$ , the evolution of local composition fluctuation can be expressed by the following equation as

$$\frac{\partial \phi}{\partial t} = M \nabla^2 [-\kappa \nabla^2 \phi + \frac{\partial f}{\partial \phi}], \quad (3.8)$$

where  $M$  is the mobility,  $\kappa$  represents the coefficient for the penalty in free energy arising from the local concentration gradient square,  $f$  stands for the local free energy. The chemical potential  $\mu$  can be expressed as:

$$\mu = \frac{\partial F}{\partial \phi}, \quad (3.9)$$

where  $F$  is the free energy defined by:

$$F(\phi) = \int dx [f(\phi(x)) + \frac{1}{2} \kappa |\nabla \phi|^2]. \quad (3.10)$$

By linearization with  $\phi(r,t) = \phi_0 + \delta\phi(r,t)$ , one can get

$$\frac{\partial \delta\phi}{\partial t} = \left\{ M \left( \frac{\partial^2 f}{\partial \phi^2} \right) \Big|_{\phi_0} \right\} \nabla^2 \delta\phi - M \nabla^2 \kappa \nabla^2 \delta\phi \quad (3.11)$$

If one considers long wavelength fluctuations only, the second term in Eq. (3.11) can be neglected, resulting in a diffusion equation as

$$\frac{\partial \delta\phi}{\partial t} = D \nabla^2 \delta\phi \quad , \quad (3.12)$$

where  $D$  is the diffusion coefficient expressed as

$$D \equiv M \left( \frac{\partial^2 f}{\partial \phi^2} \right) \Big|_{\phi_0} . \quad (3.13)$$

For a system under spinodal decomposition, i.e.  $\left( \frac{\partial^2 f}{\partial \phi^2} \right) \Big|_{\phi_0} < 0$ , the diffusivity is less than zero, and the system favors diffusion of the solute from a low concentration to a high concentration, i.e. uphill diffusion (Strobl, 1997).

If one applies Fourier transform  $\delta\phi(k, t) = \int dx \delta\phi(x, t) e^{ikx}$  in Eq. (3.11), it gives

$$\frac{\partial}{\partial t} \delta\phi_k(t) = -\omega_k \delta\phi_k \quad , \quad (3.14)$$

where  $\omega_k = M\kappa k^2 [k^2 + \kappa^{-1} \left( \frac{\partial^2 f}{\partial \phi^2} \right)]$  ,  $\delta\phi_k(t) = \delta\phi_k(t=0) e^{-\omega_k t}$  . Figure 3.2 depicted the relationship between  $-\omega_k$  and  $k$ .

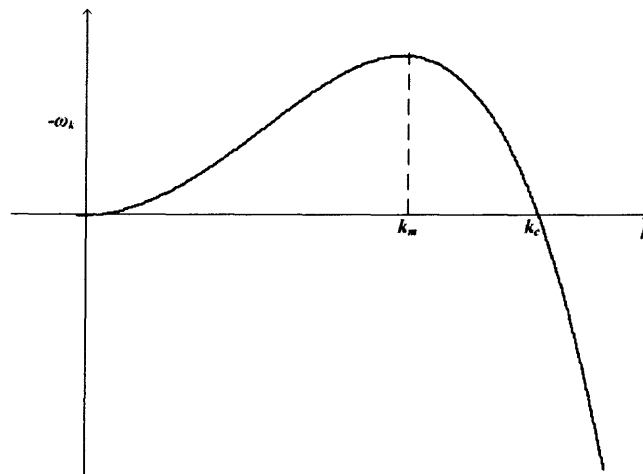


**Figure 3.2** Scheme of growing mode ( $-\omega_k$ ) vs. wavelength of fluctuation ( $k$ ) in spinodal decomposition. (Regenerated from: Gunton, J.D., San Miguel, M., Sahni, P.S. (1983) Phase Transitions and Critical Phenomena, Vol.8, Chapter 3, Academic Press, London, pp321.)



In a spinodal decomposition, long wavelength (small  $k$ ) fluctuations will grow exponentially, while short wavelength (large  $k$ ) fluctuations will decay exponentially. As shown in Figure 3.2,  $k_c$  represents the threshold wavelength for the growth of fluctuations, while  $k_m$  is the fastest growing mode for the system. In the late stage of SD, the coarsening of structures may result in an interconnected structure pattern.

The comparison of general features of NG and SD is listed in Table 3.1 (Sperling, 2001a).

**Table 3.1** Comparison of the features of Phase separation mechanisms (Adopted from Sperling, 2001, pp137).

NG	SD
Initialized by stable nucleation sites (nuclei)	Initialized by small-amplitude composition fluctuation
Downhill diffusion (positive diffusion coefficient)	Uphill diffusion (negative diffusion coefficient)
Energy barrier required	No activation energy needed
Tends to form discrete domain	Tends to form interconnected structures

Karode et al., 1998 combined both spinodal decomposition and nucleation mechanism to predict the growth rate of nylon 610 film synthesized by interfacial polymerization. When the NG is incorporated into the polymer film growth, one can expect a more disperse molecular weight distribution. The measured polydispersity of the polymer film indicated that the spinodal decomposition is the dominant mode for phase separation within a short period of reaction time, while both mechanisms become significant for phase separation after a long period of reaction time.

## CHAPTER 4

### EXPERIMENTAL SECTION

#### 4.1 Materials

##### 4.1.1 Room Temperature Ionic Liquids

The room temperature ionic liquids used in this work include a series of imidazolium-based ionic liquids:

- 1-ethyl-3-methylimidazolium tetrafluoroborate ([emim][BF<sub>4</sub>]),
- 1-butyl-3-methylimidazolium tetrafluoroborate ([bmim][BF<sub>4</sub>]),
- 1-hexyl-3-methylimidazolium tetrafluoroborate ([hmim][BF<sub>4</sub>]),
- 1-octyl-3-methylimidazolium tetrafluoroborate ([omim][BF<sub>4</sub>]),
- 1-butyl-3-methylimidazolium hexafluorophosphate ([bmim][PF<sub>6</sub>]),
- 1-hexyl-3-methylimidazolium hexafluorophosphate ([hmim][PF<sub>6</sub>]).

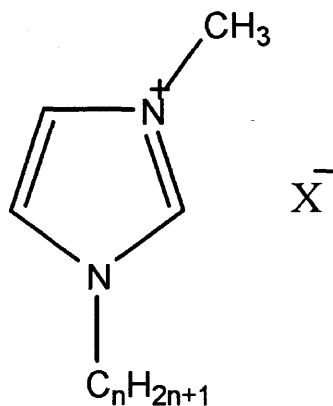
Two pyridinium-based ionic liquids were also used in some cases. They are:

- 1-butyl-4-methylpyridinium tetrafluoroborate ([bmpm][BF<sub>4</sub>]),
- 1-butyl-4-methylpyridinium hexafluorophosphate ([bmpm][PF<sub>6</sub>]).

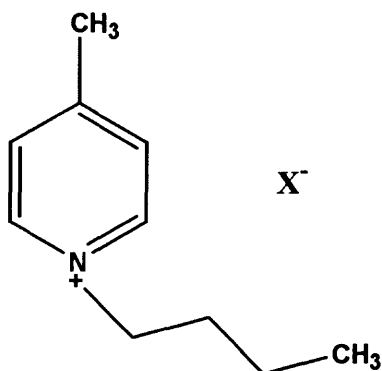
These ionic liquids were selectively used in the interfacial tension study and as solvent media for interfacial polymerization reactions. The selection of the ILs covered cations with various alkyl chain lengths and functional groups, as well as different anion groups, in order to address the effects of IL structures on the interfacial tension and the interfacial polymerization.

Figure 4.1 and Figure 4.2 depict schematic chemical structures of the two classes of ionic liquids mentioned above. All of the ionic liquids used in this work were purchased from

Sigma-Aldrich and used as received. Table 4.1 lists the CAS numbers, densities, melting points and the purity of the ILs used in this study (Sigma-Aldrich MSDS data; Huddleston et al., 2001).



**Figure 4.1** Structure of 1-alkyl-3-methylimidazolium-based room temperature ionic liquids used in this work. (For tetrafluoroborates,  $n=2,4,6,8$ ,  $X=BF_4$ ; for hexafluorophosphates,  $n=4,6$ ,  $X=PF_6$ )



**Figure 4.2** Structure of 1-butyl-4-methylpyridinium room temperature ionic liquids. ( $X=BF_4$ ,  $PF_6$ )

**Table 4.1** Material data of the ionic liquids used in this work (Sigma-Aldrich MSDS)

Ionic Liquid	CAS Number	Density (g/ml)	Melting point (°C)	Purity
[emim][BF <sub>4</sub> ]	143314-16-3	1.294 (25°C)	-	≥97.0%
[bmim][BF <sub>4</sub> ]	174501-65-6	1.21 (20°C)	-81 <sup>a</sup>	≥97.0%
[hmim][BF <sub>4</sub> ]	244193-50-8	1.149 (20°C)	-81	≥97.0%
[omim][BF <sub>4</sub> ]	244193-52-0	1.12 (20°C)	-	≥97.0%
[bmim][PF <sub>6</sub> ]	174501-64-5	1.38 (20°C)	10 <sup>a</sup>	≥96.0%
[hmim][PF <sub>6</sub> ]	304680-35-1	1.419 (20°C)	-61 <sup>a</sup>	≥97.0%
[bmpm][BF <sub>4</sub> ]	343952-33-0	1.20 (20°C)	-	≥97.0%
[bmpm][PF <sub>6</sub> ]	401788-99-6	-	45	≥97.0%

<sup>a</sup> Huddleston, J.G., Visser, A.E., Reichert W.M., Willauer, H.D., Broker, G.A. and Rogers, R.D. (2001) Characterization and Comparison of Hydrophilic and Hydrophobic Room Temperature Ionic Liquids Incorporating the Imidazolium Cation. Green Chemistry, 3, 156-164.

#### 4.1.2 Monomers for Interfacial Polymerization

The interfacial polymerization of polyureas and polyamides was investigated. Polyurea was formed by condensation polymerization of 2,4-toluene diisocyanate (TDI, ≥95.0% purity) and ethylene diamine (EDA, ≥99.0% purity) or 1,4-diaminobutane (BDA, ≥99.0% purity). Polyamides were polymerized from sebacoyl chloride (≥95.0% purity) and hexamethylene diamine (HDA, ≥95.0% purity) or 1,4-diaminobutane (BDA, ≥99.0% purity). All chemicals used in this work were purchased from Sigma-Aldrich and used as received.

#### 4.1.3 Other Materials

In the study of interfacial tension of ILs/organic solvent systems, both n-hexane (≥95.0% purity, ρ=0.664 g/ml) and Toluene (≥99.0% purity, ρ=0.865 g/ml) were employed as one of the immiscible phases in the interfacial tension measurement. in order to investigate the solvent

effects of both aliphatic and aromatic solvents on the IL/solvent interfaces. In the study of interfacial polymerization, n-hexane was adopted as the upper-phase solvent to dissolve TDI or sebacyl chloride in the synthesis of polyurea and polyamides, respectively. Both n-hexane and toluene were purchased from Sigma-Aldrich and used as received. Dechlorane 515 Plus (DCR), which is an inert particle with average size of 10-15  $\mu\text{m}$ , is selected as the core particle in the coating study. The formula of DCR 515 Plus is shown as Figure 4.3. The molecular weight of the DCR is 654 g/mol, while the density and the melting point of the DCR are 1.8g/ml and 350°C, respectively (Occidental MSDS data).

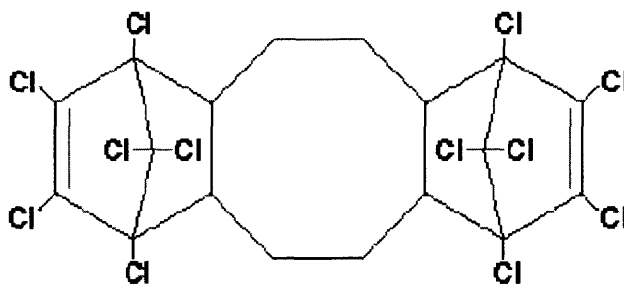


**Figure 4.3** Chemical Structure of Dechlorane 515 Plus ( $\text{C}_{18}\text{H}_{12}\text{Cl}_{12}$ ).

## 4.2 Interfacial Tension Measurement

Interfacial tension is a crucial property in the liquid-liquid chemical process such as biphasic reactions or biphasic catalysis (Olivier, 1999). In such systems, one liquid is broken up into smaller droplets under the flow field, thus, disperse uniformly in the continuous phase. The good dispersion results in a large surface area of the liquid-liquid interface, thus can improve the transport efficiency of the chemical process. The liquid droplet dispersion in the second

phase is largely dependent on the capillary number, a function of the interfacial tension. (Grace, 1982)

Interfacial tensions between selected ILs and organic solvents were measured at room temperature using a Cenco-DuNouy Interfacial Tensiometer 70545. In a typical experiment, a platinum ring with diameter of 5.992cm and a ring/wire radius ratio of 53.6 was employed. With 10 ml ionic liquid in a 50ml beaker, another 10 ml organic solvent was slowly poured onto the IL phase. 15~30 minutes are allowed before further experimentation in order to reach the phase equilibrium. Because the densities of ionic liquids are higher than those of toluene or hexane, the ring was zeroed in the light phase, and then pulled upward from the ionic liquid phase to the organic solvent phase. All data were averaged based on at least three repeated measurements. To remove possible errors resulting from the effect of ring dimensions and densities of two phases on the tension, the measured values were corrected to the true interfacial tension by the method reported by Zuidema and Waters, 1941 according to the following equation:

$$\gamma = P \cdot \{0.7250 + [0.000975P/4\pi^3R^3(D - d) + 0.04534 - 1.679/(R/r)]^{1/2}\} / 4\pi R \quad (4.1)$$

where  $\gamma$  is the true interfacial tension,  $P$  is the measurement reading value of the tensiometer,  $R$  is the radius of the ring in mm, which is 29.96mm in the current experiment;  $D$  is the density of the lower phase ( $\text{g}/\text{cm}^3$ ), which is the density of the ionic liquid used in this work (Table 4.1);  $d$  is the density ( $\text{g}/\text{cm}^3$ ) of the upper phase, which is 0.664 for n-hexane and 0.865 for toluene, respectively;  $R/r$  is the ring/wire radius ratio, which is 53.6 in the current work.

In order to examine the effect of the alkyl chain length of ILs, as well as the effect of different organic phases on the IL-solvent interfacial tension between IL and organic solvent, imidazolium-based ionic liquids include  $[\text{C}_x\text{mim}][\text{BF}_4]$  ( $x=2,4,6,8$ ) and  $[\text{C}_y\text{mim}][\text{PF}_6]$  ( $y=4,6$ ),

(See Figure 4.1) and two typical organic solvents, n-hexane and toluene, were employed for the study. A crude method of determining the miscibility of the ionic liquids and organic solvent was conducted by observing the mixture of IL/solvent at a 1:1 volumetric composition. The observation results of the ionic liquids with the above two organic solvents and water are tabulated in Table 4.2. This table facilitates the selection of appropriate test systems. It is found that [omim][BF<sub>4</sub>] has partial miscibility with toluene, so the interfacial tension of [omim][BF<sub>4</sub>]/toluene system was not measured in this work.

ILs have shown surfactant behavior in aqueous solutions as reported by Bowers et al., 2004. For amphiphilic chemicals, one can identify the critical micelle concentration (CMC) by measuring the surface/interfacial tension at various concentrations.

**Table 4.2** Miscibility observance results of ionic liquids in common solvents (1:1 volume ratio) based on visual observation

Solvent	n-hexane	Toluene	Water
[emim] <sup>+</sup> [BF <sub>4</sub> ] <sup>-</sup>	immiscible	immiscible	miscible
[bmim] <sup>+</sup> [BF <sub>4</sub> ] <sup>-</sup>	immiscible	immiscible	miscible
[hmim] <sup>+</sup> [BF <sub>4</sub> ] <sup>-</sup>	immiscible	immiscible	immiscible
[omim] <sup>+</sup> [BF <sub>4</sub> ] <sup>-</sup>	immiscible	partially miscible	immiscible
[bmim] <sup>+</sup> [PF <sub>6</sub> ] <sup>-</sup>	immiscible	immiscible	immiscible
[hmim] <sup>+</sup> [PF <sub>6</sub> ] <sup>-</sup>	immiscible	immiscible	immiscible
[bmpm] <sup>+</sup> [BF <sub>4</sub> ] <sup>-</sup>	immiscible	immiscible	miscible

To investigate the self-aggregation behavior of ionic liquid aqueous solutions in the presence of a second organic phase, the interfacial tension between n-hexane and IL aqueous solutions with various concentrations were measured. Zhao et al., 2002 reported the miscibility of the short alkyl chain imidazolium and pyridinium tetrafluoroborates in water.

[emim][BF<sub>4</sub>], [bmim][BF<sub>4</sub>] and [bmpm][BF<sub>4</sub>] were selected to prepare the aqueous solutions for interfacial tension measurement with n-hexane. The tested IL concentrations in weight percentage include 0 (pure water), 5%, 10%, 15%, 20%, 25%, 30%, 50%, 80% and 100% (pure IL). The self aggregation behavior of IL/organic solvent mixture systems was studied. Using IL as the continuous phase, ethanol was dissolved in the IL phase at various concentrations, and the surface tensions of the solutions were measured. [hmim][BF<sub>4</sub>] and [omim][BF<sub>4</sub>] are well miscible with ethanol as confirmed by the miscibility test mentioned above, the surface tension of the ethanol-IL solution systems were investigated.

### 4.3 Interfacial Polymerization

#### 4.3.1 Synthesis of Polyurea with ILs

Polyureas were synthesized from 2,4-toluene diisocyanate (TDI) and ethylene diamine (EDA) or 1,4-diaminobutane (BDA). A typical reaction between TDI and EDA can be simply expressed as Figure 4.4.

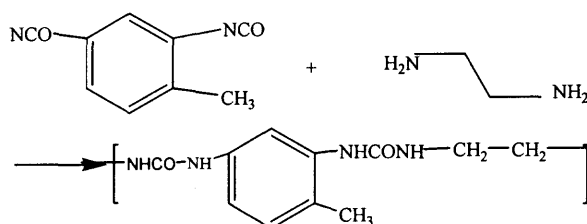


**Figure 4.4** Reaction Scheme of polyurea synthesis.

Most common ionic liquids are immiscible with n-hexane. Diamine normally shows good solubility in 1-alkyl-3-methylimidazolium ionic liquids as reported by Scavazzo et al., 2002. According to the different reactants and ionic liquid used in the synthesis, the synthesized polyurea samples were divided into three groups as follows:



Group 1: The upper phase is formed by dissolving TDI in n-hexane, while the lower phase is formed by dissolving EDA in 1-alkyl-3-methylimidazolium tetrafluoroborates, ( $[C_n\text{mim}][\text{BF}_4]$ ,  $n=2,4,6,8$ ). For comparison purposes, polyurea was also synthesized at the regular hexane-water interface from TDI and EDA.

Group 2: The upper phase is formed by dissolving TDI in n-hexane, while the lower phase is formed by dissolving BDA in 1-alkyl-3-methylimidazolium tetrafluoroborates, ( $[C_n\text{mim}][\text{BF}_4]$ ,  $n=2,4,6,8$ ). For comparison purposes, polyurea was also synthesized at the regular hexane-water interface from TDI and BDA.

Group 3: The upper phase is formed by dissolving TDI in n-hexane, while the lower phase is formed by dissolving EDA or BDA in 1-alkyl-3-methylimidazolium hexafluorophosphates, ( $[C_n\text{mim}][\text{PF}_6]$ ,  $n=4,6$ ).

The reaction characteristics of the three groups mentioned above are listed in Table 4.3, 4.4 and 4.5, respectively. All reactions have taken place at room temperature without stirring. The experimental procedure is described as follows:

In a typical experiment, TDI was dissolved in n-hexane (upper phase), while an excess amount of EDA or BDA was dissolved in pure ILs (lower phase). The upper phase was slowly poured onto the lower phase in a 10ml reaction cell without stirring. The reaction occurred immediately by forming white polyurea at the interfacial layer. After 1 hour, the white polymer precipitates were found in the upper organic phase, while the lower phase with the ionic liquids remained clear. The polymer was collected in a Buchner funnel, washed repeatedly with 1:1 ethanol/water volumetric mixture and dried under vacuum for 24 hours at 45°C. The dried products were weighed and their conversions were calculated based on the initial number of moles of the limiting reactant, i.e. TDI.

**Table 4.3** Reaction media of polyurea prepared from ethylene diamine in 1-alkyl-3-methylimidazolium tetrafluoroborates (Group 1)

Sample Name	Upper phase <sup>a</sup>	Lower phase <sup>b</sup>
PUA-0	TDI + n-hexane	EDA + water
PUA-B2E	TDI + n-hexane	EDA+ [emim][BF <sub>4</sub> ]
PUA-B4E	TDI+ n-hexane	EDA+ [bmim][BF <sub>4</sub> ]
PUA-B6E	TDI+ n-hexane	EDA + [hmim][BF <sub>4</sub> ]
PUA-B8E	TDI + n-hexane	EDA + [omim][BF <sub>4</sub> ]

<sup>a</sup>1.4mmol TDI dissolved in 2ml n-hexane.

<sup>b</sup>4mmol EDA dissolved in 1ml IL.

**Table 4.4** Reaction media of polyurea prepared from 1,4-diaminobutane in 1-alkyl-3-methylimidazolium tetrafluoroborates (Group 2)

Sample Name	Upper phase <sup>a</sup>	Lower phase <sup>b</sup>
PUA-B0	TDI + n-hexane	BDA + water
PUA-B2B	TDI+ n-hexane	BDA + [emim][BF <sub>4</sub> ]
PUA-B4B	TDI+ n-hexane	BDA + [bmim][BF <sub>4</sub> ]
PUA-B6B	TDI + n-hexane	BDA + [hmim][BF <sub>4</sub> ]
PUA-B8B	TDI + n-hexane	BDA + [omim][BF <sub>4</sub> ]

<sup>a</sup>1.4mmol TDI dissolved in 2ml n-hexane.

<sup>b</sup>3mmol BDA dissolved in 1ml IL.

**Table 4.5** Reaction media and conversion of polyurea prepared in 1-alkyl-3-methylimidazolium hexafluorophosphates (Group 3)

Sample Name	Upper phase <sup>a</sup>	Lower phase <sup>b</sup>
PUA-P4E	TDI+ n-hexane	EDA + [bmim][PF <sub>6</sub> ]
PUA-P6E	TDI + n-hexane	EDA + [hmim][PF <sub>6</sub> ]
PUA-P4B	TDI + n-hexane	BDA + [bmim][PF <sub>6</sub> ]
PUA-P6B	TDI + n-hexane	BDA + [hmim][PF <sub>6</sub> ]

<sup>a</sup>1.4mmol TDI dissolved in 2ml n-hexane.

<sup>b</sup>3mmol BDA dissolved in 1ml IL.

### 4.3.2 Synthesis of Polyurea with IL Aqueous Solutions

Synthesis of polyurea at the interface between n-hexane and aqueous solutions of ionic liquids is performed. Instead of pure ILs, a series of 10 wt% aqueous solutions of ILs are employed as the lower phase solvents to dissolve ethylene diamine. The upper phase is composed of TDI and n-hexane. For comparison purposes, polyurea was also synthesized at the regular hexane-water interface, with and without using the ionic surfactant, sodium dodecyl sulfate (SDS). All the reactions have taken place at room temperature. The same experimental procedure was followed according to section 4.3.1 and the reactant concentration ratio listed in Table 4.3 was followed. All samples prepared in the corresponding reaction media are listed in Table 4.6.

**Table 4.6** Reaction media of polyurea samples synthesized in IL aqueous solutions

Sample Name	Upper Phase	Lower Phase
PUA-0	n-hexane	Water
PUA-SDS	n-hexane	0.001M SDS aqueous solution
PUA-Ei	n-hexane	10 wt% [emim] <sup>+</sup> BF <sub>4</sub> <sup>-</sup> aqueous solution
PUA-Bi	n-hexane	10 wt% [bmim] <sup>+</sup> BF <sub>4</sub> <sup>-</sup> aqueous solution
PUA-Bp	n-hexane	10 wt% [bmpm] <sup>+</sup> BF <sub>4</sub> <sup>-</sup> aqueous solution

### 4.3.3 Synthesis of Polyamides with ILs and Kinetics Study

Polyamide films were synthesized by interfacial polymerization from sebacoyl chloride and 1,4-diaminobutane (BDA) or hexamethylene diamine (HDA). [bmim][BF<sub>4</sub>] and [omim][BF<sub>4</sub>] were selected as solvents for diamines in the reaction. The lower phase was formed by

dissolving diamine in the ionic liquid, while the upper phase was composed of the n-hexane solution of sebacoyl chloride. Table 4.7 shows the polyamide samples synthesized in this work and the corresponding reaction media. The molar concentration ratio of diamine/sebacoyl chloride is determined as 3:1. As a reference, reactions between sebacoyl chloride and both diamines were also performed at the water/n-hexane interface.

All the reactions were conducted at room temperature in a 10ml beaker without stirring. The same experimental procedure described in 4.3.1 was followed.

**Table 4.7** Reaction Systems of Polyamide Films by IP in ILs

<b>Sample Name</b>	<b>Lower Phase<sup>a</sup></b>
PA-H0	HDA + Water
PA-HB4	HDA + [bmim][BF <sub>4</sub> ]
PA-HB8	HDA + [omim][BF <sub>4</sub> ]
PA-B0	BDA + Water
PA-BB4	BDA + [bmim][BF <sub>4</sub> ]
PA-BB8	BDA + [omim][BF <sub>4</sub> ]

<sup>a</sup>All upper phases are sebacoyl chloride dissolved in n-hexane, the diamine concentration is 1.25mol/l, the molar concentration ratio of diamine/sebacoyl chloride=3:1.

The reaction kinetics of IP in ILs were studied by the IP of nylon 610 at the [omim][BF<sub>4</sub>]/n-hexane interface. The effect of both reactant concentrations on the reaction kinetics were studied by varying the reactant concentration ratio. Six HDA/sebacoyl chloride molar concentration ratios studied in this work are: 1.25M/1.25M, 1.25M/0.84M, 1.25M/0.42M, 0.84M/0.42M, 0.42M/0.42M and 0.42M/1.25M. To exclude the reactor volume effect on the reaction kinetics, all the reactions were conducted in a 10 ml beaker

without stirring, with the upper phase (sebacoyl chloride and n-hexane) volume as 1.1 ml and the lower phase (HDA and [omim][BF<sub>4</sub>]) volume as 1.2 ml. The polymerization was allowed to continue for 24 hours. For each concentration ratio, eight reactions with reaction times of 10min, 20min, 40min, 50min, 60min, 180 min, 300 min and 24 hours were investigated. Again, the experimental procedure described in section 4.3.1 was followed. The dried samples were weighed and the conversions were calculated based on the stoichiometry. The intrinsic viscosities of the Nylon 610 samples, synthesized under the HDA/sebacoyl chloride concentration ratio of 3/1 with varying reaction times, were measured in solutions of 98% H<sub>2</sub>SO<sub>4</sub>(See experimental details in Section 4.4, part H), in order to investigate the molecular weight evolution as a function of reaction time.

#### 4.3.4 Fine Particle Coating by IP

Dechlorane 515 Plus (DCR), an inert particle with average size of 10-15  $\mu\text{m}$ , was selected as the core particle for polymer coating through interfacial polymerization. The polyurea coating layer was readily formed via the reaction between TDI and EDA. The water in the diamine solution could also react with TDI to form oligomers. However, the reactivity of isocyanate with the active hydrogen available on different functional groups is as follows (Mark et al., 1985c):

aliphatic amine > aromatic amine > primary -OH > water > secondary -OH

It is therefore assumed that the reaction between the EDA and TDI is predominant in this process, although the chemical composition of the coating layer could become complex due to the presence of water. A scheme of the experimental setup for the coating process described above is shown in Figure 4.5: The premixing was performed in a 50ml glass beaker with

sonicator on (See 1), the reaction was conducted in a 600ml glass beaker (See 3) located in a water bath with temperature control (See 4). The stirring speed during the coating was controlled by Yamato® LR400C Digital Stirrer (See 2).

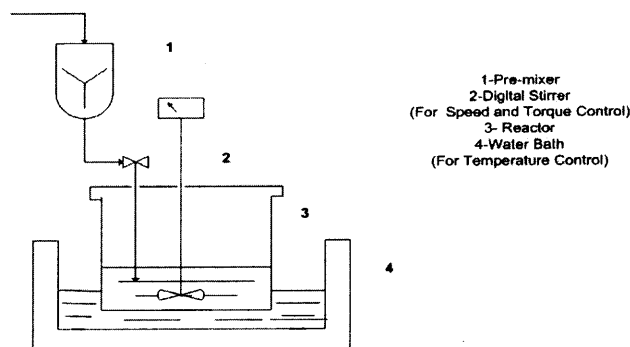


**Figure 4.5** Scheme of particle coating process by interfacial polymerization.

A typical coating operation procedure is described as follows:

1. DCR was premixed with TDI in a ratio of 5g : 2.5ml. The mixing was carried out in 1 with sonicator on for 10 minutes in order to form a uniform DCR paste.
2. Ethylene diamine was dissolved in deionized water in 3 with a predetermined volume ratio, typically in excessive amount with respect to TDI. Typical volume concentrations of the EDA solution used for the coating were 30% and 50%.
3. The paste was introduced by spatula to the solution in 3 under a controlled stirring speed. The coating by in-situ interfacial polymerization was performed under room temperature for one hour under a stable stirring. The rotation speed of the impeller was controlled by 2. In the current work, the stirring speed was varied from 100 rpm to 900 rpm. The temperature was controlled at 25°C by the water bath (4 in Figure 4.5).
4. The product was filtered and rinsed with alcohol/H<sub>2</sub>O mixture, then dried at 45°C under vacuum for 24 hours.

The coating performance of the fine particles were characterized through the following three aspects: 1) surface coverage and morphology, which was observed by SEM in this work; 2) particle size of the coated particles, which was studied by particle size analyzer ; and 3) coating weight percentage, which was analyzed by TGA. Detailed experimental methods will be presented in Section 4.4.

The initial monomer concentration and the hydrodynamic force are two of the important factors that affect the polymerization rate and the coating layer formation. Therefore, the EDA concentration and the stirring speed were employed as two major controlled parameters in the experimental work, in order to study their effects on the coating performance.

The coating with ionic liquids was preliminarily studied in this work. Ionic liquid was incorporated as a reaction additive by dissolving in the organic phase with pre-mixing. Two selected ionic liquids, [bmpm][BF<sub>4</sub>] and [bmpm][PF<sub>6</sub>], The volume ratio of TDI to IL is 10:1. The EDA volume concentration and stirring speed was determined as 30% and 600rpm, respectively. The surface morphology of the coated particles was observed by SEM.

#### **4.4 Material Characterization Methods**

The physical and chemical properties of the synthesized polymers or polymer coated particles are determined by a series of characterization methods as follow.

##### **A. Fourier Transform Infrared (FTIR)**

FTIR was used to examine the chemical composition of the synthesized polymers. FTIR spectra were recorded by Perkin Elmer SpectrumOne<sup>®</sup> FTIR spectrometer by using KBr (potassium bromide) disk as a background. The polymer solids were mixed with the dried KBr powder and pressed into a translucent thin disk for the scan. The liquid sample of ILs was

measured by using two NaCl (sodium chloride) disks. One drop of the liquid sample was spread on one of the disks and sandwiched in between before the spectra scan. All the samples undergo 25 scans from 4000 to 1000 wavenumbers, and an average spectrum was obtained.

### **B. Scanning Electron Microscopy (SEM)**

Leo 1530VP<sup>®</sup> SEM was employed to examine the surface morphology and microstructure of the polymer materials. The sample was stuck on the top of the tape on the sample holder, and fixed with compressed air. All the samples undergo a carbon thin-film coating with BAL TEC MED 20 HR Sputtering Coater before the microscopic characterization. The coating was conducted at high vacuum ( $<2 \times 10^{-5}$  bar). All the microscopies are performed under 1kV, with a working distance range of 3-5mm.

### **C. Differential Scanning Calorimetry (DSC)**

DSC was used to measure the glass transition temperature of the synthesized polymers and the thermal behavior of pure ILs to investigate the local glassy behavior of ILs. Two typical hexafluoroborate ionic liquids, [bmpm][PF<sub>6</sub>] and [hmim][PF<sub>6</sub>], were selected to study the glassy phase behavior of ILs. The reported melting temperatures are 45°C and -61°C for [bmpm][PF<sub>6</sub>] and [hmim][PF<sub>6</sub>], respectively. (Sigma-Aldrich MSDA data; Huddleston et al., 2001) Based on their different melting points, the testing temperature range has been set as -20~100°C and -80~100°C for [bmpm][PF<sub>6</sub>] and [hmim][PF<sub>6</sub>], respectively. The equipment model used in this work was TA-Q100<sup>®</sup> DSC. The DSC measurements for the polymer samples were performed at a heating rate of 5°C/min; while the DSC for the IL samples were conducted with a heating-cooling-heating cycle, at a heating rate of 10°C and a cooling rate of 5°C, respectively, in which the glass formation of ILs upon cooling is expected to be caught up.

### **D. Thermogravimetric Analysis (TGA)**



TA-Q50<sup>®</sup> TGA was employed to investigate the thermal stability of the nylon films and the coating weight percentage of the polymer coated particles. The TGA measurements were performed at a heating rate of 10<sup>°</sup>C/min, under the dry nitrogen atmosphere with a nitrogen flow rate of 40ml/min.

### **E. Particle Size Analysis**

Particle Size Analysis of the coated particulates was performed by Beckman Coulter LS230<sup>®</sup> Laser Diffraction Analyzer. The system is capable of measuring sample particles ranging from 0.04 to 2000  $\mu\text{m}$ . It can either measure particles suspended in a liquid with its Fluid Module, or measure sample particles suspended in air with Dry Powder Module. In the current work, the particle size analysis of the polyurea-coated particulates was performed by using the water suspension of the particles with the fluid module. The operation procedure is described as below:

1. Sample Preparation: Disperse the particle sample in water to ensure proper wetting and prevent agglomeration.
2. Filling microvolume cell with the background liquid (water) and run the background measurement.
3. With sonicator on, slowly pour the suspension into microvolume cell at appropriate quantities until obscuration is approximately 10%.
4. Run the measurement cycle for 60 seconds, repeat the cycle for three times.
5. Collect the averaged converted data

Both the volume averaged particle size distribution and particle mean size of the samples were obtained.

### **F. X-ray diffraction (XRD)**

XRD was utilized to probe the crystallization behavior of polymers produced by IP in ILs. In the X-ray diffraction experiment, two scattering X-rays will be completely in phase if the path difference is equal to a whole number  $n$  of wavelengths. This relationship is known as Bragg's law. Considering only the first-order reflection from planes, the Bragg's law can be written as

$$\lambda = 2d \sin \theta \quad (4.2)$$

where  $\lambda$  is the X-ray wavelength,  $d$  is the spacing distance,  $2\theta$  is the scattering angle. Following the requirement of the Bragg law, diffraction occurs only when the wavelength of the X-ray wave motion is of the same magnitude as the repeat distance between scattering centers, i.e. the characteristic length  $d$ . (Cullity, 1978)

In the case of X-ray diffraction study for polymers, the scattering maximum indicates the chain spacing distance. The scattering intensity data were plotted against the scattering vector  $Q$ , which is also called the inverse space with the unit of  $\text{\AA}^{-1}$ . The parameter  $Q$  can be correlated to  $d$  or  $\theta$  via the following equation: (Sperling, 2001b)

$$Q = \frac{2\pi}{d} = \frac{4\pi \sin \theta}{\lambda} \quad (4.3)$$

In the present work, the XRD pattern was recorded by Panalytical® PW3040 MPD XRD equipment, where the wavelength of the impinged X-ray is 1.54 $\text{\AA}$ .

### **G. Small-wide angle synchrotron X-ray Scattering (S-WAXS)**

S-WAXS was performed by Dr. Jing Zhang and Professor Jing Wu at the Brookhaven National Lab Beamline 27C, with the X-ray wavelength of 1.37 $\text{\AA}$ . The local structural study of ionic liquids was investigated by WAXS on selected short alkyl chain hexafluorophosphates ionic liquids. The two tested ionic liquids are [hmim][PF<sub>6</sub>] and [bmpm][PF<sub>6</sub>], among which the latter one has a melting point of 45°C. The testing temperatures for the two samples are

20°C and 50°C, respectively. The long range order of the polyurea samples synthesized by IP with ILs was also probed by SAXS. The testing temperature of SAXS measurement for the polymer samples was 25°C. Again, the correlation distance  $d$  was obtained via equation (4.3).

### H. Intrinsic viscosities

Intrinsic viscosities of the polyamide films,  $[\eta]$ , were measured by Cannon<sup>®</sup> 150 K333 Ubbelohde viscometer. The  $[\eta]$  is obtained by the one-point measurement and calculated by Solomon-Ciuta equation as follow (Solomon and Ciuta, 1962):

$$[\eta] = \frac{\sqrt{2(\eta_{sp} - \ln \eta_r)}}{c} \quad (4.4)$$

where

$$\begin{aligned} \eta_{sp} &= \frac{\eta - \eta_0}{\eta_0} \\ \eta_r &= \frac{\eta}{\eta_0} \end{aligned} \quad (4.5)$$

where  $\eta$  and  $\eta_0$  are viscosity of polymer solution and pure solvent, respectively;  $c$  is the concentration of polymer in dilute solution in the unit of g/100ml. Because  $\eta/\eta_0 = t/t_0$ , where  $t$  and  $t_0$  are flow times of polymer solution and pure solvent in the viscometer, respectively, we thus have

$$[\eta] = \frac{\sqrt{2\left(\frac{t-t_0}{t_0} - \ln \frac{t}{t_0}\right)}}{c} \quad (4.6)$$

Polyamide solutions were prepared by dissolving 0.01g polymer in 10ml 98% H<sub>2</sub>SO<sub>4</sub>, giving a  $c$  of 0.1g/100ml. The unit of  $[\eta]$  is 100ml/g. All the measurements were performed at 25°C and averaged on three readings for each sample.

## CHAPTER 5

### RESULTS AND DISCUSSIONS

The present chapter is divided into six sections. Section 5.1 presents the study of some physical properties of ILs that are relevant to this work. These include the measurement of interfacial tensions study between ILs and organic solvents, the structures, and thermal behavior of the ILs. Section 5.2 presents the synthesis of polyureas with ILs and their characterization. Section 5.3 presents the synthesis of polyureas with aqueous solutions and their characterization. Section 5.4 presents the synthesis of polyamides films with ionic liquids and their characterization. Section 5.5 presents the application of IP in fine particle coating and the incorporation of ILs. Section 5.6 presents the study of the reaction kinetics of polyamide films growth with ILs.

#### 5.1 Study of the Physical Properties of Ionic Liquids

In this section, the following physical properties relevant to our work were measured:

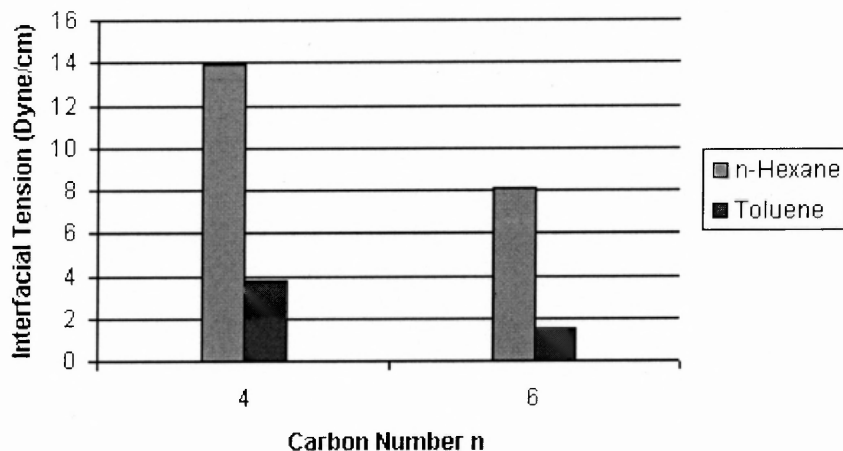
- 1) Interfacial tension between ILs with various alkyl chain lengths and two typical organic solvents: aliphatic n-hexane and aromatic toluene.
- 2) Self aggregation of ILs in aqueous solutions and self aggregation of ethanol in ILs.
- 3) DSC study of the thermal behavior of [hmim][PF<sub>6</sub>] and [bmpm][PF<sub>6</sub>].
- 4) WAXS study of the local molecular structure of [hmim][PF<sub>6</sub>] and [bmpm][PF<sub>6</sub>].

##### 5.1.1 Interfacial Tension between ILs and Organic Solvents

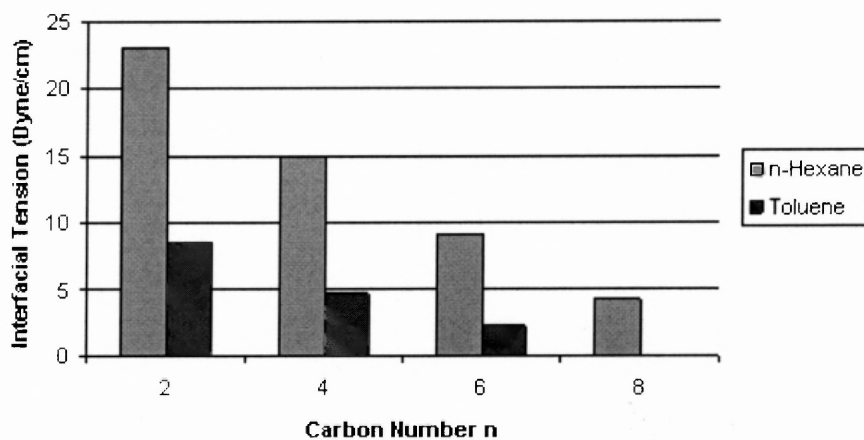
Figure 5.1 (a) shows the interfacial tensions between PF<sub>6</sub><sup>-</sup> based ILs and two organic solvents, n-hexane and toluene. It is observed that the interfacial tension decreases almost linearly with the increase of alkyl chain length, and the interfacial tension between the IL and n-hexane is

higher than the one between IL and toluene. Figure 5.1 (b) shows the interfacial tensions between  $\text{BF}_4^-$  based ILs and the organic solvents. The interfacial tension between  $[\text{omim}][\text{BF}_4]$  and toluene was not measured because of their partial miscibility. A similar trend was observed for the  $\text{BF}_4^-$  based ILs. For both types of ILs, the interfacial tensions between organic solvents and ionic liquids were found to be lower than the interfacial tension between water and the organic solvents, ranging from 1 to 25 dyne/cm. Detailed experimental data was summarized in Appendix A.

Law and Watson, 2001b used direct recoil spectroscopy (DRS) to measure the molecular orientation of  $[\text{C}_n\text{mim}][\text{BF}_4]$  ( $n=2\sim 8$ ) at the IL/air interface and concluded that longer alkyl chain substituents of 1-alkyl-3-methylimidazolium ILs result in an increased exposure of the methyl group to the IL/air interface and a lower surface tension. The same trend was also reported by Iimori et al., 2004 by sum frequency generation spectroscopy (SFG). Considering that non-polar n-hexane may resemble the air, a similar explanation based on the molecular orientation could be applied to our systems. Note that the interfacial tension between the ILs and toluene is lower than the one with n-hexane, which may result from the  $\pi$ - $\pi$  interaction between the toluene molecules and the imidazolium ring of the ILs that enhances the chemical affinity.



(a)



(b)

**Figure 5.1** Interfacial tensions between organic solvents and two series of ionic liquids: 1-alkyl-3-methylimidazolium hexafluorophosphates (a) and 1-alkyl-3-methylimidazolium tetrafluoroborates (b). The carbon number is pertaining to the one on the N-alkyl group.

### 5.1.2 Self-aggregations of ILs in Aqueous Solution/Organic Solvent Systems

In this subsection, the interfacial tension between IL aqueous solutions and n-hexane was measured to investigate molecular self-aggregation of ILs in an aqueous solution. Figure 5.2 depicts the interfacial tension against the molar concentration of three different IL aqueous solutions. Data are tabulated in Appendix B.

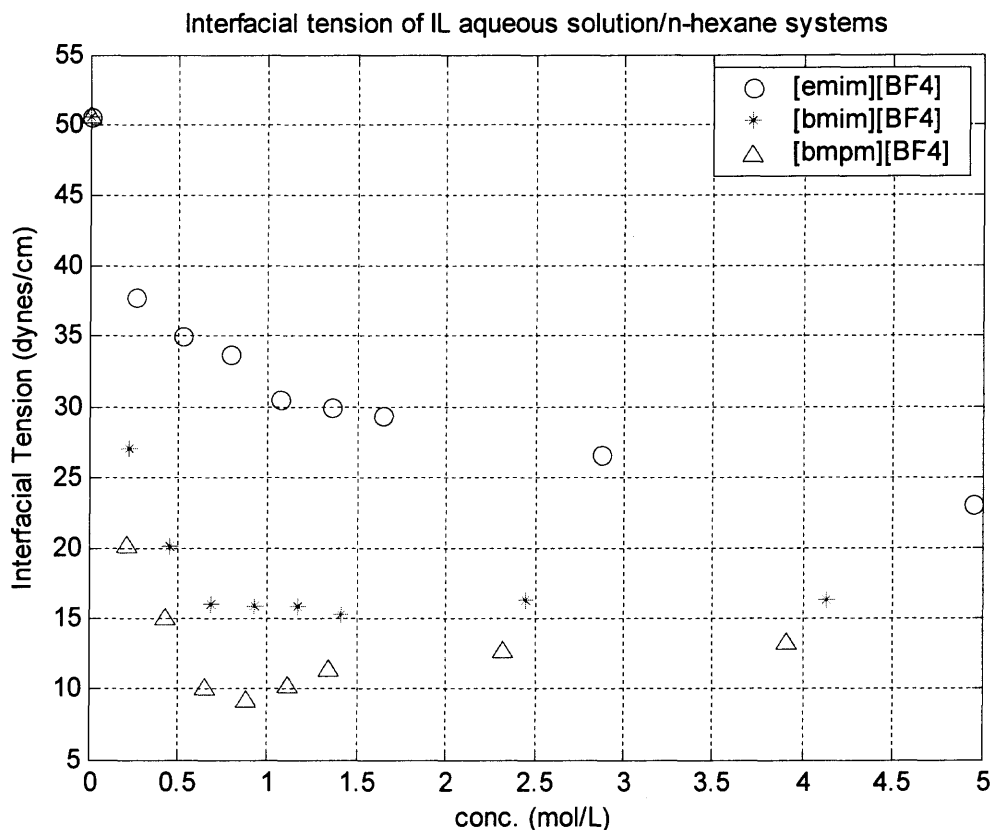


**Figure 5.2** IL aqueous solutions/n-hexane interfacial tensions under various IL concentrations in water solutions.

The measured water/n-hexane interfacial tension was 50.8 dynes/cm, in agreement with the reported value of 51.1 dynes/cm at 20°C (Weast et al., 1983). The measured interfacial tensions of the [emim][BF<sub>4</sub>]/n-hexane, [bmim][BF<sub>4</sub>]/n-hexane and [bmpm][BF<sub>4</sub>]/n-hexane were 23.0 dynes/cm, 15.0 dynes/cm and 12.7 dynes/cm, respectively.

As shown in Figure 5.2, the circle symbols stand for [emim][BF<sub>4</sub>] (n=2, imidazolium based) aqueous solution, while the data points marked with stars and triangles represent [bmim][BF<sub>4</sub>] (n=4, imidazolium based) aqueous solution and [bmpm][BF<sub>4</sub>] (n=4, pyridinium based) aqueous solution, respectively. In general, as the IL concentration increases, the interfacial tension decreases from the water/n-hexane interfacial tension ( $\gamma_{\infty}$ ) towards the value of pure IL/n-hexane interfacial tension ( $\gamma_0$ ). In the case of [bmim][BF<sub>4</sub>], the interfacial tension

decreases quickly as the concentration increases and then levels off at  $c=0.75\text{mol/L}$  to the value of  $\gamma_0$  (15.0 dynes/cm). This trend becomes more pronounced for the [bmpm][BF<sub>4</sub>] case where the interfacial tension exhibits a dip at  $c=0.9\text{mol/L}$  and then levels off to the value of  $\gamma_\infty$  (12.7 dynes/cm). For the [emim][BF<sub>4</sub>] case, the interfacial tension monotonically decreases with increasing IL concentration. This observation suggests the existence of a critical concentration for self-aggregation of IL molecules in aqueous solutions.

Bowers et al., 2004 reported the formation of IL aggregates in water by measuring surface tension, conductivity and as small angle neutron scattering (SANS). A critical aggregation concentration (CAC) of 0.8-1mol/L was identified for the [bmim][BF<sub>4</sub>] water solution. From SANS results and fitting for a core-shell model, it was suggested that the [bmim][BF<sub>4</sub>] aggregates could exhibit a spherical geometry with a core radius of  $\sim 10.5\text{\AA}$  and a shell thickness of  $6\sim 7\text{\AA}$ . In the present work, the critical aggregation concentration occurs at 0.75M for [bmim][BF<sub>4</sub>] aqueous solution and 0.9M for [bmpm][BF<sub>4</sub>] aqueous solution. The results agree well with the CAC reported by Bowers et al, 2004. Other methods such as small angle X-ray scattering (SAXS) and SANS can be used to probe the aggregates structure of the IL solution. Self aggregation of IL molecules in water was found only for those molecules with adequately long alkyl chains. No self aggregation was found for [emim][BF<sub>4</sub>] aqueous solution by interfacial tension measurement.

### 5.1.3 Self-aggregation of Ethanol in IL Solutions

The similar polarity of ethanol to the imidazolium-based ILs as shown in Table 2.4, as well as the amphiphilic nature of ILs, implicated a possibility of self-aggregates formation of the IL-ethanol system. Self-aggregation of ethanol in IL solutions was investigated by measuring



surface tension of the ethanol-IL solutions. The solutions were prepared by dissolving anhydrous ethanol in two types of ILs, [hmim][BF<sub>4</sub>] and [omim][BF<sub>4</sub>], at various concentrations. Figure 5.3 depicts the surface tension versus ethanol concentration in [hmim][BF<sub>4</sub>] (cross symbol) and [omim][BF<sub>4</sub>](oval symbol).

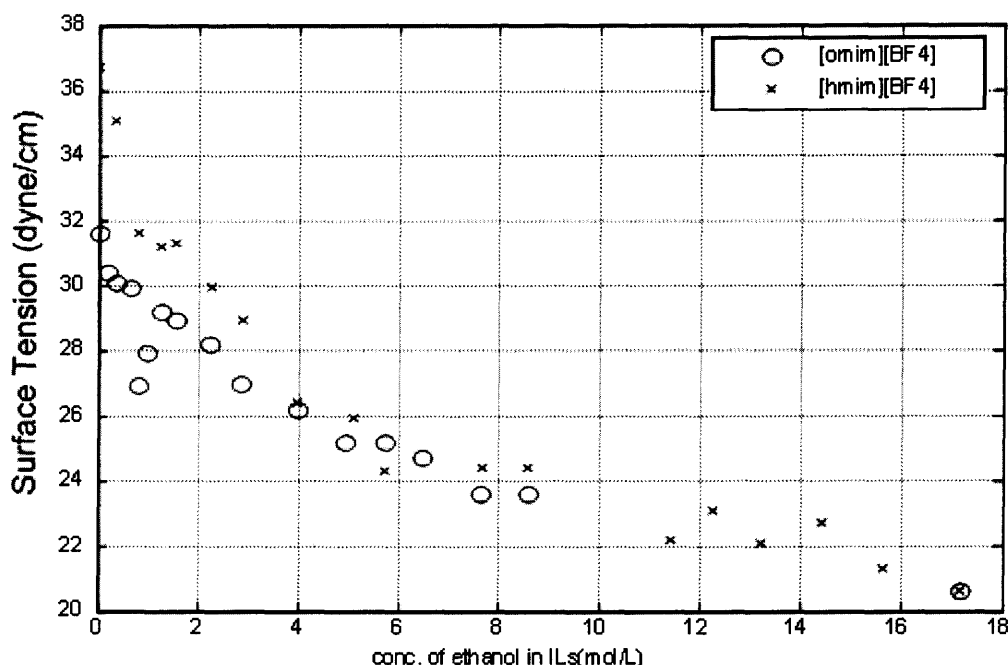


**Figure 5.3** Surface Tension vs. ethanol concentration in ethanol/IL inverse phase solution.

It is observed that for the ethanol-[hmim][BF<sub>4</sub>] system, the surface tension curve presents a shoulder at the ethanol concentration of ~1.2 M; while for the ethanol-[omim][BF<sub>4</sub>] case, an abrupt decrease of surface tension was found at ~0.8 M. These features implicate that ethanol molecules form self-aggregates in ILs. However, detailed structures of the aggregates are not known. One possibility is that the ethanol molecules form aggregation with hydroxyl groups residing at the outer surface of the aggregate surrounded by the anions. It is also noted from the data that ILs with longer alkyl chain can facilitate the self-aggregation of ethanol by

lowering the CAC. In any case, other characterization methods such as SANS with deuterated ethanol can be employed to investigate detailed structures of the aggregates.

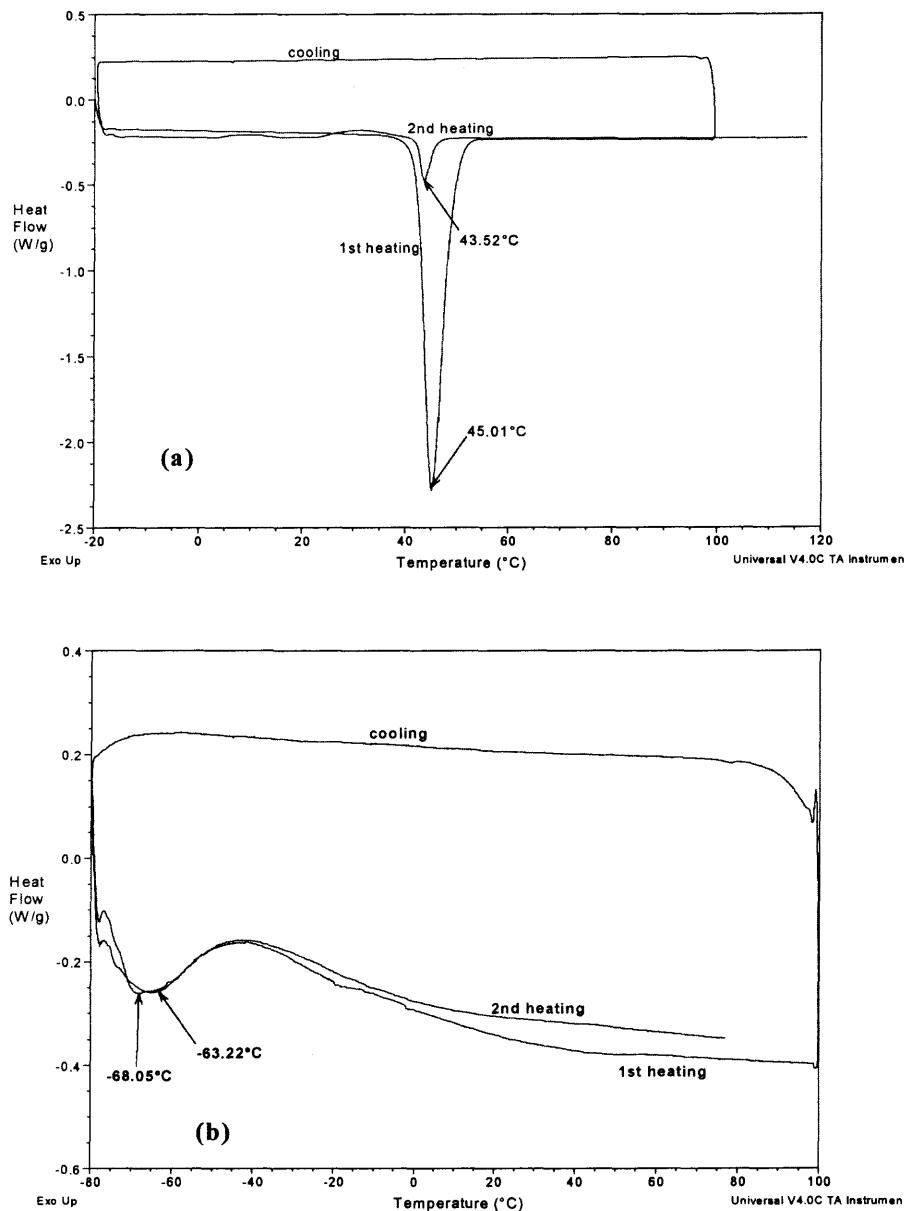
#### 5.1.4 Thermal Behavior of ILs

Figure 5.4 depicts the DSC study results by heating-cooling-heating cycle for two selected ionic liquids: [bmpm][PF<sub>6</sub>] and [hmim][PF<sub>6</sub>].

Figure 5.4 (a) shows a melting temperature ( $T_m$ ) of  $\sim 45^\circ\text{C}$  under the heating rate of  $10^\circ\text{C}/\text{min}$  for [bmpm][PF<sub>6</sub>], which is consistent with the value provided by the Sigma-Aldrich MSDS data. However, there is no crystallization peak found on cooling for [bmpm][PF<sub>6</sub>] under the testing cooling rate. Figure 5.4 (b) shows a  $T_m$  of  $\sim 65^\circ\text{C}$  for [hmim][PF<sub>6</sub>] at the heating rate of  $10^\circ\text{C}/\text{min}$ . The measured  $T_m$  agrees quite well with the literature value of  $-61^\circ\text{C}$  reported by Huddleston et al., 2001. Again, no crystallization peaks were observed upon cooling process.

This glassy supercooling behavior is well known as reported by Holbrey and Seddon, 1999 for tetrafluoroborate ionic liquids at the same cooling rate. The phenomena could be ascribed to the highly asymmetrical structure of ionic liquids, reducing the lattice energies and disrupting the packing efficiencies. Recently, Cadena et al., 2005 reported simulations of the relaxation of ILs, indicating that the typical relaxation time for rotational and translational motion of ILs is in the order of several nanoseconds, which is much slower than simple fluids, normally in the order of pico-seconds. The extended molecular correlations and low mobility can hinder the ordered packing of IL molecules and lead to the glass state. The enthalpy change of melting was not measured due to the lack of information of the original crystallinity.

However, the decrease of the heat of fusion on the second heating cycle reveals the decrease of crystallinity after the first cooling.



**Figure 5.4** DSC study results of ionic liquids: (a) [bmpm][PF<sub>6</sub>]; (b) [hmim][PF<sub>6</sub>]. (Test performed by heating-cooling-heating cycle, heating rate is 10°C/min, cooling rate is 5°C/min)

### 5.1.5 WAXS Study of the Structures of ILs

Figure 5.5 shows the scattering intensity ( $I$ ) versus scattering vector ( $Q$ ) for two selected ILs, [hmim][PF<sub>6</sub>] at 25°C and [bmpm][PF<sub>6</sub>] at 50°C. The two peaks at  $\sim 0.95 \text{ \AA}^{-1}$  and  $\sim 1.37 \text{ \AA}^{-1}$  for [hmim][PF<sub>6</sub>] correspond to the length scale of 6.6 Å and 4.58 Å. The same correlation distances were found for [bmpm][PF<sub>6</sub>]. These peaks revealed the local structures and the correlations among IL molecules. Morrow and Maginn, 2002 have computed the center-of-mass radial distance functions (RDF) on [bmim][PF<sub>6</sub>]. It was found that the first solvation shell of cation-anion ion pairs occurs at 4.3 Å at 298K, while the first peak for cation-cation RDF and anion-anion RDF occur at 8 Å and 6.5 Å, respectively. A similar correlation distance of 4.5 Å was reported by Hardacre et al., 2003 who studied the liquid structure of dimethylimidazolium chloride ([dmim][Cl]) via neutron diffraction. The WAXS results presented here are quite consistent with the simulation results and previous experimental work. Therefore, the short-range order could be attributed to the solvation shell formed between ion pairs. The correlation distance of 4.58 Å for both ILs can be originated from the [hmim]<sup>+</sup>-[PF<sub>6</sub>]<sup>-</sup> solvation shell and [bmpm]<sup>+</sup>-[PF<sub>6</sub>]<sup>-</sup> solvation shell. The correlation distance of 6.6 Å exhibited by both ILs can be attributed to the solvation shell of the [PF<sub>6</sub>]<sup>-</sup>-[PF<sub>6</sub>]<sup>-</sup> ion pairs. The WAXS results in the current work, as well as the previous works mentioned above, suggested that ILs are a class of highly self-organized fluids with extended local molecular ordering.

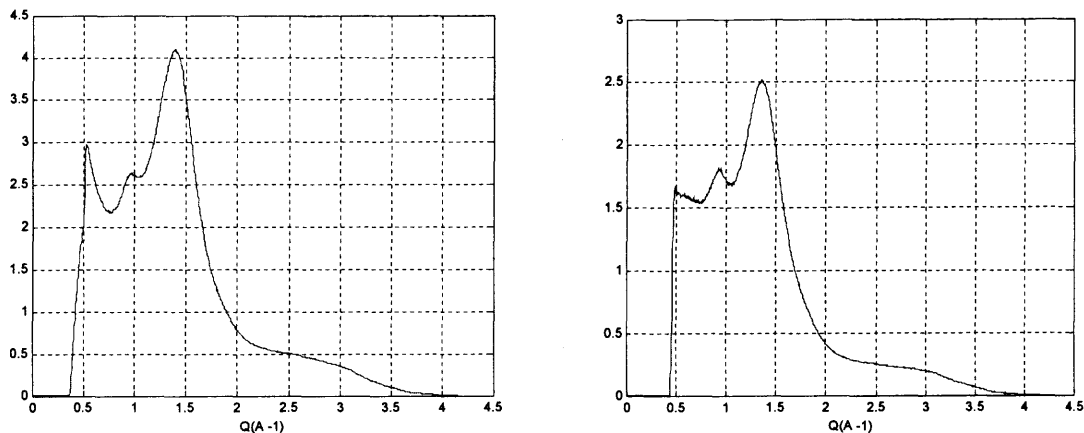


**Figure 5.5** WAXS data of [hmim][PF<sub>6</sub>] at 20°C (Left) and [bmpm][PF<sub>6</sub>] at 50°C (Right). (The y axis is scattering intensity in arbitrary unit)

## 5.2 Synthesis of Polyurea at IL/n-hexane Interface

In this section, we report a systematic study of polyurea synthesis via interfacial polymerization between a n-hexane phase and an IL phase. The effect of ILs on the chemical composition and reaction conversion of the final polymer products were studied by comparing the results with the polyurea synthesized in a water/n-hexane system. The morphology of the synthesized polymer was examined by scanning electron microscopy (SEM). SAXS and XRD were used to study the molecular structures of polyurea.

### 5.2.1 Reaction Conversion

The reaction conversion was determined at room temperature, with a reaction time of 1 hour. Under the same reaction conditions, Table 5.1 shows the conversions of the samples of Group 1, Group 2 and Group 3 (See sample details in Section 4.3). In Group 1, the conversions of polyurea prepared in [C<sub>n</sub>mim][BF<sub>4</sub>] from EDA and TDI increased remarkably compared to the polyurea synthesized at the water/n-hexane interface (PUA-0). It can be seen that the

conversion rate increases with the alkyl chain length of  $[C_n\text{mim}][\text{BF}_4]$ . In Group 2, all the polyurea synthesized from BDA and TDI also exhibit higher conversions than the one synthesized at the water/n-hexane interface (PUA-B0). However, no strong correlation was observed between the alkyl chain length and conversion for this group. In Group 3, a decrease of conversion with ascending alkyl chain length of  $\text{PF}_6^-$  based ILs was found. Most of the samples showed higher conversion than their water/n-hexane counterpart, except PUA-P6B. These results clearly demonstrated the enhancement of IP conversion by using IL as a reaction medium. Also, the replacement of water with ILs eliminated possible reaction of TDI with water, and thus increased the overall reaction conversion.

Since interfacial polymerization is a diffusion-controlled reaction, lower conversions represent a thicker diffusion barrier for reaction which prevents the polymerization from proceeding further. The diffusion barrier could largely depend on the morphology of the polymer and the ILs used for the reaction, including the alkyl chain lengths and anions, etc. An investigation of the polymer surface morphology can give more lucid information to understand the reaction conversion results presented here.

**Table 5.1** Reaction conversion of the polyureas synthesized with ILs

<b>Sample Group</b>	<b>Sample Name</b>	<b>Conversion (%)</b>
<b>GROUP 1</b>	PUA-0	22.3
	PUA-B2E	33.3
	PUA-B4E	44.0
	PUA-B6E	62.9
	PUA-B8E	75.3
<b>GROUP 2</b>	PUA-B0	22.0
	PUA-B2B	42.7
	PUA-B4B	39.5
	PUA-B6B	40.4
	PUA-B8B	23.5
<b>GROUP 3</b>	PUA-P4E	37.1
	PUA-P6E	27.5
	PUA-P4B	36.2
	PUA-P6B	14.6

### 5.2.2 FTIR Analysis

FTIR spectra of neat [bmim][BF<sub>4</sub>], polyurea synthesized at the water-hexane interface, PUA-B4E and PUA-B8E are depicted in Figure 5.6 in order to compare the chemical structures of polyurea prepared in different systems. The spectra (a) and (b) depict the IR results of neat [bmim][BF<sub>4</sub>] and polyurea synthesized at the water/n-hexane interface, respectively. Spectra (c) and (d) show the IR results of PUA-B4E and PUA-B8E prepared at the interface of n-hexane/[bmim][BF<sub>4</sub>] and n-hexane/[omim][BF<sub>4</sub>], respectively.

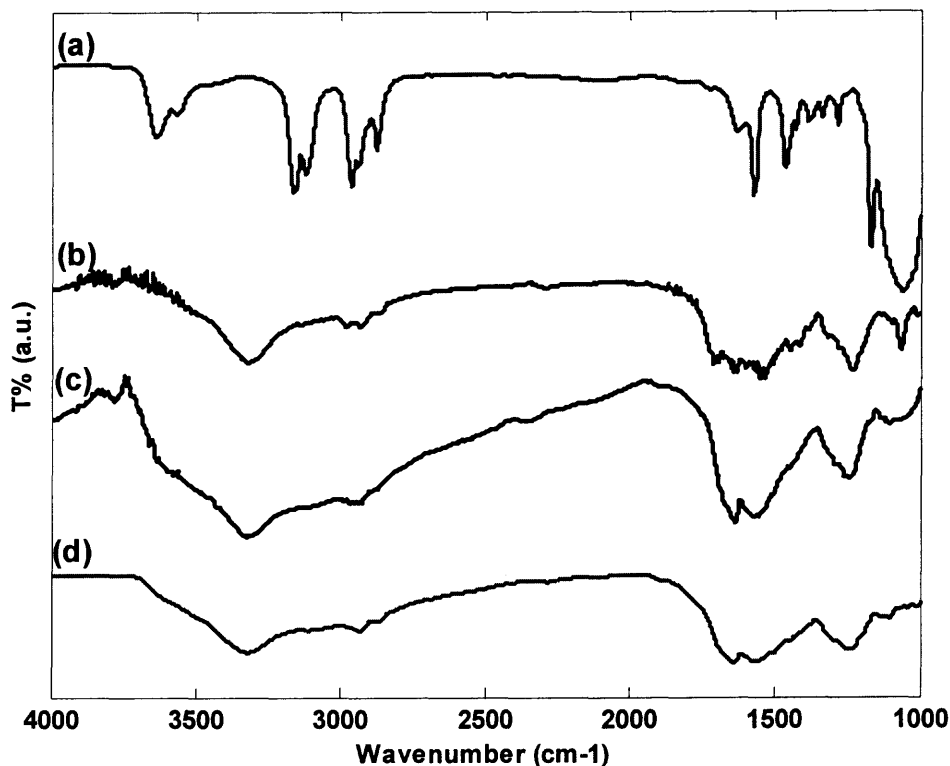


**Figure 5.6** FTIR spectra of neat ionic liquid and typical polyurea samples by interfacial polymerization: (a) [bmim][BF<sub>4</sub>]; (b) PUA-0; (c) PUA-B4E; (d) PUA-B8E.

It is shown that the polyurea samples exhibited the same features in FTIR spectra (b), (c) and (d). The main  $\text{-NH-}$  stretching peak at  $3280\text{--}3300\text{ cm}^{-1}$  and the carbonyl bonding peak at  $\sim 1600\text{ cm}^{-1}$  indicate the existence of strong linkages of  $\text{-CO-NH-}$  in all the samples, the essential structure of polyurea. On the other hand, the  $\nu_{\text{C-H}}$  peak between  $3200$  and  $3050\text{ cm}^{-1}$  observed in spectrum (a), which denotes the C-H stretching vibration of the imidazolium ring, has disappeared in spectrum (c) and (d), indicating the complete removal of the ionic liquids from the final polymer products (Szymanski and Erickson, 1970). The FTIR results indicate that there is no significant difference in the composition of polyurea synthesized in various IL phases or in aqueous phase. The results also demonstrate that the difference in morphological



features exhibited by the polymer, which will be discussed in detail in this dissertation work, is not due to the chemical difference but the role of ILs in the kinetics of phase separation.

### 5.2.3 Thermal Analysis

Thermal analysis of the polyurea was conducted by using differential scanning calorimetry (DSC) under the heating rate of 5°C/min. Figure 5.7 depicted DSC results of two typical samples prepared at the IL/n-hexane interface, PUA-B4B and PUA-B8B. A thermal decomposition temperature of 241.44°C was found for the PUA-B4B case and 255.56°C for the PUA-B8B case. The glass transition temperatures of 69.52°C for PUA-B4B and 61.21°C for PUA-B8B, agree quite well with the ones of regular polyurea reported in the literature, which ranges from 45~65°C depending on the monomers (Brandrup et al., 1985). Mark et al., 1985 reported that aromatic polyureas have a melting temperature ranging from 290-320°C, which is largely dependent on the molecular weight of the polyurea. In the present work, the melting temperature of the polyureas could not be identified from the DSC results, probably because the melting temperature is close to the thermal decomposition point.

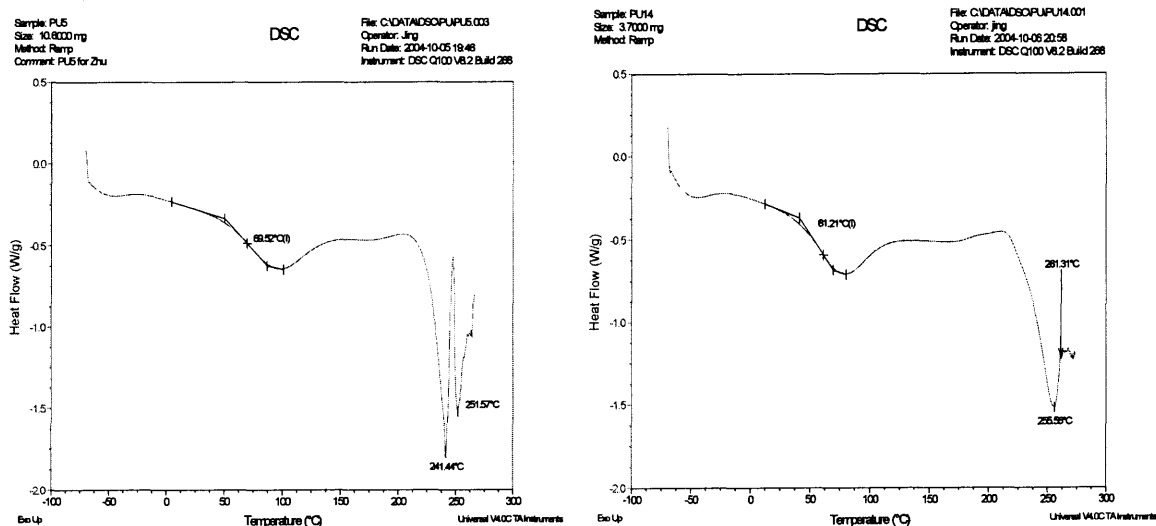


**Figure 5.7** DSC study results of PUA-B4B (left) and PUA-B8B (right) under the heating rate of 5°C/min.

## 5.2.4 Surface Morphology

SEM was performed to examine the surface morphology for all the polyurea samples prepared.

### 5.2.4.1 Polyureas Synthesized from Ethylene Diamine in $[C_n\text{mim}][\text{BF}_4]$ Ionic Liquids

The SEM pictures of PUA-0 are presented in Figure 5.8 for comparison. Dense agglomerates without any porous structures were found in the PUA-0 case. Figure 5.9 shows the SEM micrographs of the polyurea samples prepared with  $[C_n\text{mim}][\text{BF}_4]$  from ethylene diamine. The polyurea synthesized from EDA in short carbon-chain ionic liquids exhibit nanofibrous structure with primary sizes around 50~100nm. These primary particles form interconnected porous agglomerates with pore size ~1 $\mu\text{m}$ . When the carbon number on alkyl chain of ILs increases to 6 and 8, interconnected alveolate structures with pore size from 200~500nm were observed.

From the SEM images, it is found that the polymers form primary fiber-like structures with sizes around 50-100 nm. No significant difference in the primary structures was observed

for samples prepared with ILs of various alkyl chain lengths. However, in the case of [omim][BF<sub>4</sub>] (n=8), a clear feature of bicontinuous interconnected structures was observed. As described in Section 5.2.1, the reaction conversions for this group were found to increase with the alkyl chain length of the IL used. The more pronounced porous structures with increasing alkyl chain length may reduce the diffusion barrier at the interface, rendering increasing reaction conversions.

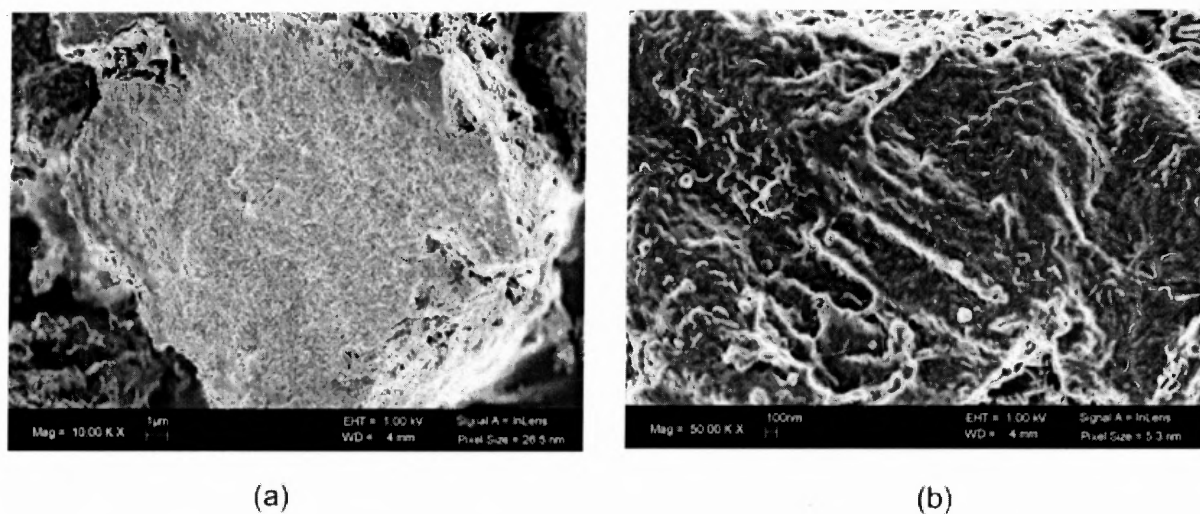


**Figure 5.8** SEM images of regular polyurea synthesized at water/n-hexane interface: (a) 10,000X; (b) 50,000X.

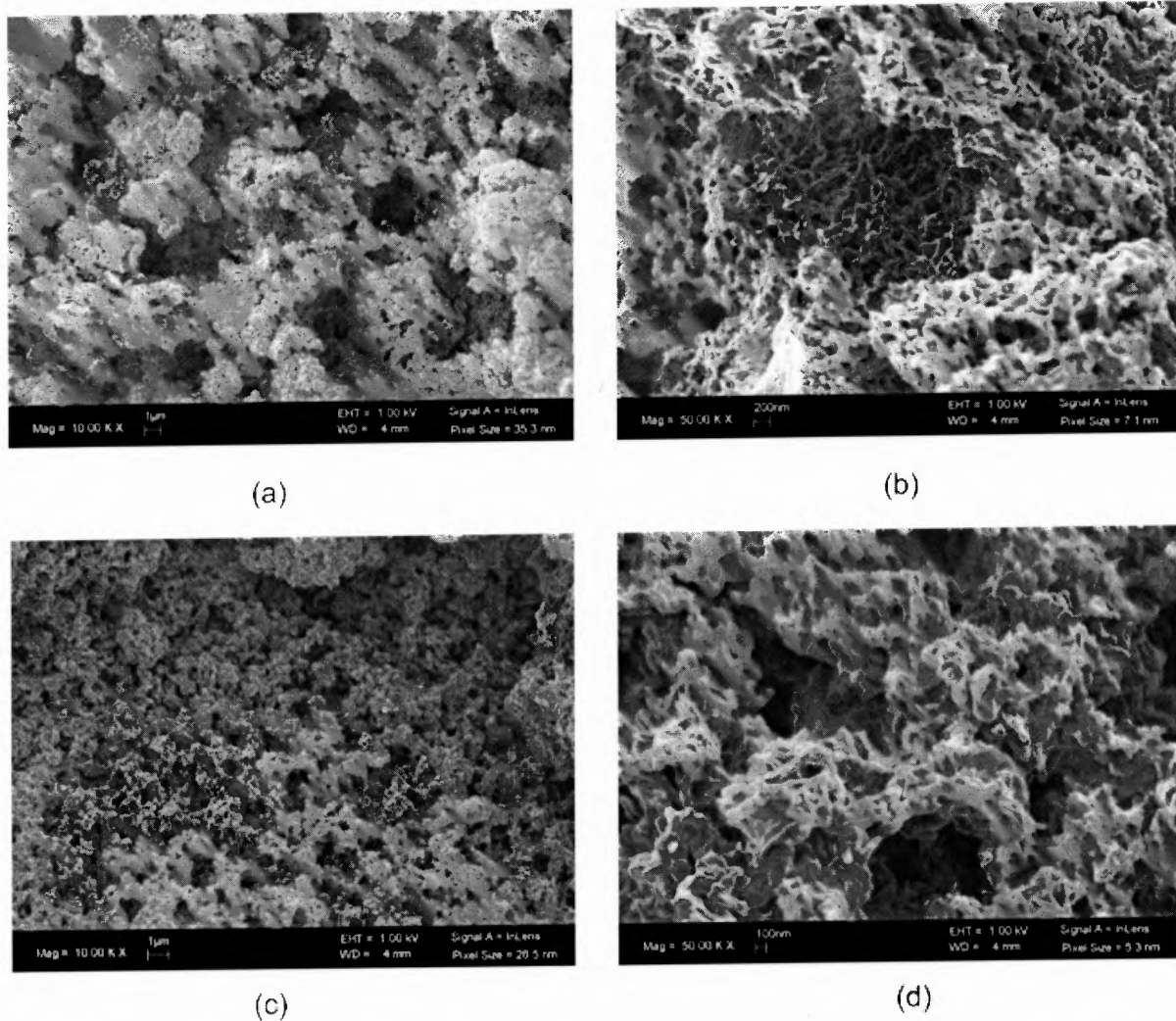


**Figure 5.9** Scanning Electron Microscopy (SEM) images of the polyureas synthesized from ethylene diamine in  $[C_n\text{mim}][\text{BF}_4]$  ionic liquids: (a) PUA-B2E (10,000X); (b) PUA-B2E (50,000X); (c) PUA-B4E (10,000X); (d) PUA-B4E (50,000X).

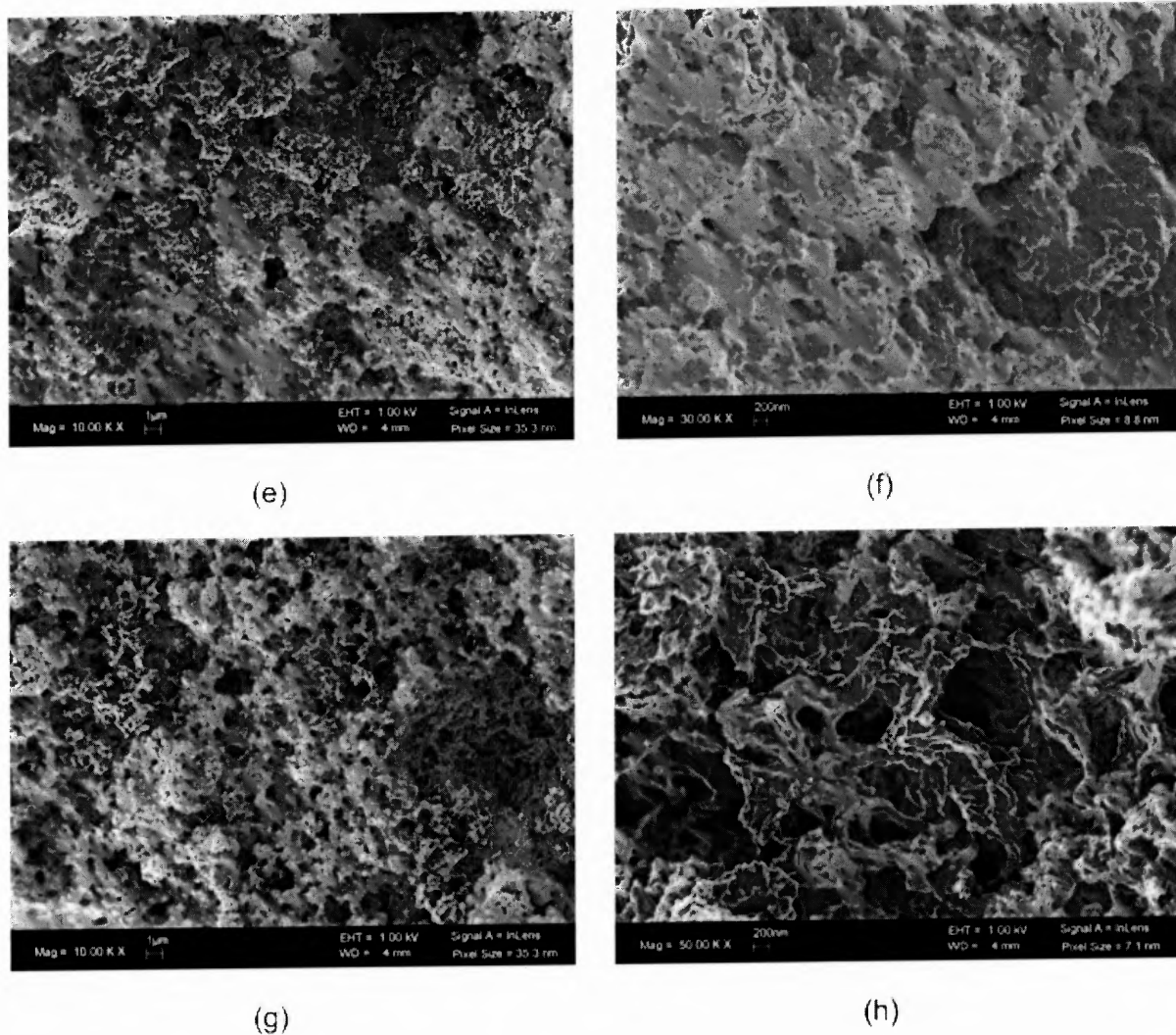


**Figure 5.9 (Cont'd)** Scanning Electron Microscopy (SEM) images of the polyureas synthesized from ethylene diamine in  $[C_n\text{mim}][\text{BF}_4]$  ionic liquids: (e) PUA-B6E (10,000X); (f) PUA-B6E (50,000X); (g) PUA-B8E (10,000X); (h) PUA-B8E (50,000X).

**5.2.4.2 Polyureas Synthesized from 1,4-diaminobutane (BDA) in  $[C_n\text{mim}][\text{BF}_4]$**  The SEM images of polyureas prepared from BDA in  $[C_n\text{mim}][\text{BF}_4]$  are displayed in Figure 5.10. All the four samples show consistent interconnected alveolate structures with sizes about 100~200nm. These porous structures are comprised of fiber-like or rod-like primary structures with sizes around 100 nm. There is no significant difference in the surface morphologies by

varying the alkyl chain lengths of the cations. Compared to Group 1, which was synthesized from EDA and TDI, this group shows more pronounced porous structures on the polymer surface, probably due to a longer aliphatic chain of the diamine used in this case. Considering the nature of diffusion-controlled polymerization, porous structures will enhance the diffusion of reactants to the reaction site and improve the overall reaction conversion. Therefore, the observed surface morphology are consistent with the increase of reaction conversion as mentioned earlier.

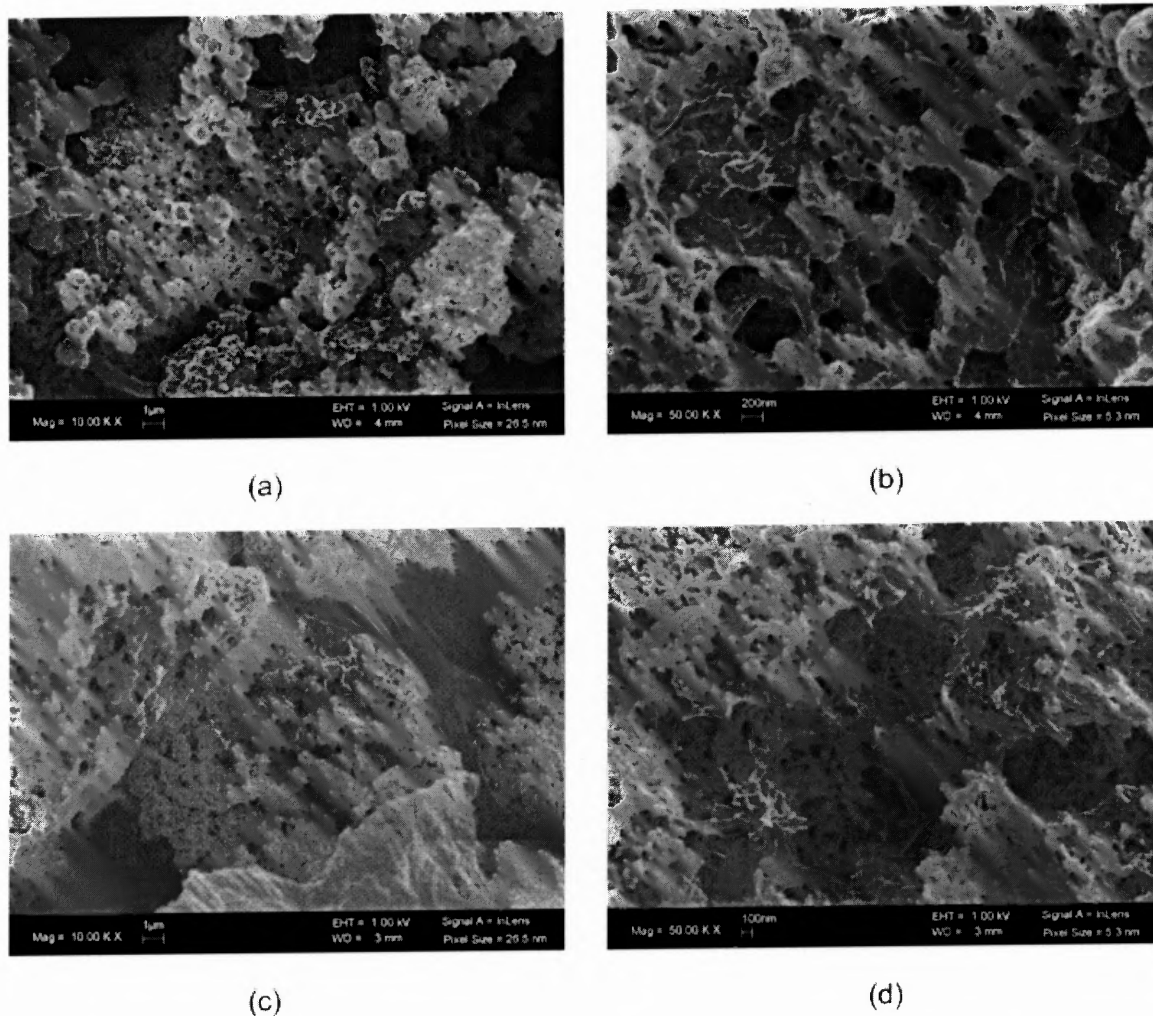


**Figure 5.10** Scanning Electron Microscopy (SEM) images of the polyureas synthesized from 1,4-diaminobutane in  $[C_n\text{mim}][\text{BF}_4]$  ionic liquids: (a) PUA-B2B (10,000X); (b) PUA-B2B (50,000X); (c) PUA-B4B (10,000X); (d) PUA-B4B (50,000X).

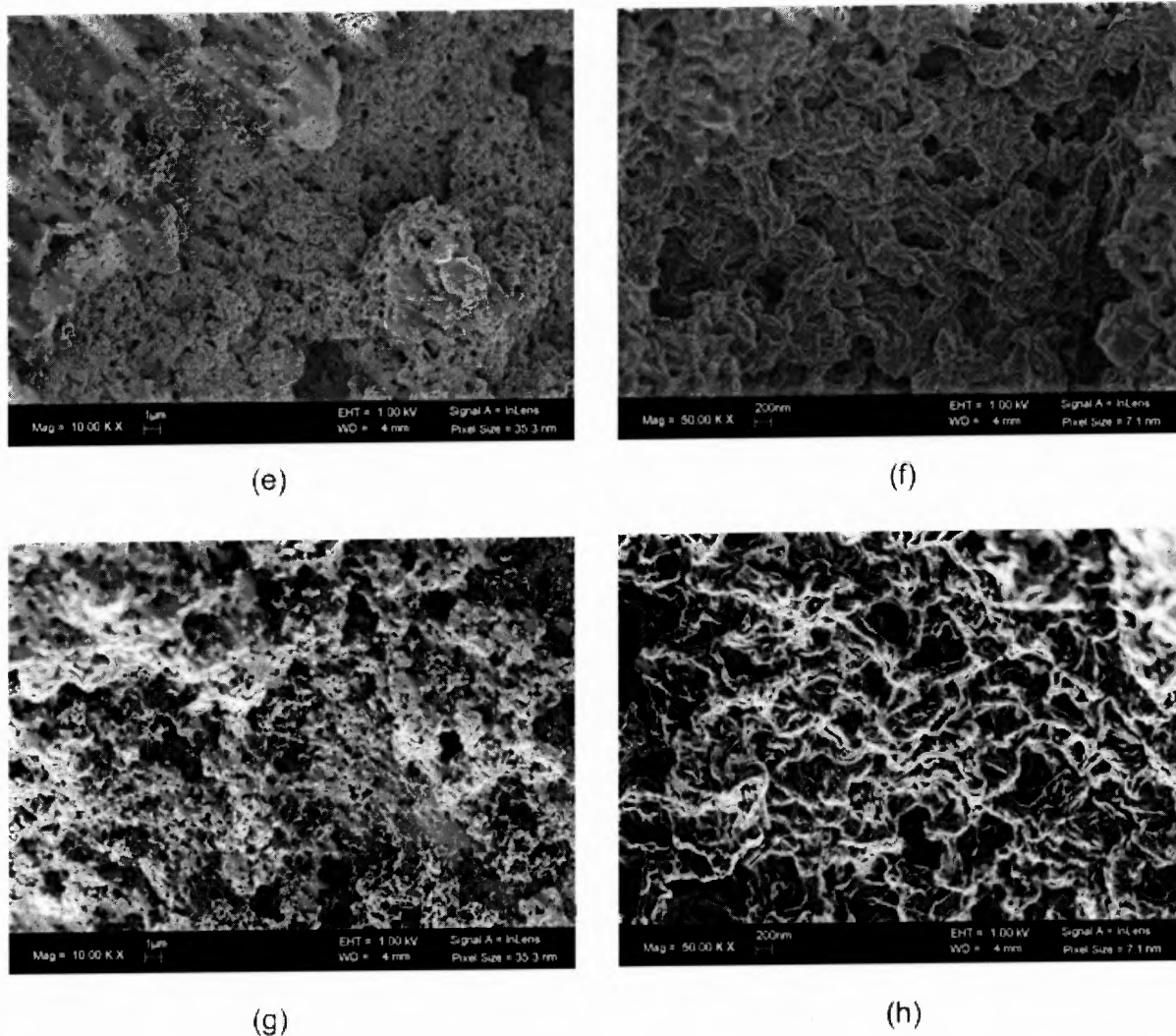


**Figure 5.10 (Cont'd)** Scanning Electron Microscopy (SEM) images of the polyureas synthesized from 1,4-diaminobutane in  $[C_n\text{mim}][\text{BF}_4]$  ionic liquids: (e) PUA-B6B (10,000X); (f) PUA-B6B (50,000X); (g) PUA-B8B (10,000X); (h) PUA-B8B (50,000X).

**5.2.4.3 Polyureas Synthesized from Ethylene Diamine (EDA) in  $[C_n\text{mim}][\text{PF}_6]$**  Figure 5.11 shows the surface morphology of polyurea synthesized from EDA and TDI in  $[C_n\text{mim}][\text{PF}_6]$ . A reef-like network structure with open pores of 100~200 nm was found on the PUA-P4E (EDA+TDI,  $[C_4\text{mim}][\text{PF}_6]$ ) surface. Its counterpart prepared in the  $[\text{BF}_4^-]$  based ILs, PUA-B4E (EDA+TDI,  $[C_4\text{mim}][\text{BF}_4^-]$ ) shows nanofibrous structure aggregates without exhibiting apparent porosity (See Figure 5.9 (c) and (d)). A volcano-like structure was

observed at the PUA-P6E (EDA+TDI,  $[C_6\text{mim}][PF_6]$ ) surface. Meanwhile, only slightly porous surface morphology was observed for its counterpart prepared in the  $[BF_4^-]$  based ILs, PUA-B6E (EDA+TDI,  $[C_6\text{mim}][BF_4]$ ) (See Figure 5.9 (e) and (f)). The results implicate that the anion of ILs also play an important role in the formation of the surface structures.

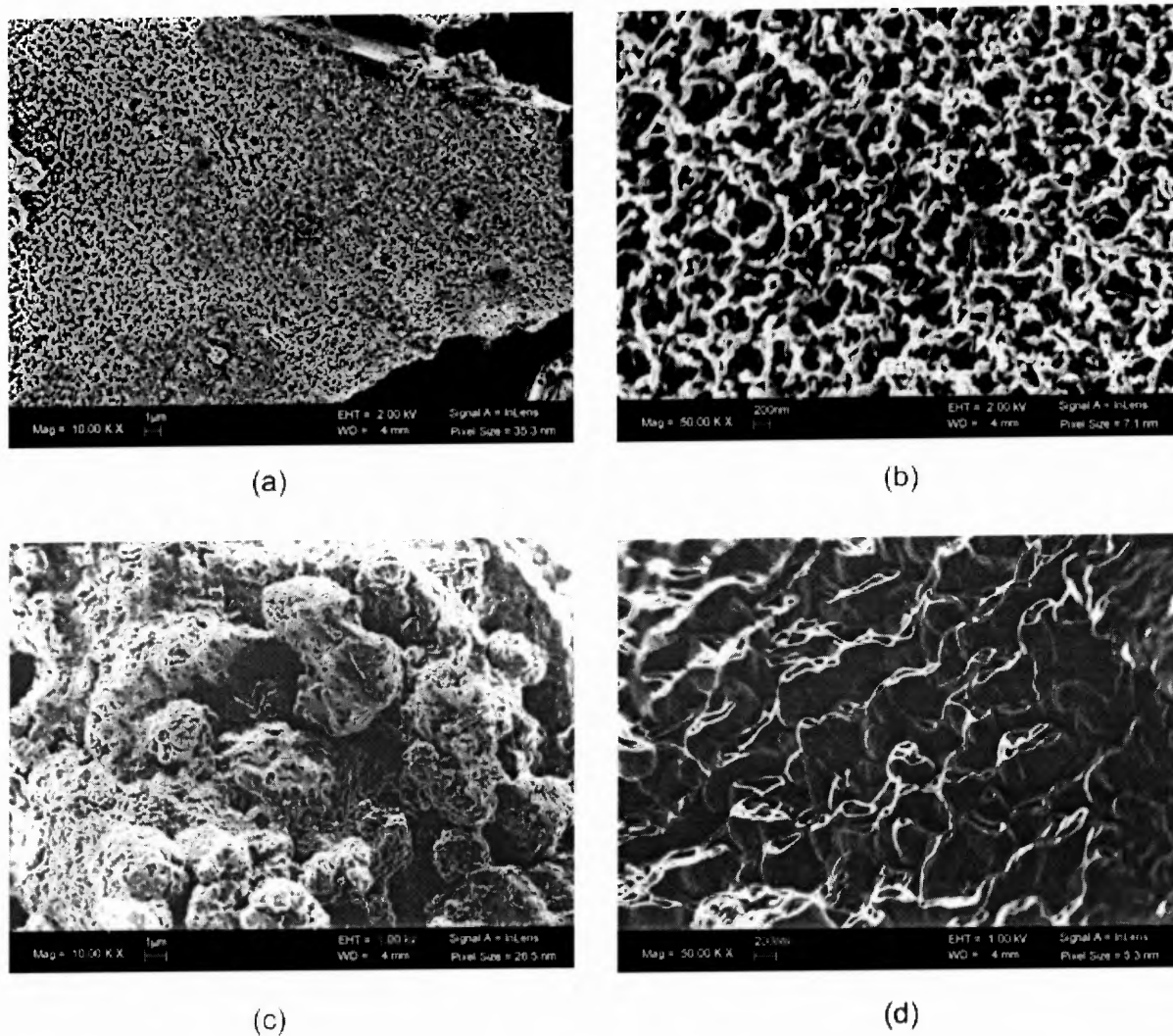


**Figure 5.11** Scanning Electron Microscopy (SEM) images of the polyureas synthesized in  $[C_n\text{mim}][PF_6]$  ionic liquids: (a) PUA-P4E (10,000X); (b) PUA-P4E (50,000X); (c) PUA-P6E (10,000X); (d) PUA-P6E (50,000X).



**5.2.4.4 Summary of surface morphologies** Table 5.2 shows the comparison of the polyureas prepared with various ILs. In brief, ionic liquids can be used as a medium of interfacial polymerization to fabricate porous polymeric films. In this particular study, different types of surface structures such as nanofibrils and interconnected nanopores with sizes ranging from 50-500nm, were produced by varying either the cations or anions part of ionic liquids. The microscopic structures of the polyurea that could affect the observed morphology, were probed by SAXS and XRD in more detail in the following two subsections.

**Table 5.2** Summary of surface morphology of polyurea synthesized in ionic liquids

Alkyl Chain length of ILs	No ILs	[emim][BF <sub>4</sub> ] (C <sub>n</sub> =2)	[bmim][BF <sub>4</sub> ] (C <sub>n</sub> =4)	[hmim][BF <sub>4</sub> ] (C <sub>n</sub> =6)	[omim][BF <sub>4</sub> ] (C <sub>n</sub> =8)	[bmim][PF <sub>6</sub> ] (C <sub>n</sub> =4)	[hmim][PF <sub>6</sub> ] (C <sub>n</sub> =6)
<b>TDI + Ethylene diamine</b>	Flat non-porous surface	Coral-like nanoporous structure	Nanofibrous structure	Slightly porous structure	Alveolate structure	Nanoporous network	Volcano-like structure
<b>TDI +1,4-diaminobutane</b>	Flat non-porous surface	Alveolate structure	Alveolate structure	Alveolate structure	Alveolate structure	Nanosphere structure	Nanofibrous structure

### 5.2.5 Results by Small Angle X-ray Scattering (SAXS)

Figure 5.10 shows the SAXS results of typical polyurea samples synthesized in [C<sub>n</sub>mim][BF<sub>4</sub>] via interfacial polymerization. Figure 5.12 (a) presents the scattering intensity (I)-scattering vector (Q) plot for PUA-B2E (n=2), with a shoulder observed at Q=0.030Å<sup>-1</sup>, indicating a characteristic length of 20.9nm. Figure 5.12 (b) presents the I-Q curve for PUA-B4E (n=4), shows a shoulder at Q=0.030 Å<sup>-1</sup>. Figure 5.12 (c) shows the I-Q curve for PUA-B8E (n=8); a more evident peak at Q=0.032 Å<sup>-1</sup> is observed, indicating a correlation length of 19.6 nm.

Figure 5.12 (d) presents the I-Q curve for PUA-B8B ( $n=8$ , synthesized from BDA). A shoulder is found at  $Q=0.028 \text{ \AA}^{-1}$ , which represents a correlation length of 22.4 nm.

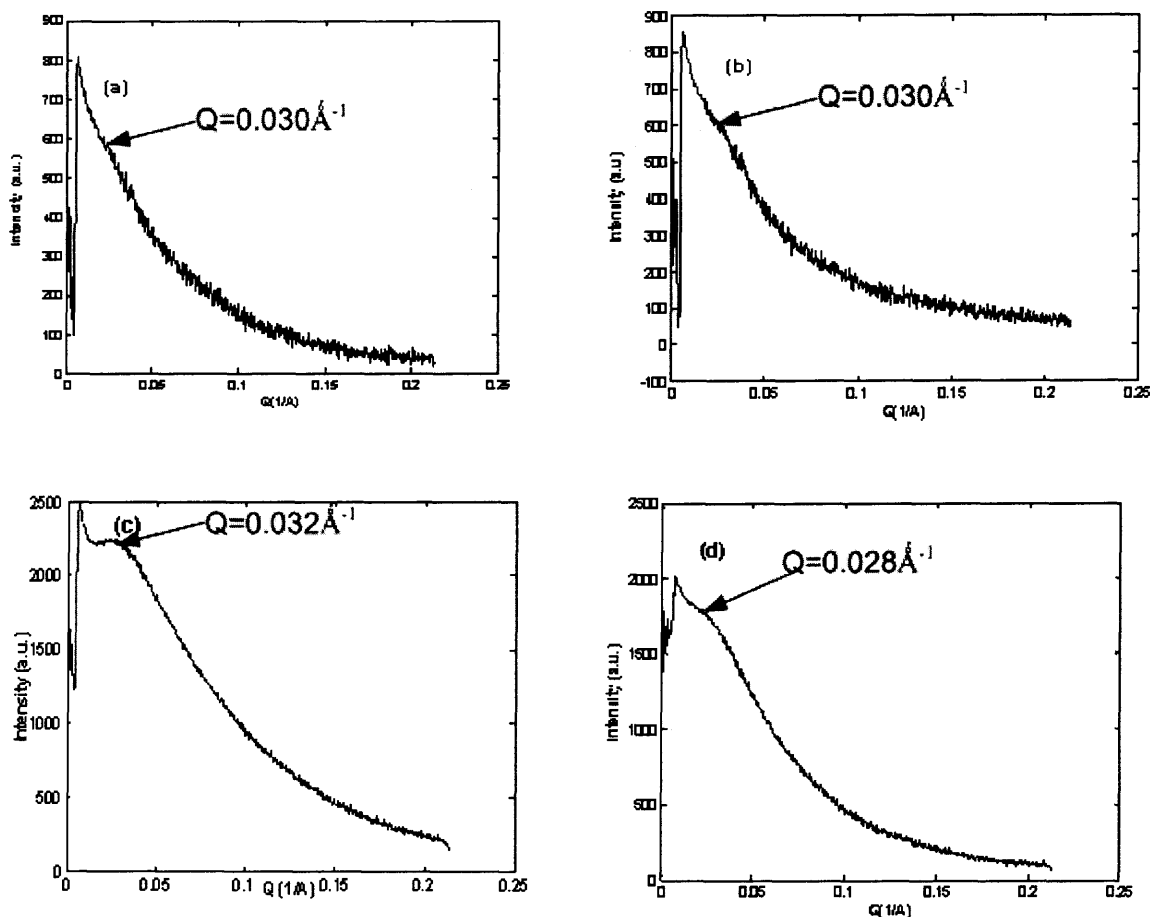
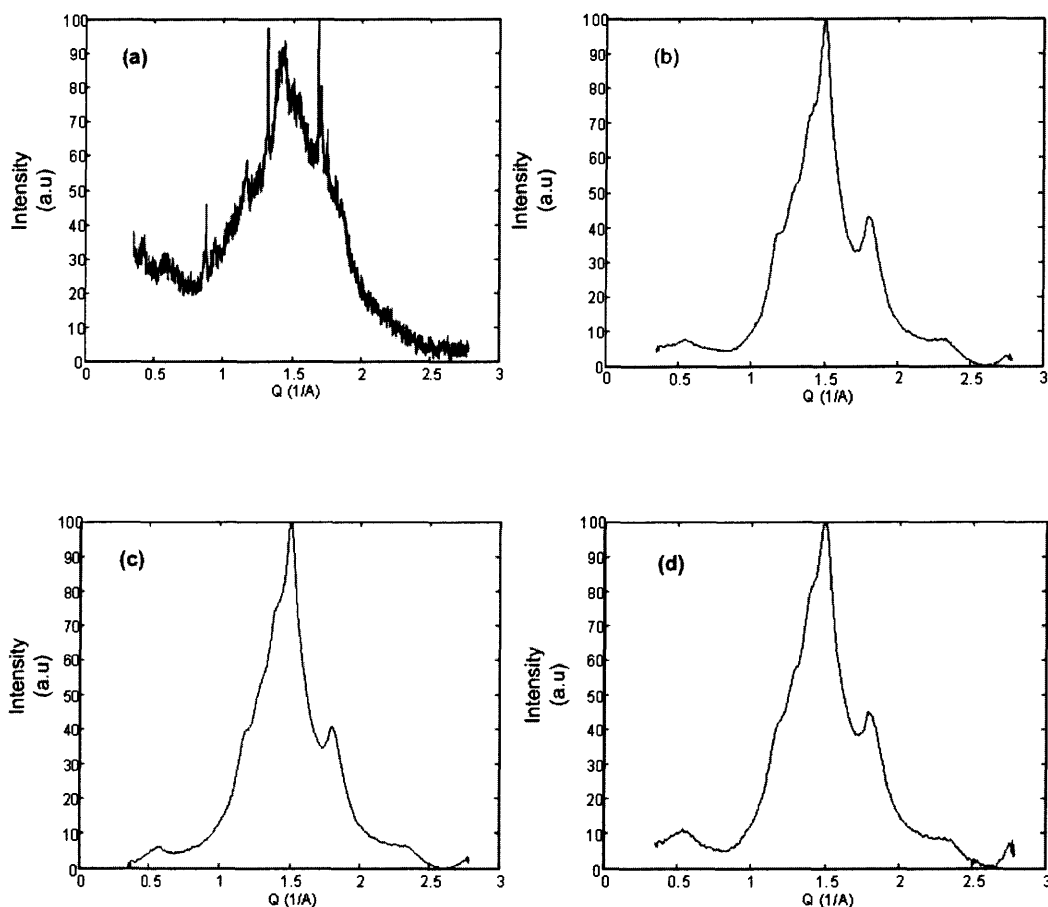


**Figure 5.12** SAXS results of the polyurea synthesized by IP in ILs: (a) PUA-B2E; (b) PUA-B4E; (c) PUA-B8E; (d) PUA-B8B.

The correlation distance of  $\sim 20\text{nm}$  observed by all four samples could be ascribed to either the lamellar spacing of the crystalline structure in polyurea or small crystallites formed via polymerization induced precipitation. However, no primary structures with this size were found under SEM as presented in Section 5.2.4. It is thus suggested that the correlation length could be originated from the spacing distance between the lamellar layers formed in the polyurea.

### 5.2.6 X-ray Diffraction Measurement

The crystalline structures of polyurea samples as well as the effect of ILs on the polymer crystallization were probed by powder X-ray diffraction (XRD). XRD data of polyurea synthesized from EDA at the water/n-hexane interface and a series of polyurea synthesized from EDA with  $[C_n\text{mim}][\text{BF}_4]$  were plotted in Figure 5.13, where *Intensity* stands for the diffraction intensity and  $Q$  denotes the scattering vector, which is inversely proportional to the  $d$  spacing according to Eq. (4.3).



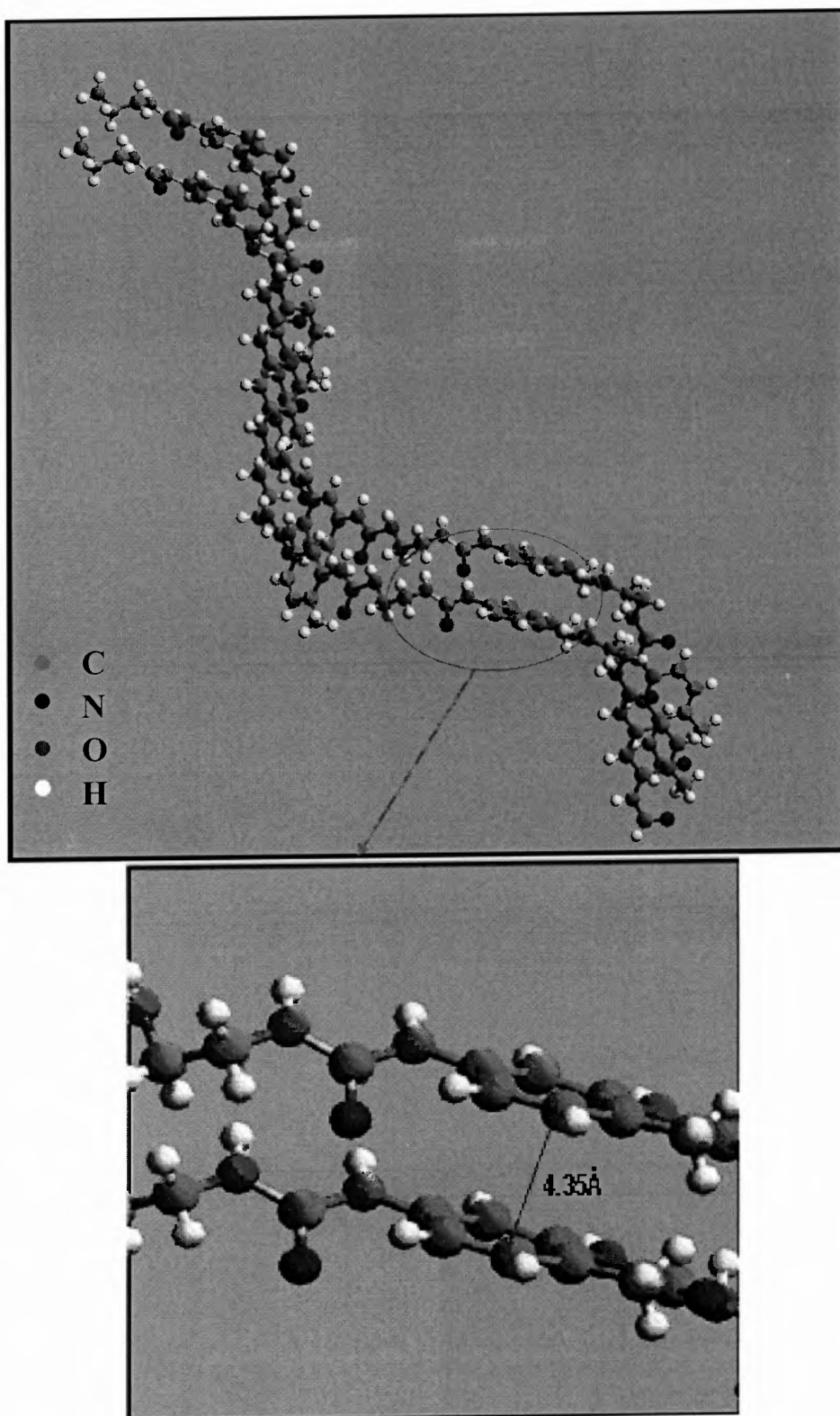
**Figure 5.13** XRD patterns of the polyureas synthesized by IP in ILs: (a) PUA-0 (regular polyurea); (b) PUA-B2E; (c) PUA-B4E; (d) PUA-B8E.

Figure 5.13 (a) presents the diffraction patterns of the polyurea synthesized at the water/n-hexane interface, showing a number of Bragg peaks in the range of  $Q=1-2 \text{ \AA}^{-1}$ . Figure

5.13 (b) presents the XRD pattern of PUA-B2E (n=2). Compared to Figure 5.13 (a), many Bragg peaks were suppressed in Figure 5.13 (b); however a major peak located at  $Q=1.42 \text{ \AA}^{-1}$ , indicating that the characteristic distance of  $4.35 \text{ \AA}$  remains the same. Figure 5.13 (c) and (d) present the XRD pattern of PUA-B4E (n=4) and PUA-B8E (n=8), respectively. Both patterns exhibited the same feature as in PUA-B2E, with a major peak at  $Q=1.42 \text{ \AA}^{-1}$ .

Ishihara et al., 1983 and Hong et al., 2000 studied the crystalline structures of polyurea and reported that the major peak resembles the intermolecular distance of  $4.35\sim 4.44 \text{ \AA}$  between the urea-ring planes on the two neighboring polyurea chains. A scheme of molecular structures reproduced by Cerius II<sup>®</sup> is used to depict the conformation of two neighboring polyurea chains as shown in Figure 5.14. The  $\pi$ - $\pi$  stacking distance of  $4.35 \text{ \AA}$  is displayed. It turns out that the ionic liquid can affect the molecular packing and crystallization of the polymer.

Yadav et al., 1996 reported the crystallization behavior of polyurea by XRD and kinetics study. It was found that when polymers formed and precipitated out at a high rate, a more amorphous structure was produced, probably because the polymers did not get sufficient time to arrange themselves into an ordered lattice under such a high rate. A reduced three dimensional (3-D) molecular structure presented in this work could be ascribed to the high polymerization rate due to the incorporation of ionic liquids, which reduced the diffusion barrier with the formation of porous structures and eliminated the side reaction between TDI and water. Higher polymerization rate renders faster precipitation and a lower crystallinity.



**Figure 5.14** Molecular structure of polyurea schemed by Cerius II<sup>®</sup>.

Zhou et al., 2004 reported wormlike structures found in SiO<sub>2</sub> synthesized by a sol-gel process in IL and proposed a hydrogen bonding -co-  $\pi$ - $\pi$  interaction mechanism to interpret the observation. In our case, the imidazolium rings of ILs and the aromatic moieties of the polyurea can form  $\pi$ - $\pi$  interactions. In addition, the -NH- groups of the polyurea can form hydrogen bonds with the BF<sub>4</sub><sup>-</sup> anion, which further connected to the extended molecular network formed in ILs. These interactions will affect the packing of the polymer chains and the crystallization, as revealed in the XRD data.

### **5.2.7 Molecular Interactions and the Formation of Polymeric Nanostructures in Various ILs**

The origins of forming the surface nanostructure in polyurea could be very complicated. Due to the amphiphilic nature of the ILs employed, the reduction of interfacial tension in the presence of ionic liquids can render an enhanced nucleation rate and affect the morphology accordingly. However, reduction in interfacial tension alone can not explain the nanostructures observed in the polymer products. To demonstrate this, a surfactant SDS (sodium dodecyl sulfate) was added to the water phase to decrease the interfacial tension between the oligomers and the solvents during the interfacial polymerization. A completely different porous morphology, featuring large pore sizes and smooth surface (details in Sect. 5.3) was observed.

Special orientations and spatial correlations of ionic liquid molecules have been found recently. Fukushima et al. 2004 reported the ordering of short chain ionic liquid aligned by single-walled carbon nanotubes (SWNT) in a gel of 1-butyl-3-methylimidazolium bis(trifluoromethylsulfonyl)imide containing 0.5wt% of SWNT. A spacing of 4.6Å was found

under XRD, possibly due to cation- $\pi$  interaction (Ma and Dougherty, 1997). Bowers and Vergara-Gutierrez, 2004 examined molecular structures of two ionic liquids, [bmim][BF<sub>4</sub>] and [omim][PF<sub>6</sub>], near the free surface by neutron reflectivity (NR). These IL molecules were found to form an ordered lamellar structure near the surface with segregated head and tail groups; such an ordering can extend into the bulk for a depth longer than  $\sim 40\text{\AA}$ .

A number of molecular simulations have been employed to investigate the molecular ordering of ionic liquids in the bulk phase or near the surface. Urahata and Ribeiro, 2004 reported a systematic study on 1-alkyl-3-methylimidazolium ionic liquids and concluded the existence of an intermediate range of order in ILs. Using molecular dynamics (MD), Lynden-Bell, 2003 reported that the cation of dimethylimidazolium chloride ([dmim][Cl]) has a preferred ring plane perpendicular to the surface. Hanke et al., 2003 used MD simulations to study the interactions between benzene and [dmim][Cl] and dimethylimidazolium hexafluorophosphate ([dmim][PF<sub>6</sub>]). An oscillating pattern of ion charges was found to propagate in an extended distance of 5-10 $\text{\AA}$ . In short, the ionic interactions can lead to a charge-ordering effect and affect local liquid structures.

Based on the previous experimental and theoretical investigations of ionic liquids, the surface nanostructures found in polyurea are likely to result from the interactions between polyurea and the IL, which exhibits extended correlations in positions and orientations. It is also known that the amino groups (-NH<sub>2</sub>) and the anions will form hydrogen bonds. Whether the interactions between the ionic liquid molecules and polyurea perturb the correlations among the cations and anions, and bring the rather drastic morphological features to the polymer is to be studied. Here FTIR was used to monitor such interactions. Figure 5.15 depicts the IR spectra of (a) neat [bmim][BF<sub>4</sub>], (b) polyurea prepared at the

[bmim][BF<sub>4</sub>]/n-hexane interface *before* the removal of the IL (i.e. unwashed PUA-B4E with residual [bmim][BF<sub>4</sub>]), and (c) neat PUA-B4E without IL. Two new peaks located at 2082cm<sup>-1</sup> and 1508cm<sup>-1</sup> (marked with asterisks) in spectrum (b) were observed when compared with spectra (a) and (c). Also found was broadening of  $\nu_{\text{C-H}}$  peak between 3200 and 3050cm<sup>-1</sup>, denoting the C-H stretching vibration of the imidazolium ring as compared to the peak (triangle mark) on spectrum (a) from the neat IL. This broadening arises from molecular interactions of ionic liquids, e.g. stacking of the imidazolium rings ([bmim]) and  $\pi$ - $\pi$  interactions that reduce the local electron density, or other interactions. As the hydrogen bonds can render surface localization of anions, such localization could also induce the alignment of the adjacent cation rings. In any case, the new peaks and broaden absorption bands found in spectrum (b) strongly suggest the existence of rather significant intermolecular interactions between IL and the polyurea when they were mixed; once the IL was removed from the surface of polyurea by repeated washes, these features disappeared.



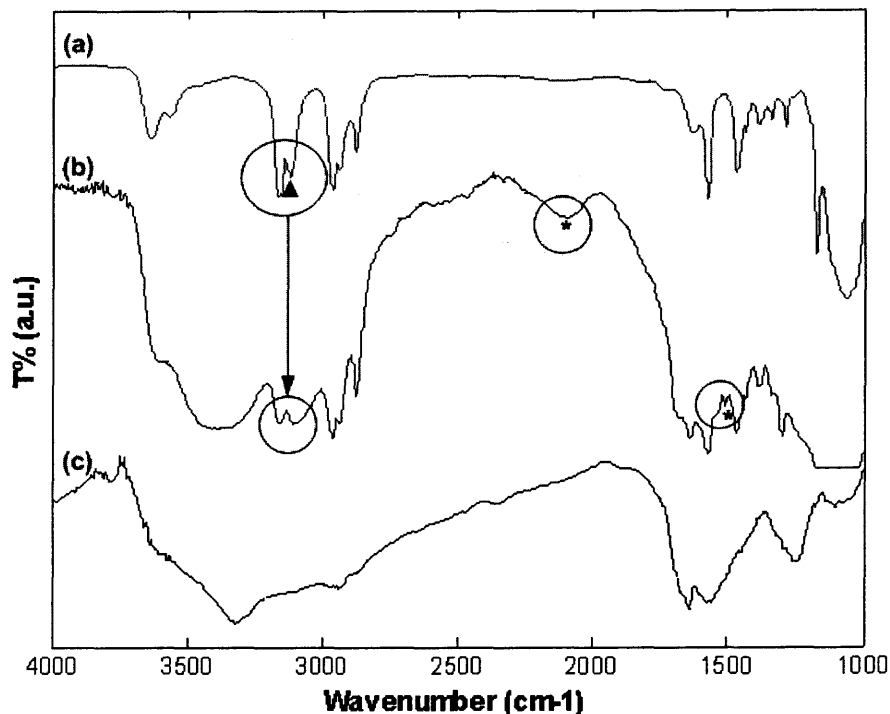


**Figure 5.15** FTIR spectra of neat [bmim][BF<sub>4</sub>] (a), unwashed PUA-B4E with residual [bmim][BF<sub>4</sub>] (b), and PUA-B4E after repeated washes (c).

The above spectral features from FTIR data are not a single event. As shown in Figure 5.16, similar measurements were taken for another set of samples: (a) neat [omim][BF<sub>4</sub>], (b) unwashed PUA-B8E with residual [omim][BF<sub>4</sub>], and (c) neat PUA-B8E without the ionic liquid. A new peak at  $\sim 2100\text{cm}^{-1}$  and broadening of the peak between  $3200$  and  $3050\text{cm}^{-1}$ , denoting the stretching vibration modes of the C-H bonds in [omim] rings were found in spectrum (b) compared with spectra (a) and (c). With the same broadening feature found in different imidazolium rings, similar scenarios of the interactions and intermolecular structures are expected. To complete our discussion, standard FTIR spectra of the unreacted EDA and TDI were examined to exclude possible artifacts caused by the residual reactants. As shown in Figure 5.17 (a), the spectrum of EDA shows no peaks in the range of  $2000$ - $2500\text{cm}^{-1}$ . The spectrum of TDI (Figure 5.17 (b)) shows no peak between  $1800$ - $2500\text{cm}^{-1}$  except an N=C=O

bond at  $2280\text{cm}^{-1}$ . These spectra could hardly be matched to the new peaks as indicated in Figure 5.15 (b) and Figure 5.16 (b). This comparison demonstrates that the observed new peaks in the unwashed polyurea with residual IL samples are not from the reactants or the solvents but a direct consequence from the intermolecular interactions between the ionic liquid and polyurea.

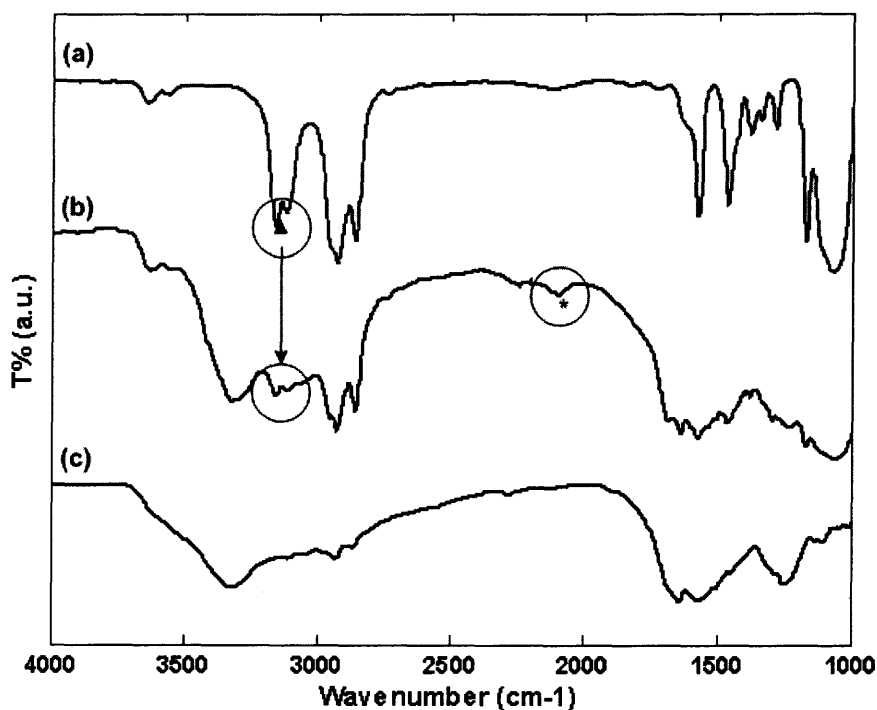


**Figure 5.16** FTIR spectra of neat [omim][BF<sub>4</sub>] (a), unwashed PUA-B8E with residual [omim][BF<sub>4</sub>] (b), and PUA-B8E after repeated washes (c).

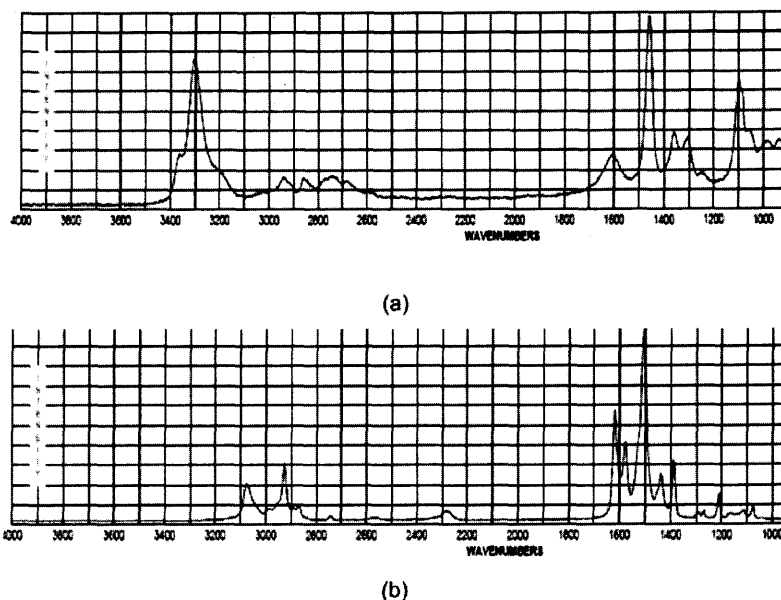


**Figure 5.17** Standard FTIR absorbance spectra of (a) Ethylene Diamine and (b) TDI. (From Sigma-Aldrich Technical data) No peaks at  $\sim 2100\text{cm}^{-1}$  were found in both spectra, while the peak at  $\sim 2280\text{cm}^{-1}$  for TDI is assigned to the  $\text{N}=\text{C}=\text{O}$  bonding.

Antonietti and his coworkers (Zhou et al., 2004) reported the observation of similar broadening of the  $\nu_{\text{C-H}}$  peak of [bmim] imidazolium rings from the IR data of nanoporous silica mixed with [bmim][ $\text{BF}_4$ ]. Interestingly, the [ $\text{BF}_4^-$ ] anions also formed hydrogen bonds with the hydroxyl groups on the silica surface. They explained the broadening is originated from the  $\pi$ - $\pi$  interaction of the imidazolium rings that reduces the local electron density in the rings and affects the vibrations of the C-H bonds.  $\pi$ - $\pi$  interaction is a noncovalent interaction originated from intermolecular overlapping of p-orbitals in  $\pi$ -conjugated systems such as aromatic rings (Hunter and Sanders, 1990). These authors further gave a hypothetical hydrogen-bond-co- $\pi$ - $\pi$  interaction model to explain the structures of the nanoporous silica, which mimic the superstructures formed by the ionic liquids. Their explanations of molecular interactions and local molecular structures were supported by FTIR, NMR and UV-vis. Our systems share similar physical ground as theirs: the interactions between the anions and the amino groups could affect the structures of the adjacent imidazolium cations and further affects the

vibrations of the C-H bonds in the imidazolium rings. The interactions could also affect the crystallization of the polyurea as revealed by the XRD results. More experiments, e.g. NMR, to this account are in need for better understanding of the relations between the observed polymer morphology and the physical and chemical properties of ILs.

### **5.3 Interfacial Polymerization with Aqueous Solution of ILs**

In this section, IL aqueous solutions were employed in the interfacial polymerization to synthesize polyurea. The reactants TDI and ethylene diamine were dissolved in n-hexane and IL aqueous solutions, respectively. The FTIR results and surface morphologies of the polymer products are presented and compared with the ones synthesized in water with and without ionic surfactant sodium dodecyl sulfate (SDS).

#### **5.3.1 FTIR Analysis of Polyurea Synthesized with Aqueous Solutions of ILs**

The FTIR spectrum of polyurea synthesized at the regular water/n-hexane interface is shown in Figure 5.18(a), which will be used as a reference for comparison. Figure 5.18(b) depicts the FTIR spectra of polyurea samples prepared with aqueous solutions of three ILs and with the aqueous solution of SDS.

All the synthesized samples exhibited very similar FTIR spectra. The main  $\text{-NH-}$  peaks at  $3280\sim 3300\text{ cm}^{-1}$  and the carbonyl bonding peak at  $\sim 1600\text{ cm}^{-1}$  indicate the existence of strong linkages of  $\text{-CO-NH-}$  in all the samples (Szymanski and Erickson., 1970). Again, no peak is found in the range of  $3050\sim 3200\text{ cm}^{-1}$ , indicating complete removal of the ILs from the final polymers. The FTIR results confirm that the product from the interfacial polymerization at the

hexane-IL aqueous solution interface is polyurea and there is no significant change in chemical structures upon the addition of ILs.

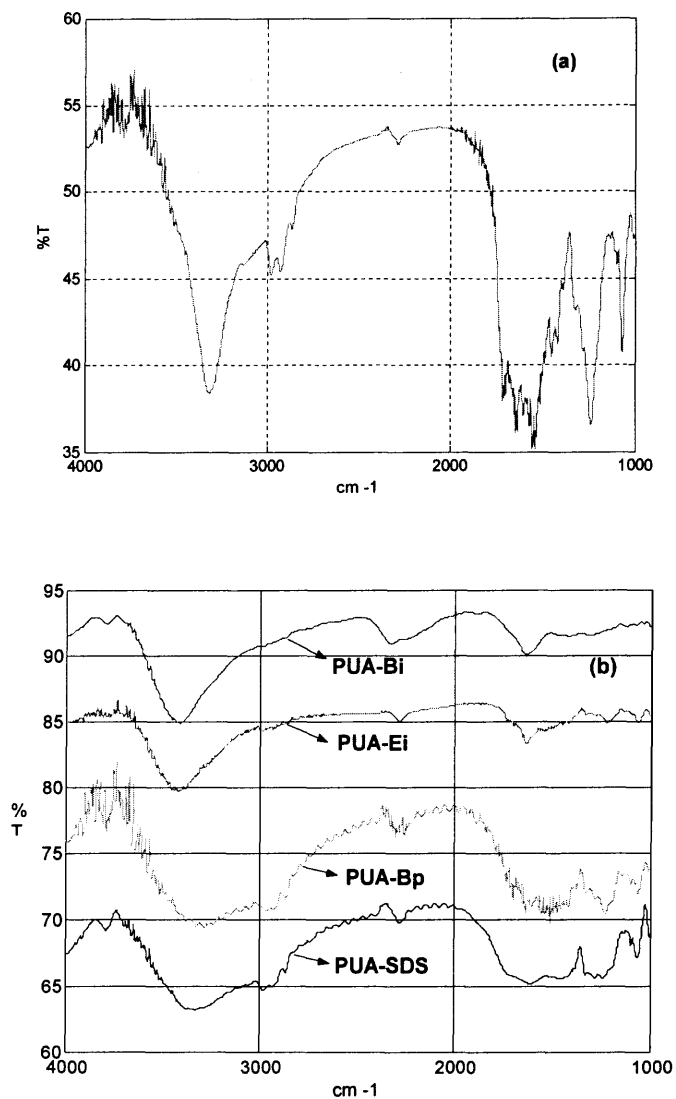


**Figure 5.18** FTIR spectra of the polyurea samples by interfacial polymerization in various reaction media: (a) water/n-hexane; (b) n-hexane and aqueous solutions of three different ILs and aqueous solution of SDS.

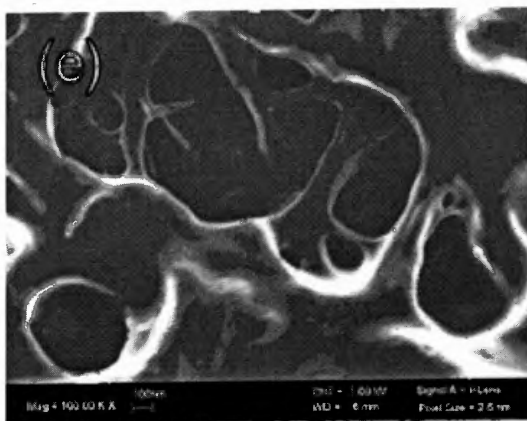
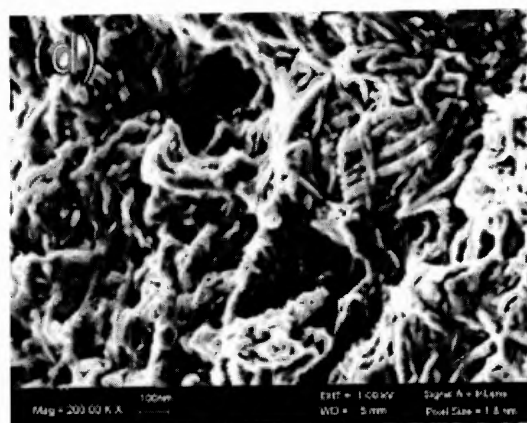
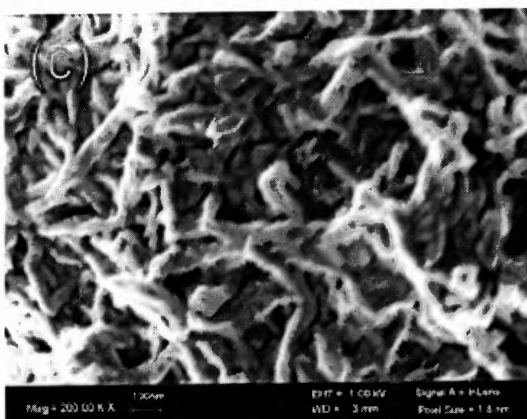
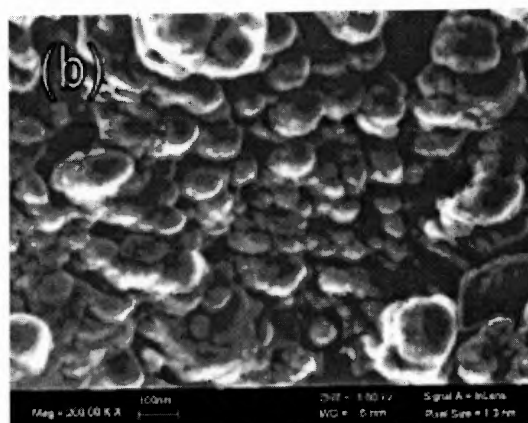
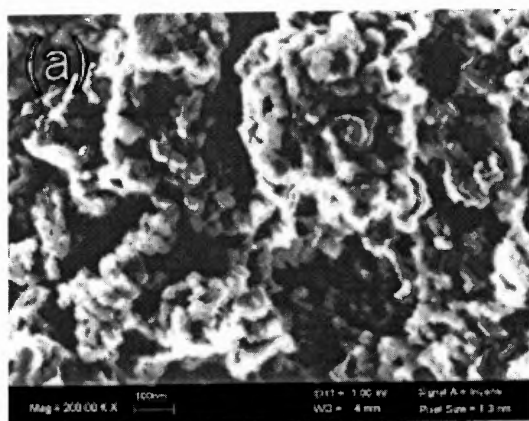
### 5.3.2 Surface Morphology of Polyurea Synthesized in Aqueous Solutions of ILs

Figure 5.19 shows the SEM micrographs of the polyureas synthesized at the interface of n-hexane and IL aqueous solutions compared to the polyurea synthesized at a regular water/n-hexane interface. Exotic surface nanostructures were observed for all the three samples prepared in IL aqueous solutions. Short nanoscale fibril structures were found on the surface of PUA-Ei (EDA+TDI, [emim][BF<sub>4</sub>] aqueous solution) and PUA-Bp (EDA+TDI, [bmpm][BF<sub>4</sub>] aqueous solution). The lengths of these primary structures are about 100nm, while for the PUA-Bi (EDA+TDI, [bmim][BF<sub>4</sub>] aqueous solution) surface, elliptical nanostructures of the size of 20nm have been observed. These surface morphologies are consistent with aggregated nanosize particles. In contrast, the polyurea synthesized with SDS solution exhibits a porous structure with a smooth surface. The pore sizes are in a wide range from 10<sup>2</sup>~10<sup>3</sup> nm. Densely packed random agglomeration was found for PUA-0 (EDA+TDI, water/n-hexane). Table 5.3 summarizes the morphology results for comparison.

**Table 5.3** Surface morphology of polyureas\* synthesized in various aqueous solutions

<b>Sample Name</b>	<b>Reaction Medium</b>	<b>Surface Morphology</b>
PUA-0	Water/n-hexane	Random agglomeration
PUA-SDS	0.001M SDS aqueous solution/n-hexane	Interconnected porous structure (10 <sup>2</sup> ~10 <sup>3</sup> nm)
PUA-Ei	[emim][BF <sub>4</sub> ] aqueous solution/n-hexane	Discrete ellipsoids (~20nm)
PUA-Bi	[bmim][BF <sub>4</sub> ] aqueous solution/n-hexane	Nanofibrous Structures (~100nm)
PUA-Bp	[bmpm][BF <sub>4</sub> ] aqueous solution/n-hexane	Nanofibrous Structures (~100nm)

\*All polyureas were synthesized from EDA and TDI.



**Figure 5.19** SEM micrographs of the polyureas synthesized with ionic liquid aqueous solutions: (a) PUA-0; (b) PUA-Bi; (c) PUA-Ei; (d) PUA-Bp; (e) PUA-SDS.

The effect of interfacial tension on the morphology has been investigated by comparing the interfacial tension between n-hexane and different IL aqueous solutions. Based on the results measured in Section 5.1, the comparison is depicted as Figure 5.20. The interfacial tension of n-hexane/0.001M SDS solution was 22.4 dynes/cm, which is much lower than the one of water/n-hexane system. The decrease of interfacial tension will increase the nucleation rate and facilitate the formation of small-size polymeric structures.

From the three samples synthesized with IL solutions, totally different surface morphologies were observed as shown in Figure 5.19(b), (c) and (d); however, the interfacial tensions of these samples are similar to the SDS solution. Thus, the nanostructures found in the polyurea synthesized with IL solutions can only be partly attributed to the decrease of the interfacial tension.

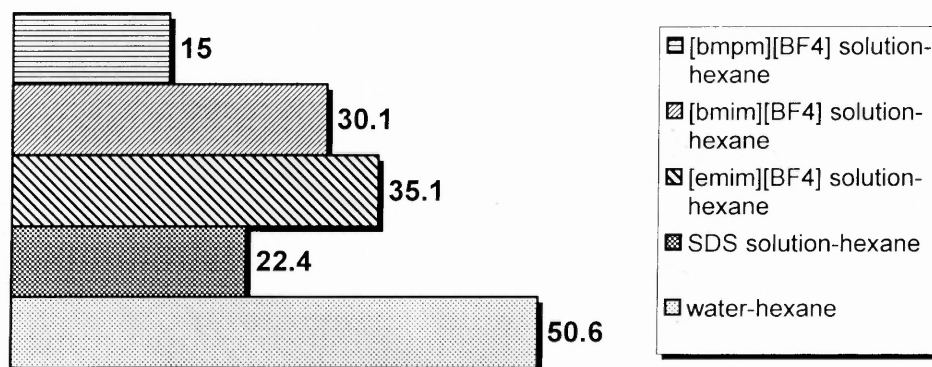


**Figure 5.20** Interfacial Tension between n-hexane and various aqueous-based solutions. (The labeled numbers next to the bars are tension values in the unit of dyne/cm)

It is known that there exists cation- $\pi$  interaction between an aromatic group and organic cation in aqueous media (Ma et al., 1997). TDI is an aromatic compound which can interact with imidazolium or pyridinium cations at the interface by the cation- $\pi$  interaction which can



further affect the molecular structures of the polyurea in the reaction zone and induce the surface nanostructures.

Recent SAXS study of 1-decyl-3-methylimidazolium bromide ( $[\text{C}_{10}\text{mim}][\text{Br}]$ ) showed that  $[\text{C}_{10}\text{mim}][\text{Br}]$  can self assemble in water and eventually forms lyotropic lamellar layers with a lattice spacing varying from 5 to  $40\text{\AA}$ , depending on water concentration. Hydrogen bonding is considered to be essential to form such self-assembly in water (Dietz et al., 2003). It has been demonstrated by Baldelli, 2003 that the existence of hydrogen bonding, though weak compared to ionic interaction, is strong enough to change the surface orientation of ionic liquids. It is proposed that the hydrogen bonding between anion and water may help to form an intermolecular network at the interface (See Figure 5.21). Though there is no evidence that there are self-assembled structures in the IL aqueous solutions used in our study, the observed nanostructures could result from the reason that polymer was immersed in and affected by a “IL-water network” in the vicinity of the interface due to the intermolecular interactions between the ILs and the polymer (Sect.5.2.7) during the precipitation process.

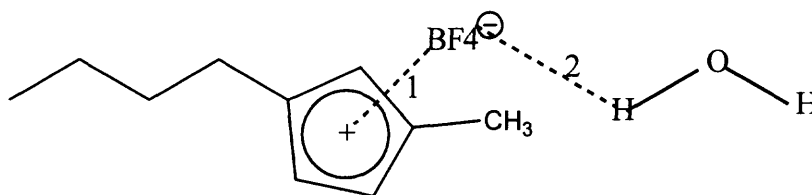


**Figure 5.21** Scheme of intermolecular network between  $[\text{bmim}][\text{BF}_4]$  and water: 1. Coulombic Force; 2. Hydrogen bond.

It is also found that different types of anions will lead to different surface morphologies, as shown in Figure 5.19(b) and (d), so do various alkyl chain lengths attached to the imidazolium rings in the comparison of figure 5.19(b) and (c). Further complementary techniques such as

NMR are needed to fully understand the formation mechanism of polymer nanostructures in IL aqueous solutions.

#### 5.4 Synthesis of Polyamide Film with ILs

In this section, we report the synthesis and characterization of poly(hexamethylene sebacamide) (Nylon 610) and poly(butylene sebacamide) (Nylon 410) films by IP in room temperature ionic liquids.

##### 5.4.1 FTIR Analysis of Polyamide Films by IP in ILs

FTIR was employed to examine the chemical structures of the polyamide products. Figure 5.22 depicts the comparison of the FTIR spectra from two typical polyamides synthesized in our work, PA-B0 (Nylon 410, water) and PA-BB4 (Nylon 410, [bmim][BF<sub>4</sub>]), and the spectrum from [bmim][BF<sub>4</sub>]. The main peaks at  $\sim 3300\text{cm}^{-1}$  and  $\sim 1600\text{cm}^{-1}$  found in both polymer samples indicate the  $-\text{NH}-\text{CO}-$  linkage of polyamide. The disappearance of the C-H vibration peak of the imidazolium ring at  $3050\sim 3200\text{cm}^{-1}$  in spectrum (c) compared to spectrum (a) suggests complete removal of [bmim][BF<sub>4</sub>] from the PA-BB4. The results identify the film products as polyamide and suggest that the application of room temperature ionic liquids has no significant effect on the chemical structures of the polyamide, an observation similar to the synthesis of polyurea with ILs.

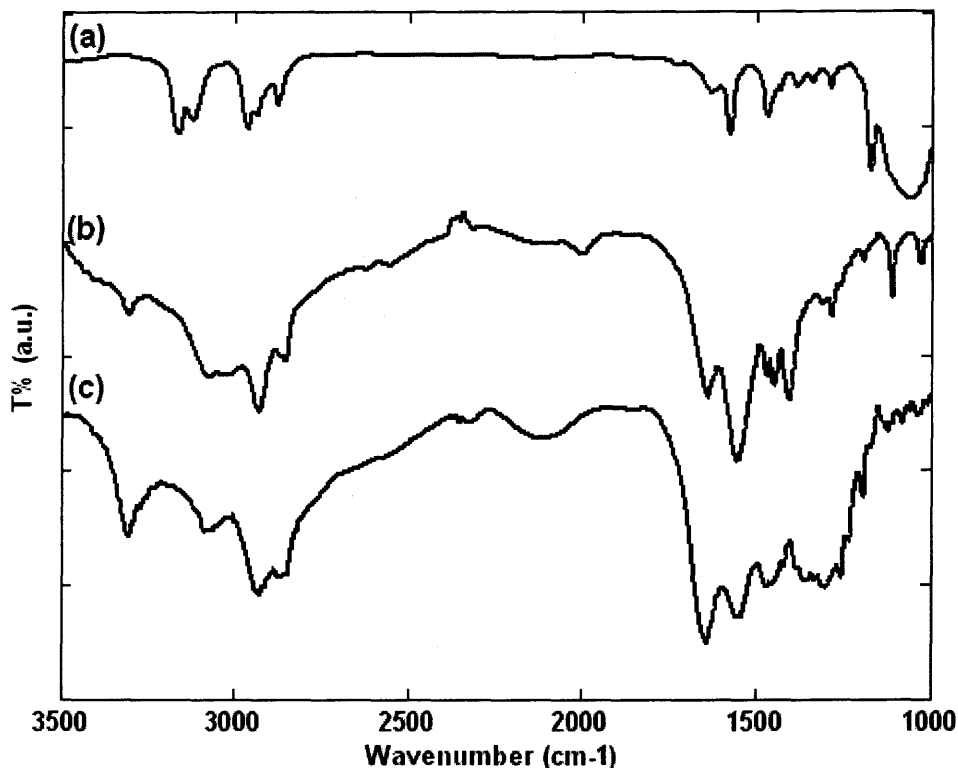


**Figure 5.22** FTIR spectra of polyamides by interfacial polymerization at various conditions: (a) [bmim][BF<sub>4</sub>]; (b) PA-B0; (c) PA-BB4.

#### 5.4.2 Effect of Ionic Liquids on Molecular Weight of Polyamides

Intrinsic viscosity,  $[\eta]$ , can be correlated to polymer molecular weight by Mark-Houwink equation as:  $[\eta]=KM^\alpha$ , where  $K$  and  $\alpha$  are constants for a particular polymer-solvent system

(Sperling, 2001c). The value of  $K$  can be given by  $K = \Phi\left(\frac{r_0^2}{M}\right)^{3/2}$ , where  $r_0^2$  represents the

mean square end-to-end distance of the unperturbed polymer coil of interest. If the number average molecular weight is used,  $\Phi$  is a universal constant and is equal to  $2.5 \times 10^{21}$  dl/mol $\cdot$ cm<sup>3</sup>. Another theoretical value of  $3.6 \times 10^{21}$  dl/mol $\cdot$ cm<sup>3</sup> was calculated with the consideration of the frictional coefficients of chains. The exponent  $\alpha$  can be expressed as

$\alpha=3\nu-1$ , where  $\nu$  is the inverse fractal dimension of the polymer in the solution. When the fractal dimension is equal to two i.e. a  $\theta$  solvent,  $\alpha=0.5$ ; when the fractal is equal to  $5/3$ , i.e. a good solvent,  $\alpha=0.8$ . Therefore, the value of  $\alpha$  for random coils usually falls between 0.5 and 0.8 (Strobl, 1997). Nevertheless, if the polymer is rod-like (fractal dimension=1),  $\alpha=2$ ; if the polymer is semi-flexible or stiff coils such as cellulose trinitrate,  $\alpha=1$ .

Morgan and Kwolek, 1963 reported the molecular weight-viscosity relationship of Nylon 610 measured in m-cresol at 25°C. It was reported that for the Nylon 610/m-cresol system,  $K$  equals to  $1.35 \times 10^{-4}$ , while  $\alpha$  equals to 0.96. The high value of  $\alpha$  could result from the formation of branches or strong interactions between Nylon 610 and the solvent. The absolute molecular weight values were not calculated in the current work due to the lack of the values of  $K$  and  $\alpha$  for the Nylon 610/H<sub>2</sub>SO<sub>4</sub> system; however, by comparing the intrinsic viscosities of the same polymer species under the same solvent condition, one can still examine the relative molecular weight. Table 5.4 depicts the intrinsic viscosities of the polyamides synthesized in different ionic liquids.

**Table 5.4** Intrinsic viscosity of polyamides prepared by IP in different ILs<sup>a</sup>

Polymer Sample	$[\eta]$ , 100ml/g	Polymer Sample	$[\eta]$ , 100ml/g
PA-B0	0.58	PA-H0	0.54
PA-BB4	0.52	PA-HB4	0.66
PA-BB8	0.60	PA-HB8	0.67

<sup>a</sup>98% H<sub>2</sub>SO<sub>4</sub> is used as the solvent; polymer concentration is 0.1g/100ml.

The intrinsic viscosities of polyamides obtained in this work are comparable to the results reported by Lozinskaya, 2004 who synthesized polyamides in ILs via direct polycondensation

and measured the intrinsic viscosities by using 98% $\text{H}_2\text{SO}_4$  as solvent. From Figure 5.23, it is found that applying ILs as reaction media can increase the molecular weight in general; the trend is especially unambiguous for the nylon 610 series. The increase of molecular weight is mainly caused by replacing water with ionic liquids as reaction media due to the elimination of the hydrolysis of the diacid chloride to form diacid. The hydrolysis is normally encountered at regular water/organic solvent system. Therefore, the introduction of ionic liquids as solvent for diamine can considerably reduce the hydrolysis and increases the molecular weight. It is also found that for polyamide prepared in different ILs, the one synthesized in [omim][ $\text{BF}_4$ ] has a higher molecular weight than its counterpart in [bmim][ $\text{BF}_4$ ].

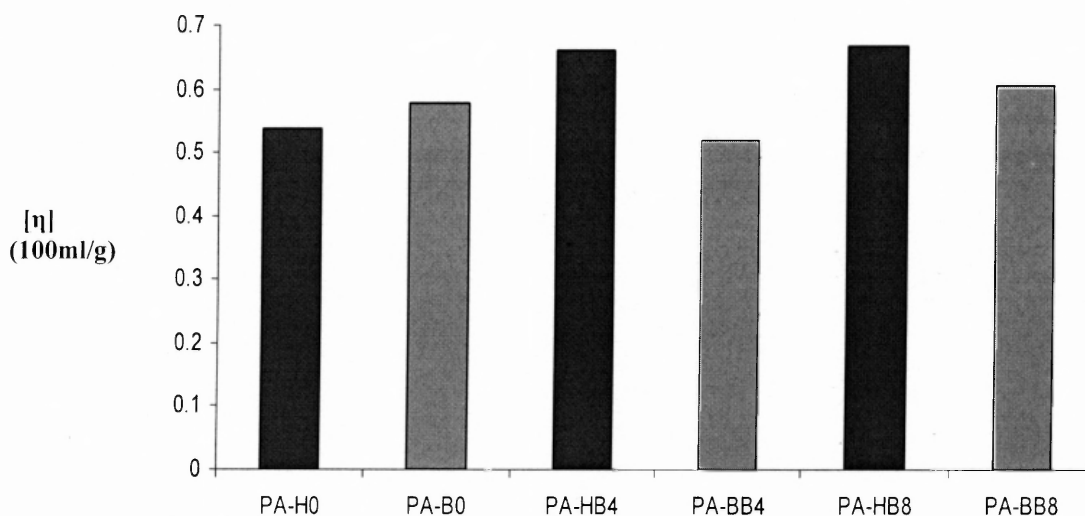


**Figure 5.23** Intrinsic viscosities of polyamides prepared with various ILs.

#### 5.4.3 Thermal Stability of Polyamide films

Thermal stability of two typical poly(hexamethylene sebacamide) (Nylon 610) film samples, PA-H0 and PA-HB8, was evaluated by TGA. Figure 5.24 depicts the comparison of the

weight loss curves. The temperature at 10% weight loss is defined as the decomposition temperature ( $T_d$ ) in the current test.

The PA-H0 sample shows a relative low thermal stability with  $T_d=199^\circ\text{C}$  and a continuous weight loss over a wide temperature range between  $160^\circ\text{C}$  and  $450^\circ\text{C}$ . The lower average molecular weight and broader molecular weight distribution could be the reason for the poor thermal stability. On the other hand, the PA-HB8 (Nylon 610, [omim][BF<sub>4</sub>]) displays an outstanding thermal stability. The PA-HB8 sample shows a decomposition temperature of  $330^\circ\text{C}$  with a sharp decomposition slope indicating a higher average molecular weight and a narrower molecular weight distribution. The agreement between the thermal stability analysis and the intrinsic viscosity described in subsection 5.4.2 suggests that one can synthesize polyamide films with a higher molecular weight and better thermal stability with ionic liquids than with water, a consequence could be resulted from the elimination of the hydrolysis of diacid chloride in the reaction.

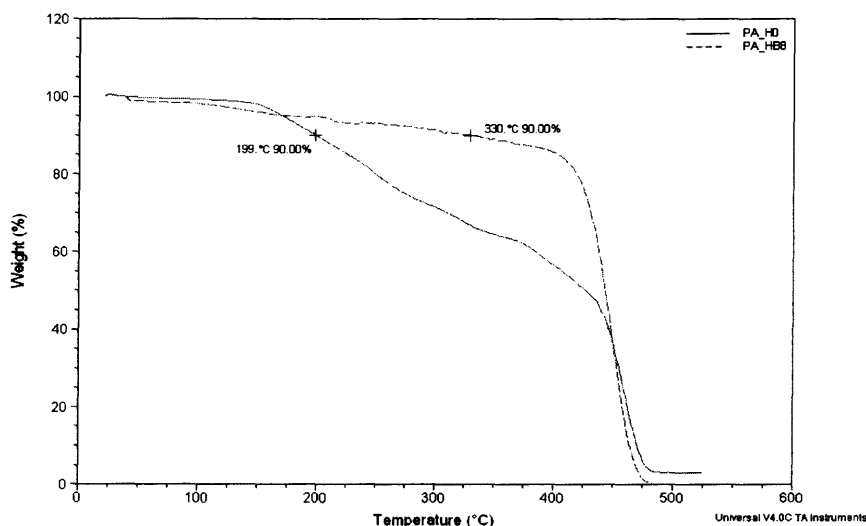


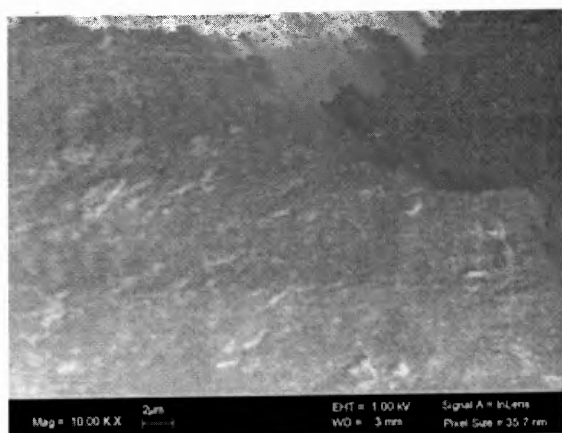
**Figure 5.24** TGA curves of Nylon 610 films by IP with different reaction media.( PA-H0: water/n-hexane interface; PA-HB8: [omim][BF<sub>4</sub>]/n-hexane interface.)

#### 5.4.4 Surface Morphology of Polyamide films Synthesized by IP in ILs

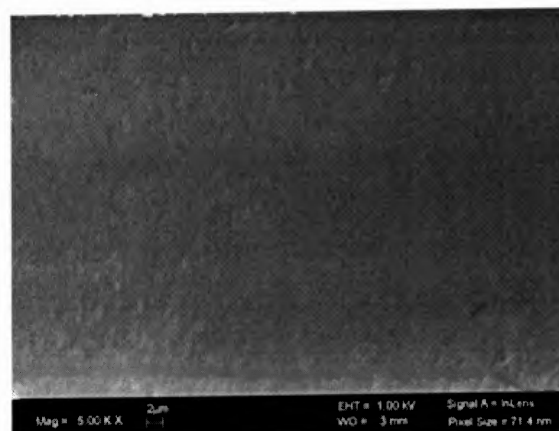
Surface morphologies of poly(butylene sebacamide) (Nylon 410) and poly(hexamethylene sebacamide) (Nylon 610) films synthesized with various media are compared in Figure 5.25.

It is observed that both nylon 410 and nylon 610 films prepared at the water-hexane interface (Figure 5.25 (a) and (b)) exhibited no special features but flat, homogeneous surfaces. However, for both samples synthesized in the [bmim][BF<sub>4</sub>] (Figure 5.25 (c) and (d)), fine nanoparticle aggregates were found on the polymer surface. This feature is more evident for the case of PA-BB8 and PA-HB8, where [omim][BF<sub>4</sub>] was used as the reaction medium (Figure 5.25 (e) and (f)). These two samples exhibit a rougher film surface consisting of submicron particles. Comparing the surface morphologies of Nylon 410 and Nylon 610 films, no significant difference was found due to the difference in the alkyl chain lengths of the diamine.

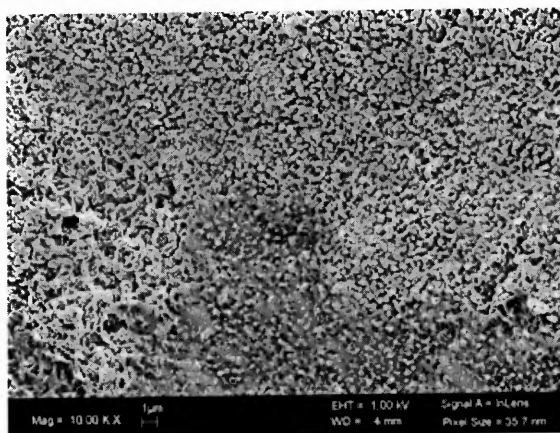
The tunability of the surface morphology of polyamide films by varying different ionic liquids as reaction media may offer a potential alternative to fabricate nanostructured materials with heat-exchanging surface, where thermal transfer can be enhanced by the augmentation of surface area. Such nanostructured surfaces can have potential applications in heat exchange and packaging materials for semiconductor devices (Lee and Chopra, 2005).



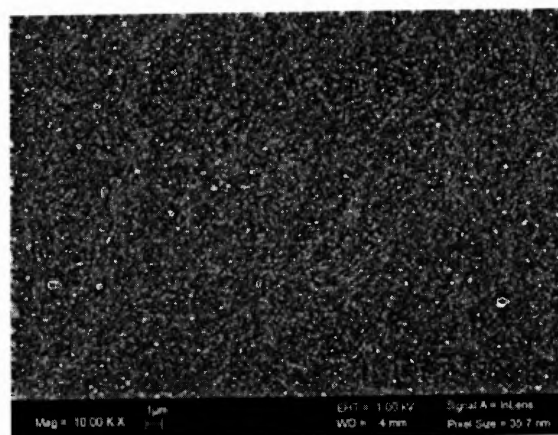
(a)



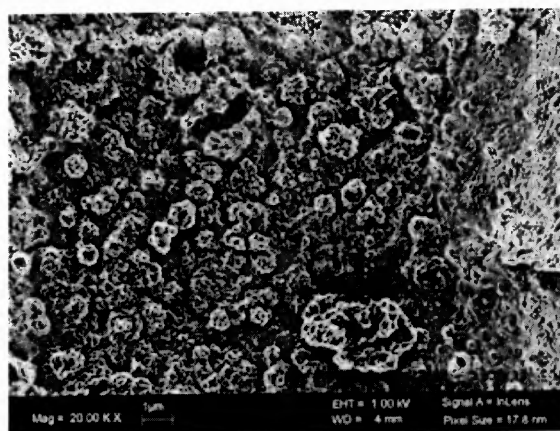
(b)



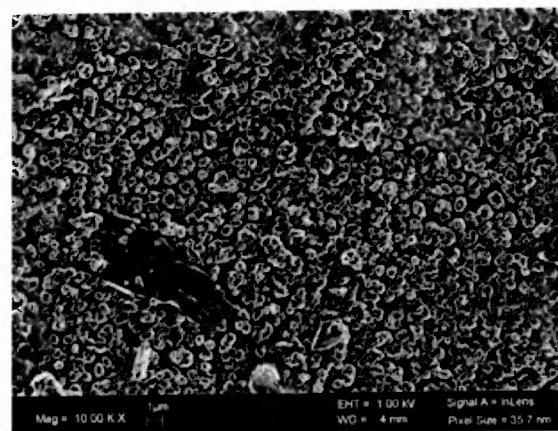
(c)



(d)



(e)



(f)

**Figure 5.25** SEM pictures of Nylon films synthesized by IP in various reaction media: (a) PA-B0; (b) PA-H0; (c) PA-BB4; (d) PA-HB4; (e) PA-BB8; (f) PA-HB8. (Magnification for the pictures is 10,000X, except 5,000X for PA-H0)



## 5.5 Fine Particulates Coating by Interfacial Polymerization

Interfacial polymerization has been widely applied to microencapsulation of liquid and membrane architecture as described in Section 2.4.2. In this section, the coating of micron-size solid particles with polymer layer by interfacial polymerization and the incorporation of ionic liquids is reported.

### 5.5.1 Surface Morphology

The fine particle coating procedure by IP was described in Section 4.3.4.

The surface morphologies of the coated particles were mainly characterized by SEM. Figure 5.26 compares the morphology of polyurea-coated DCR and bare DCR particulates. Both samples are coated at the same stirring speed of 600 rpm. Rough surfaces and sharp edges were observed for the uncoated DCR (Figure 5.26 (a)); while a smoother surface was observed on the SEM picture of the polyurea-coated DCR (Figure 5.26(b)). The SEM image shows a good surface coverage of the particle by the current coating method.

Figure 5.27 compares the surface morphology of polyurea-coated DCR under different initial EDA volume concentrations. Figure 5.27(a) shows the surface morphology of the coated particle under 30% initial EDA concentration, while Figure 5.27(b) shows the one under 50% EDA initial concentration. A higher diamine concentration leads to a rougher surface than the lower one does. The thin-film like polyurea layer in the 30% concentration case, disappears when the EDA concentration is 50%, from which the smooth surface was changed to a rougher one.

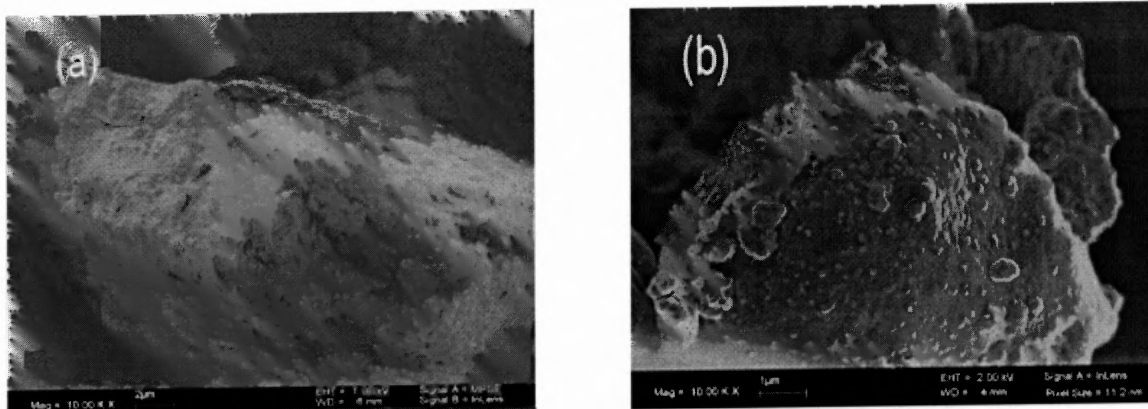


**Figure 5.26** SEM Photographs of (a): bare DCR particles and (b): polyurea-coated DCR particles.

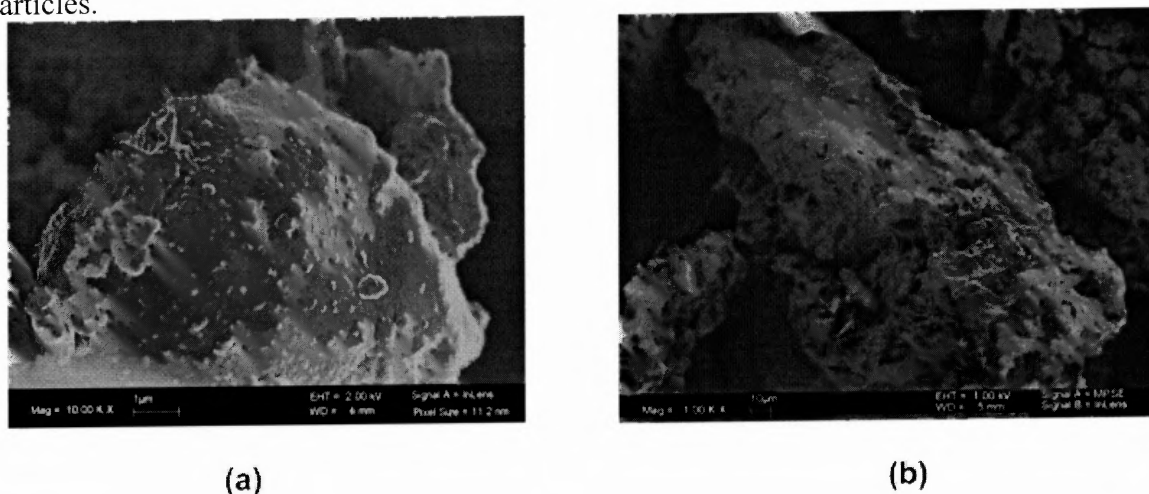


**Figure 5.27** SEM Photographs of polyurea-coated DCR under initial ethylene diamine volume concentrations of 30% (a), and 50% (b).

### 5.5.2 Particle Size Analysis

Particle size analysis was conducted to examine the effect of stirring speed and the reagent concentration. The effect of stirring on the particle size can be understood via Figure 5.28. As the stirring speed increases, the average droplet size is reduced due to the hydrodynamic stress and thus the coated particle sizes. The size of the coated particle agglomerates is therefore decreased. The coating thickness is largely dependent on the agglomeration number for different particle sizes. On the other hand, the coating structure within the agglomerates could

be very complicated. Porous or sponge-like coating structures could be formed, which is relevant to the agglomeration mode and the cluster sizes of the particles in the agglomerates.

The effect of stirring on the agglomeration of coated DCR particles is studied by varying the stirring speed from 100rpm to 900rpm under the same volume concentrations of 2.5% TDI but two different volume ratios of ethylene diamine and water: 30/70 and 50/50. Figure 5.29 depicts the particle size distribution of the coated DCR under different stirring speeds at two ethylene diamine volume concentrations of 30% and 50%, respectively. It is clearly shown that in both cases, the increase of stirring rate during the coating process gives rise to a narrower size distribution of the particulates as well as a decrease of the particle mean size. At low stirring speed such as 100 rpm, the coated particles displayed a broad and almost bimodal size distribution; as the stirring speed increases from 100 rpm to 900 rpm, the size distribution becomes narrower and the average size decreases accordingly. This may attribute to the strong flow field, leading to a high shear flow, which reduces the size of TDI/DCR droplets and thus reduces the coating thickness and the degree of agglomeration.

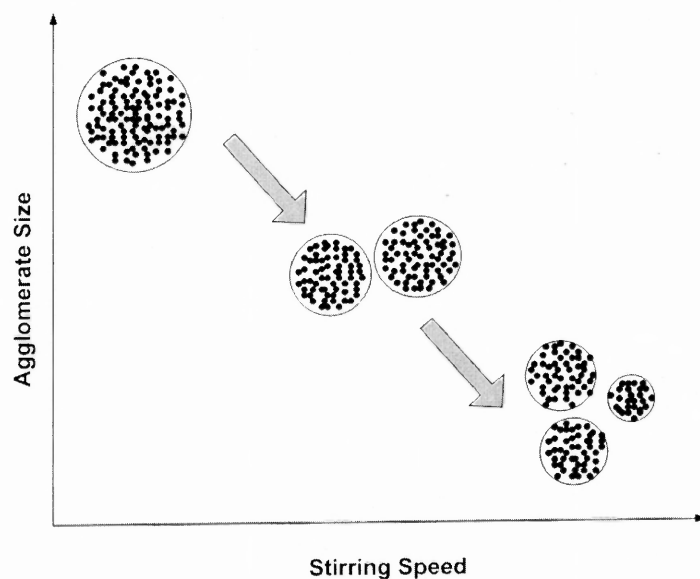
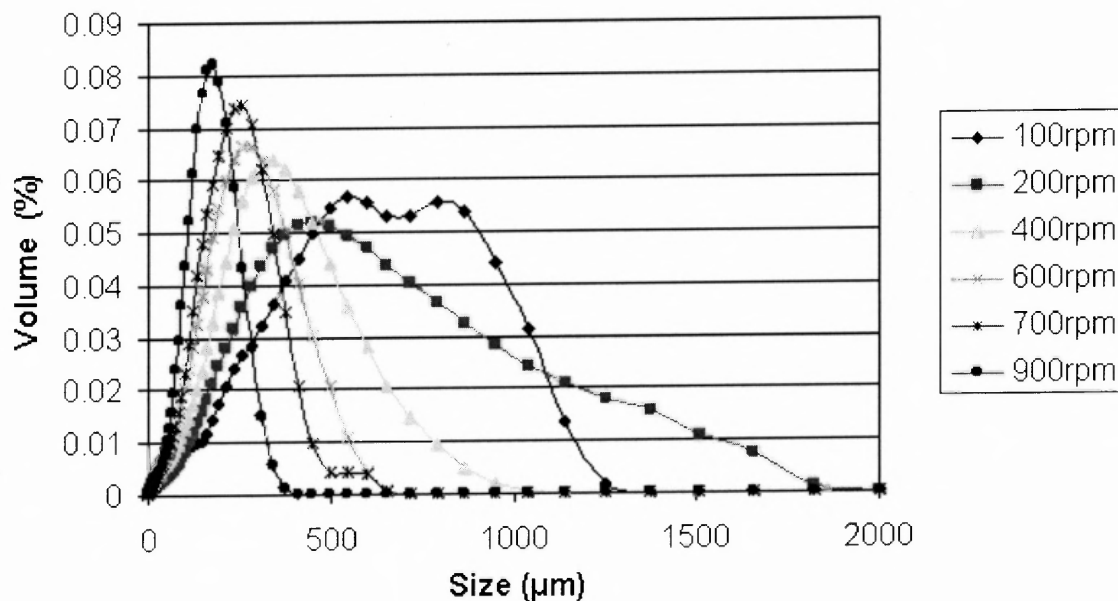
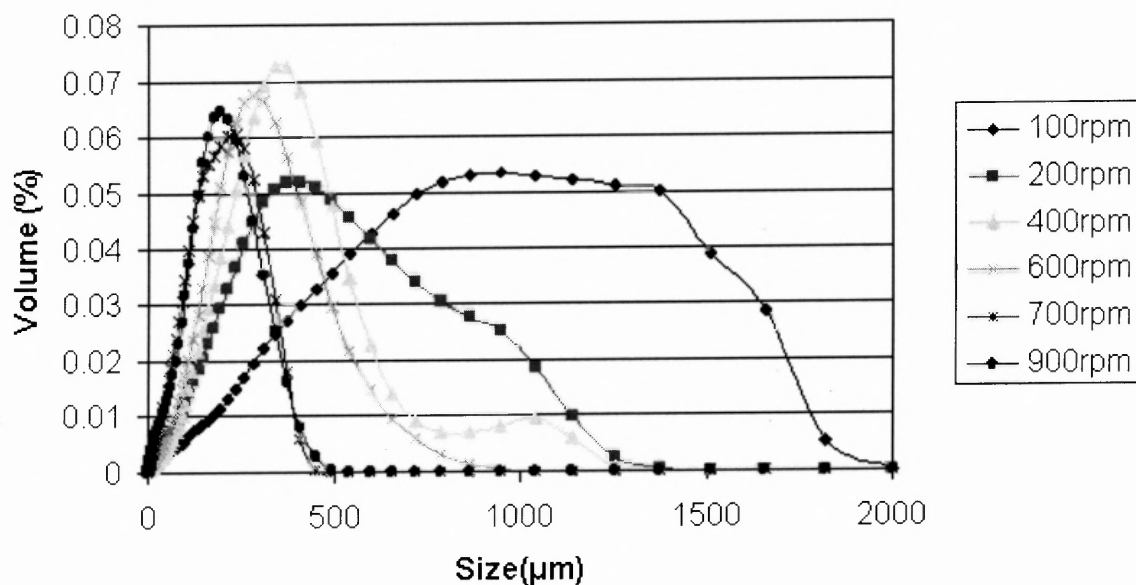


**Figure 5.28** Effect of stirring on coated-particle agglomerate size.



(a)



(b)

**Figure 5.29** Particle Size Distribution of Polyurea-Coated DCR under various stirring speeds: DCR/TDI=5g/2.5ml, Volume ratio of Diamine and water is 30:70 in (a) and 50:50 in (b).

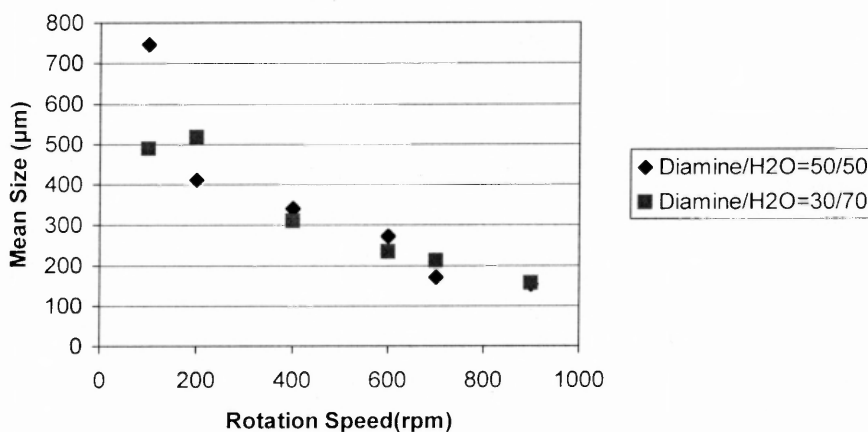


**Figure 5.30** Particle mean size of polyurea-coated DCR under various stirring speeds (DCR/TDI=5g/2.5ml).

Figure 5.30 depicts the relationship between the particle mean size of the coated particles and the stirring speed. The detailed data is shown in Appendix C. A decrease of particle mean size of the coated DCR with the increase of the stirring speed was observed. This trend is the same for both 30% and 50% diamine concentrations. The effect is extremely profound for the case of 50% diamine concentration where the particle mean size has been reduced from 746 $\mu\text{m}$  to 153  $\mu\text{m}$  with the stirring speed increasing from 100 rpm to 900 rpm. The high shear flow under a high stirring speed substantially causes the break-up of the TDI/DCR droplets and leads to a smaller observed mean size.

The effect of reactant concentration on the coated-particle sizes is studied by varying the volume concentration of ethylene diamine from 10% to 50% at a stirring speed of 900rpm. Figure 5.31 depicts the particle size distribution patterns and the mean particle size of coated DCR under different volume concentrations of diamine. The data of mean particle size at various diamine concentrations is shown in Appendix D. As ethylene diamine becomes more concentrated, the particle size distribution is narrower. A drastic decrease of particle size when

the volume concentration of diamine changed from 10% to 20% is observed. Once the concentration goes above 20%, the mean particle size remains within a narrow range between 150~170  $\mu\text{m}$ . This result implicates that the mean particle size is affected by the transport of diamine only under low concentration. Once the diamine concentration exceeds a threshold (in this case 20%), the reactant concentration becomes irrelevant to the mean particle size; the mean size is determined by the stirring speed under the high concentration limit.

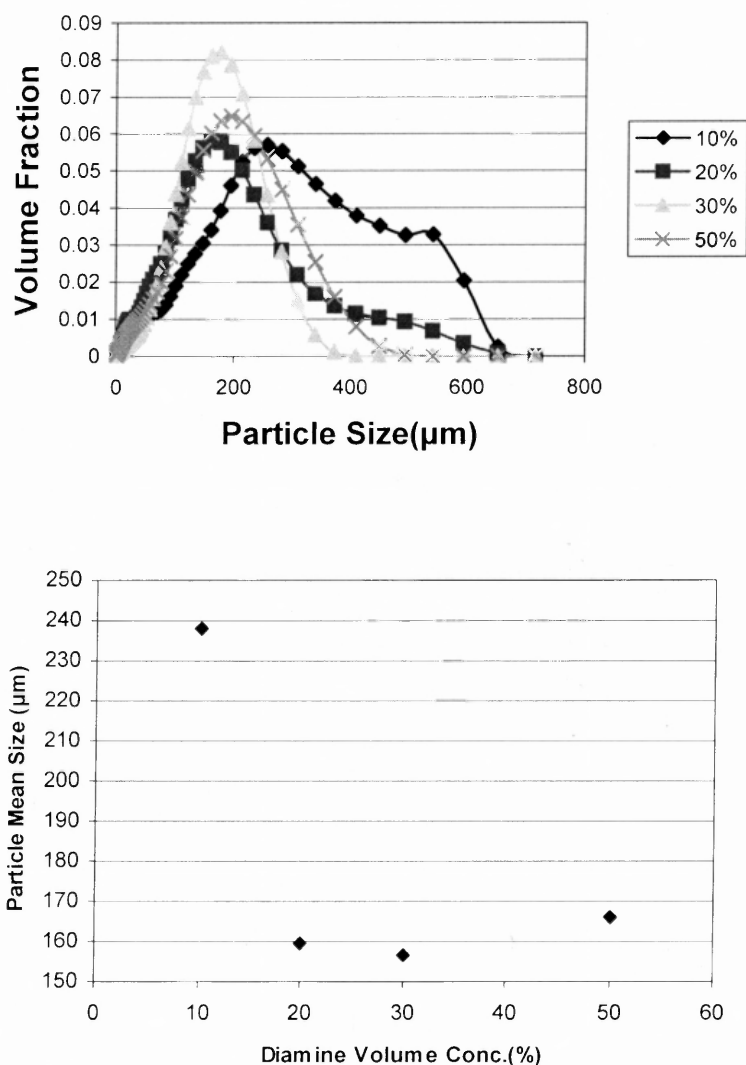


**Figure 5.31** Particle Size Distribution (top) and particle mean sizes (bottom) of polyurea-coated DCR under various ethylene diamine volume concentrations. (DCR/TDI=5g/2.5ml, 900 rpm)

### 5.5.3 Coating Weight Percentage

TGA was employed to evaluate the coating weight percentage of the particles. The onset temperature for the decomposition of pure DCR is found to be 300.94°C based on the TGA spectrum (Figure 5.32). On the other hand, Figure 5.33 presents a comparison of the TGA curves of uncoated DCR, polyurea-coated DCR and polyurea. Polyurea begins to decompose at about 150~200°C. The weight loss of coated particles depends on the coating weight percentage of polyurea on the surface of DCR. In this work, 270°C has been chosen as a reference temperature to analyze the coating weight percentage.

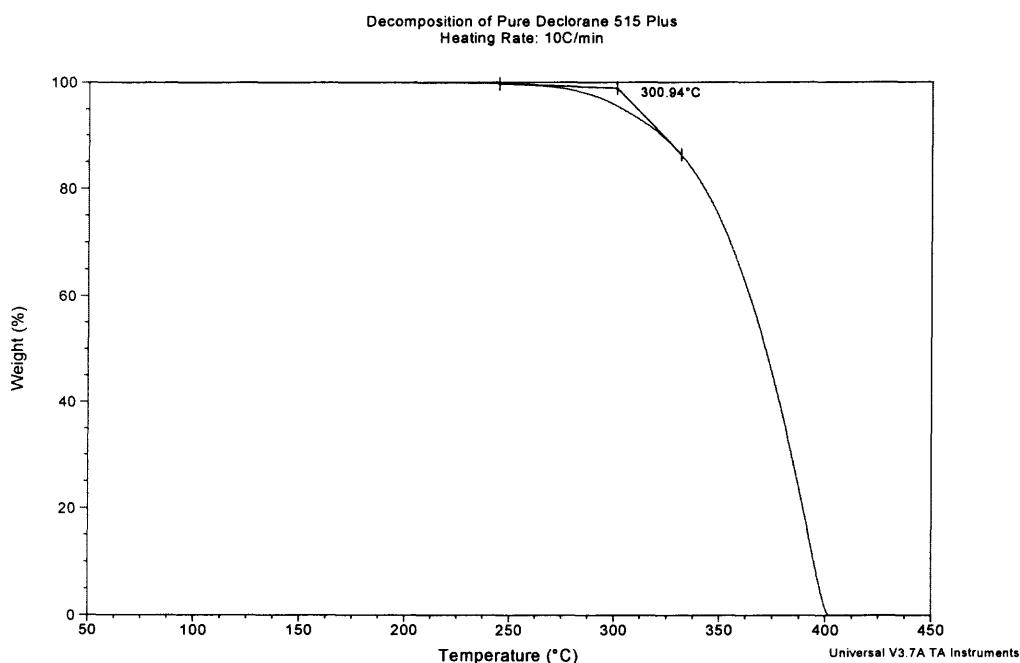


**Figure 5.32** Thermo-Gravimetric Analysis (TGA) spectra of pure DCR: Temperature range from 50°C to 400°C, Heating rate=10°C/min.

The polymer coating weight percentage can be expressed as:

$$W_c = (W_s - W_d) / (W_p - W_d) \times 100\% \quad (5.1)$$

where  $W_c$  represents actual coating weight percentage of polymer;  $W_s$ ,  $W_p$  and  $W_d$  denote weight loss percentage of the coating samples, polyurea and pure DCR at 270°C, respectively.

The polymer coating weight percentage under various stirring conditions were investigated. A

decrease of coating weight percentage of polyurea with increased stirring speed was observed in Figure 5.34. The detailed data is shown in Appendix E. At low stirring speed of 100 rpm, the coating weight percentage reaches 40%, which is close to the theoretical value of 44.9%. As the stirring speed is increased, strong hydrodynamic force “rips off” some of the polymer coating layer, therefore, results in a less amount of polyurea on the surface of DCR. The coating weight percentage decreases almost linearly with respect to the stirring speed. This result also partly accounts for the decrease of particle size when the stirring speed is increased.

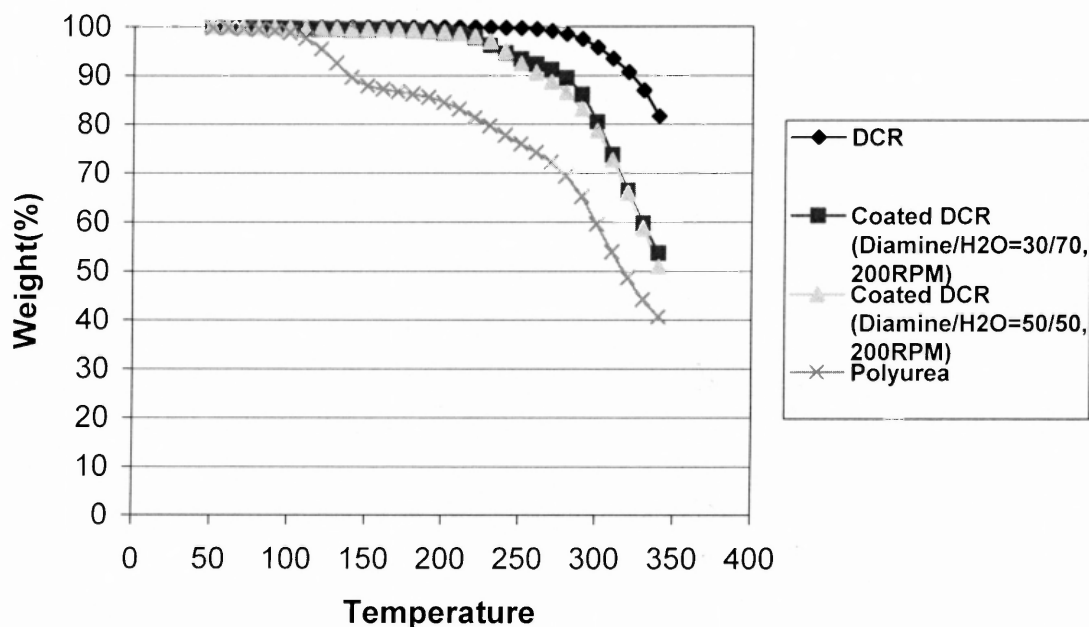


**Figure 5.33** Comparison of TGA spectra of pure DCR, polyurea-coated DCR and pure polyurea.



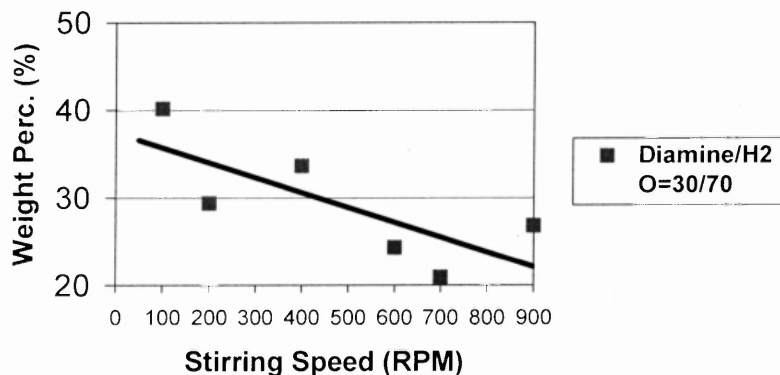


**Figure 5.34** Coating weight percentage of polyurea-coated DCR under various stirring speeds. (DCR/TDI=5g/2.5ml, Volume concentration of ethylene diamine is 30%)

#### 5.5.4 Application of Ionic Liquids in Particle Coating by IP

Two selected ionic liquids, [bmpm][BF<sub>4</sub>] and [bmpm][PF<sub>6</sub>], were used in the coating reaction, respectively, to explore the potential of applying ILs in coating fine particulates. The coating procedure is described in Section 4.3.4.

A rough surface and sharp edge was observed for the uncoated DCR particles as shown in Figure 5.35 (a). In contrast, a coated polymer layer exhibited a much smoother surface in Figure 5.35(b), which indicated the complete coating of the DCR by interfacial polymerization. In the presence of the ionic liquid, however, the polymer coating layer exhibited a coral-like porous structure, with the pore size around 100nm (See Figure 5.35(c) and (d)), which is consistent with the surface nanoporous structures described in 5.2.4, in terms of both the structure size and the shape. The unique surface features of the coating layer may have resulted from the intermolecular interactions between ionic liquids and polyurea as described

in Section 5.2.7. The effect of the coating substrate on those interactions needs to be studied in more details.

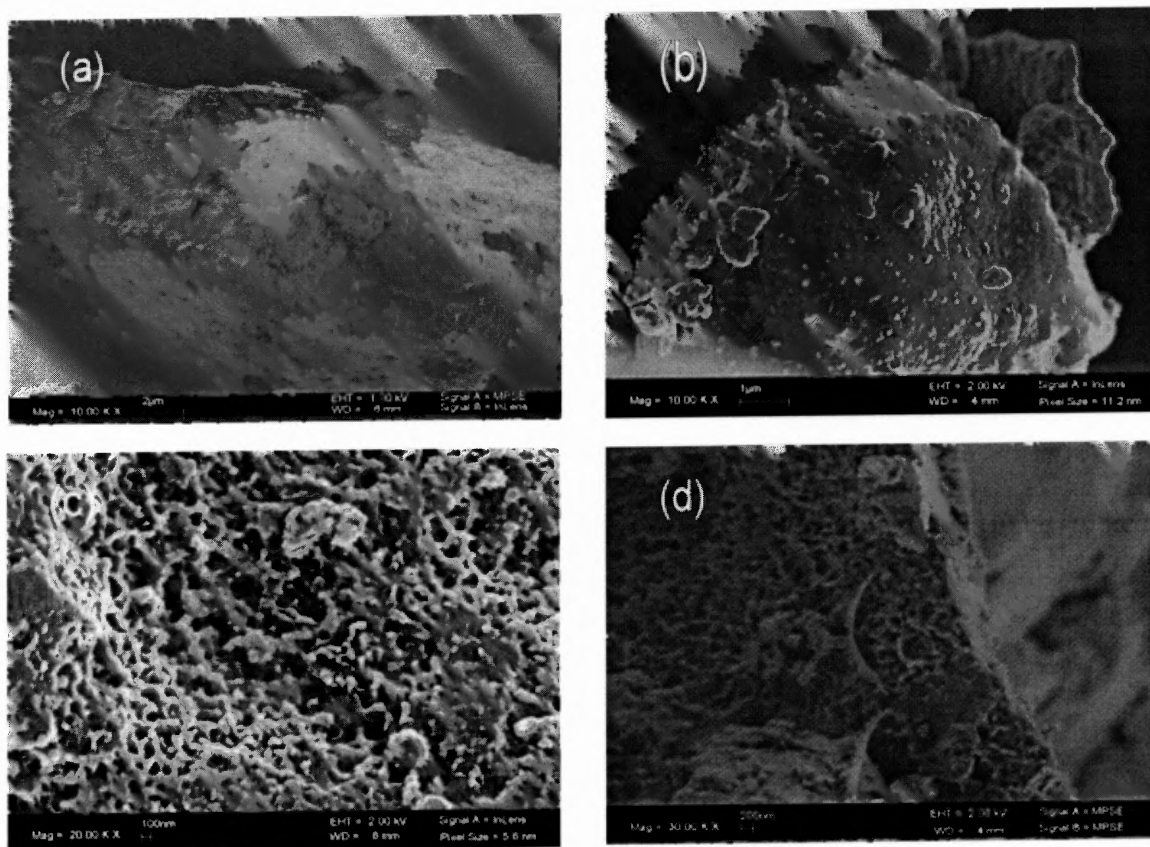


**Figure 5.35** SEM pictures for evaluation of DCR coating by IP of polyurea with ionic liquids: (a) bare DCR; (b) polyurea-coated DCR without IL; (c) polyurea-coated DCR with [bmpm][BF<sub>4</sub>]; (d) polyurea-coated DCR with [bmpm][PF<sub>6</sub>].

The formation of porous coating layer by interfacial polymerization in ionic liquids suggests a potential application of ionic liquids in microencapsulation or coating technique, where the porous polymer layer can be used in controlled release (Kim et al., 2005) and polymeric antireflection materials. (Walheim et al., 1999) However, further development of particulates coating or microencapsulation with room temperature ionic liquids has to be economically justified with the extent of commercialization of the IL.

## 5.6 Kinetics Study of Interfacial Polymerization in ILs

In this section, the study of the kinetics in interfacial polymerization with ILs is presented. The synthesis of nylon 610 at the [omim][BF<sub>4</sub>]/n-hexane interface (PA-HB8) was used as a model system for investigating the relations of the production rate and the reaction time at various reactant concentrations. The increase of the average molecular weight of polymer was monitored by measuring the intrinsic viscosity of the products. The microstructure evolution of the film with reaction time was monitored by SEM. A simplified diffusion-controlled mathematical model of IP with ILs was developed and fitted with the experimental results.

### 5.6.1 Mathematical Model of IP with ILs

It is well known that interfacial polymerization is a diffusion controlled reaction. In the present work, a simplified mathematical model is constructed to predict the growth of nylon 610 film at the n-hexane/[omim][BF<sub>4</sub>] interface. The mathematical model for a system under general consideration is illustrated in Figure 5.36.

In Figure 5.36, Regime I, II, III represent the IL phase, n-hexane phase, and interfacial reaction region (polymer film), respectively. The reactants in IL phase and n-hexane phase are hexamethylene diamine (HDA) and sebacyl chloride;  $L_1$ ,  $L_2$  and  $L$  represent the dimensions of regime I, II and III, respectively.  $c_{A0}$  and  $c_{Ab}$  stand for the initial concentration of HDA and the concentration at  $x_1=L_1$ , i.e. the IL/film interface, while  $c_{B0}$  and  $c_{Bb}$  denote the initial concentration of sebacyl chloride and the concentration at  $x_2=L_2$ , i.e. the n-hexane/film interface, respectively.  $x_1$ ,  $x_2$  and  $y$  denote the one-dimensional coordinates of the three regimes as shown in the figure.

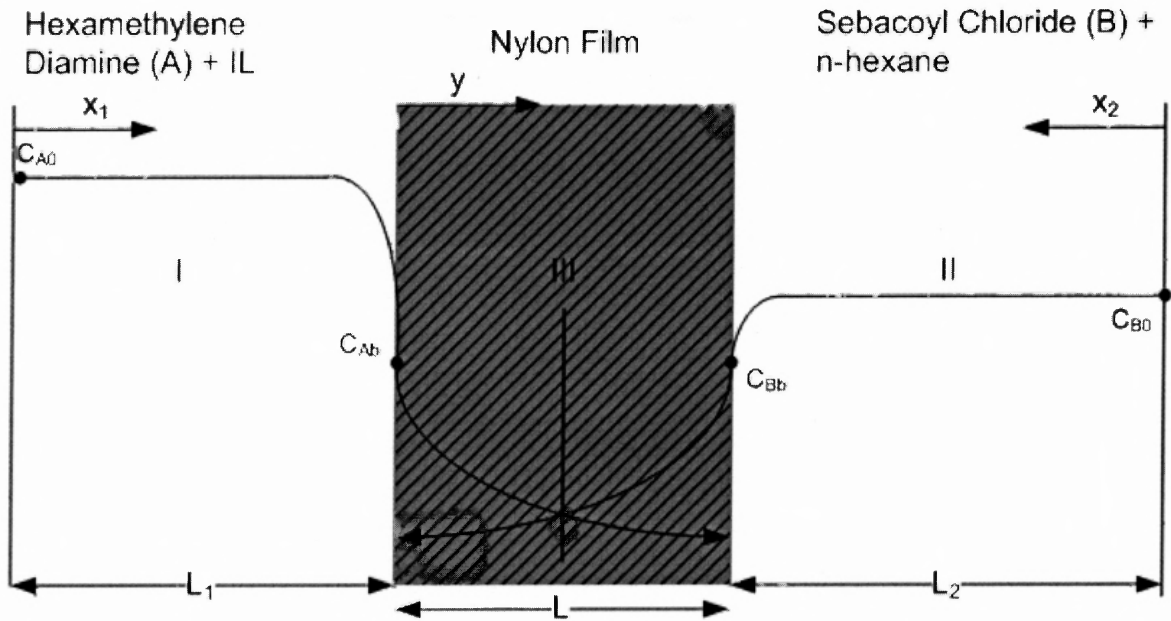


**Figure 5.36** Schematic illustration of interfacial polymerization model at the n-hexane/IL interface.

Morgan, 1965 reported that the interfacial polymerization rate is sensitive to the initial concentrations of both monomers, and the reaction rate was within the order between  $10^{-1} \sim 10^3$   $\text{m}^3/\text{mol} \cdot \text{s}$ . Karode et al., 1998 reported an apparent reaction rate constant of  $700 \text{ kmol}/\text{m}^3 \cdot \text{s}$  by fitting experimental data (Johnson, 1985). In this work, the polymerization is assumed to be a second order reaction that is proportional to the concentrations of both reactants. The general governing equations for the concentrations in the three regimes can be written as follows.

### Regime I

$$\frac{\partial c_A}{\partial t} = D_1 \frac{\partial^2 c_A}{\partial x_1^2}$$

$$I.C.: t = 0, c_A(x_1, 0) = c_{A0}$$
(5.2)

$$B.C.1: x_1 = 0, \frac{\partial c_A}{\partial x_1} = 0$$

$$B.C.2: x_1 = L_1, -D_1 \frac{\partial c_A}{\partial x_1} = -D_A \frac{\partial c_A}{\partial y} \Big|_{y=0}$$

**Regime II**

$$\frac{\partial c_B}{\partial t} = D_2 \frac{\partial^2 c_B}{\partial x_2^2}$$

$$I.C.: t = 0, c_B(x_2, 0) = c_{B0}$$

$$B.C.1: x_2 = 0, \frac{\partial c_B}{\partial x_2} = 0$$

$$B.C.2: x_2 = L_2, -D_2 \frac{\partial c_B}{\partial x_2} = D_B \frac{\partial c_B}{\partial y} \Big|_{y=L}$$
(5.3)

**Regime III**

$$\frac{\partial c_A}{\partial t} = D_A^{eff} \frac{\partial^2 c_A}{\partial y^2} - kc_A c_B$$

$$\frac{\partial c_B}{\partial t} = D_B^{eff} \frac{\partial^2 c_B}{\partial y^2} - kc_A c_B$$

$$I.C.1: t = 0, c_A = c_{A0}$$

$$I.C.2: t = 0, c_B = c_{B0}$$

$$B.C.1: y = 0, -D_A \frac{\partial c_A}{\partial y} = -D_1 \frac{\partial c_A}{\partial x_1} \Big|_{x_1=L_1}$$

$$B.C.2: y = 0, c_B = 0$$

$$B.C.3: y = L, -D_B \frac{\partial c_B}{\partial y} = D_2 \frac{\partial c_B}{\partial x_2} \Big|_{x_2=L_2}$$

$$B.C.4: y = L, c_A = 0$$
(5.4)

where  $D_1$  and  $D_A^{eff}$  represent the diffusivities of HDA in the IL phase and in the polymer film, respectively;  $D_2$  and  $D_B^{eff}$  stand for the diffusivities of sebacyl chloride in the n-hexane phase and in the polymer film, respectively. The rate of change of the polymer film thickness  $L$  can be expressed as

$$(1 - \varepsilon) \frac{\rho_p A}{M_w} \frac{dL}{dt} = A \int_0^{L(t)} kc_A(t)c_B(t)dy$$
(5.5)

where  $\rho_p$  and  $M_w$  are the density of the polymer and the molecular weight of the repeat unit, respectively.  $A$  is the surface area of the interface,  $k$  is the reaction constant.  $\varepsilon$  is the time-dependent porosity of the film which can be expressed as:

$$\varepsilon(t) = 1 - \frac{V_p(t)}{V_{film}(t)}. \quad (5.6)$$

$V_p(t)$  is the volume of the synthesized polymer;  $V_{film}(t) = AL$  is the apparent volume of the film. The effective diffusivities of the reactants in the porous polymer film are functions of the porosity and the tortuosity, which can be expressed as: (Cussler, 1991; Winston Ho and Sirkar, 2001)

$$D_i^{eff}(t) = \frac{D_{io}\varepsilon(t)}{\tau(t)} \quad ; i = A \text{ and } B, \quad (5.7)$$

where  $\tau$  is the tortuosity and is dependent on the structures of the pores;  $D_{io}$  is the free diffusivity of reactant A and B at  $t=0$ .

The solution for the above equations in principle can be solved by numerical methods if adequate information for the parameters and the porous polymer film is provided. Nevertheless, it is difficult to have the effective diffusivities of the reactants inside the porous polymer film measured since the structure of the nylon film changes with time. The effective diffusivities are thus affected by and reversely affecting the kinetics of the morphological development of the polymer film. Despite many publications addressing the kinetics of interfacial polymerization in the past several decades, the structural changes and the time-dependence of the effective diffusivity inside the polymer film were not well discussed. Interestingly, the effective diffusivities in polymer film of any interfacial polymerization are the kernel of the diffusion-control process. Many studies in the past have focused on the mass transfer in both the liquid phases, either under quiescence or with convection, and their impacts

to the kinetics of the film thickness. The mass transfer in liquid phase plays a rather insignificant role in the slowing down of the polymerization compared to the barrier from the polymer film at the interface. However, hydrodynamics forces may affect the kinetics of the phase separation during the formation of the polymer films and thus affect the structure and the effective transport property associated with it.

In this work, a simplified diffusion-controlled model is derived to calculate the mass flux on both sides of the bulk phases into the interfacial reaction zone. The following assumptions were made:

- 1) The mass of the polymer product is proportional to the thickness of the polymer film and can be expressed as  $M_p = (1-\varepsilon)\rho_p AL$ , where  $M_p$  is the mass of the polymer film.
- 2) The reaction of IP occurs instantly when the two reactants encounter each other (diffusion-control limit); the growth of  $L$  is therefore dictated by the diffusion of the monomers.
- 3) The reaction takes place at the vicinity of the IL/polymer interface. This assumption is primarily based on the large difference in viscosities between n-hexane and [omim][BF<sub>4</sub>]. The diffusivity of the solute in solvent is largely dependent on the solvent viscosity. The relationship between diffusivity and solvent viscosity for non-aqueous solvents can be correlated by  $D \propto \eta^q$ , where  $D$  is the diffusivity,  $\eta$  is the solvent viscosity, and the value of  $q$  varies from -0.5 to -1 (Reid et al., 1988). The viscosity of n-hexane at 20°C is 0.3 mPa·s. The viscosity of [omim][BF<sub>4</sub>] is 239 mPa·s at 25°C as measured by Ubbelohde viscometer in our lab; the viscosity of [omim][BF<sub>4</sub>] is at least 800 times larger than that of n-hexane.

Therefore, the diffusivity of sebacoyl chloride in n-hexane is estimated to be  $10^2$ - $10^3$  times larger than the diffusivity of HDA in [omim][BF<sub>4</sub>].

- 4) Assuming a thin film is formed, the concentration profile through the polymer film is considered to be linear. The diffusion of sebacoyl chloride in the polymer film is further regarded as in a pseudo-steady state.

Based on the above assumptions, a simplified model is illustrated in Figure 5.37. From mass balance, Eq. (5.5) can be written as

$$(1 - \varepsilon) \frac{\rho_p A}{M_w} \frac{dL}{dt} = k c_A c_B \cdot A \quad (5.8)$$

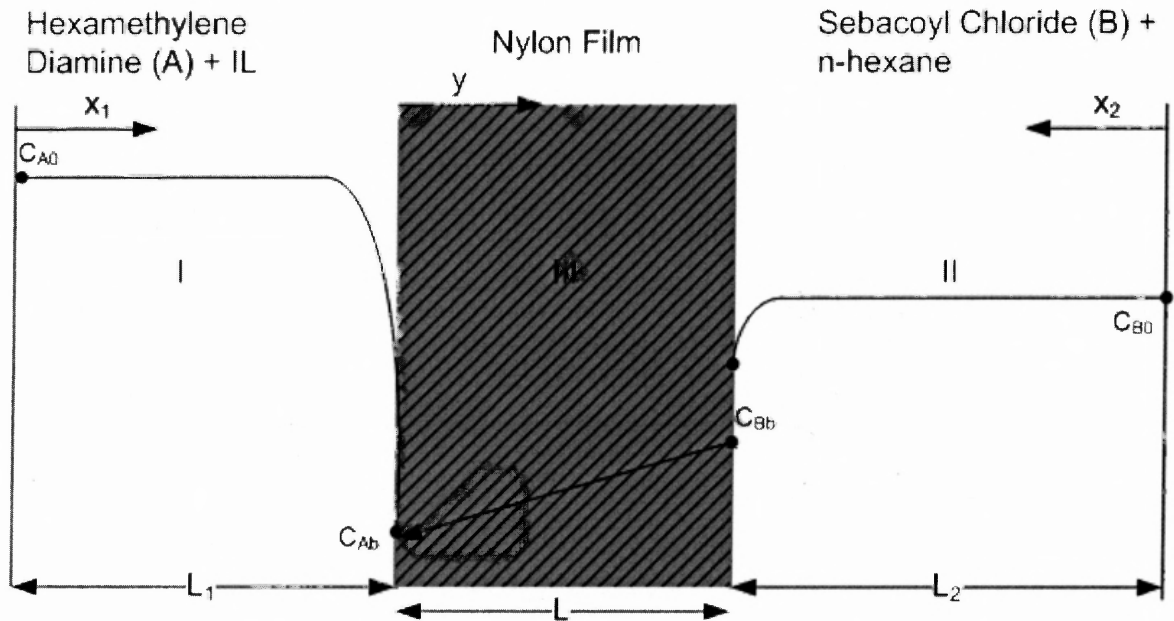


**Figure 5.37** Conceptual illustration of simplified IP model at the n-hexane/IL interface.

From the assumption of pseudo-steady state, the mass flux across the polymer film is balanced with reaction rate and is expressed as:



$$D_B^{eff} \frac{c_{Bb} - c_B}{L} = kc_A c_B \quad (5.9)$$

By combining Eq. (5.8) and Eq. (5.9), we have

$$\frac{\rho_p A}{M_w} \frac{dL}{dt} = -\frac{D_B^{eff}(t) \Delta c}{(1-\varepsilon) L} \cdot A = -\frac{D_{Bo} \varepsilon}{\tau(1-\varepsilon)} \frac{\Delta c}{L} \cdot A, \quad (5.10)$$

where  $\Delta c$  is the concentration difference of sebacoyl chloride between the two sides of the film, which is regarded as a constant after a certain period of induction time when the diffusion control limit is also reached. Under the assumption of diffusion control limit, the porosity must be adequately small; the term  $(1-\varepsilon)$  in the denominator can thus be approximated as one. Nevertheless, the time dependence of the porosity and the tortuosity are still not known. An assumption of a power-law relation is proposed hereby in order to facilitate our analysis, i.e.

$\frac{\varepsilon}{\tau} \propto t^{-n}$  for large  $t$ . Therefore the effective diffusivity can be expressed as:

$$D_B^{eff}(t) = D_{Bo} \frac{1}{1 + a^2 t^n}, \quad (5.11)$$

where  $a$  is a constant related to the decaying rate of the diffusivity;  $n$  is the exponent that characterizes the time-dependent diffusivity. The time-dependent diffusivity is originated from the continuous coarsening of the polymer that reduces the pore size of the film and renders a growing barrier to diffusion. This proposed effective diffusivity will be tested by the growth kinetics of the film and the morphological development of the nylon films observed under SEM, which will be shown in the following two sections.

Note that when  $n=0$ , the diffusivity has no dependence of time; the thickness of the polymer layer is thus proportional to the square root of time, i.e. the growth of the film will stop only until the limiting reactant is used up when the conversion is 100%. This particular case has been widely employed in many previous studies of interfacial polymerization. If

$n=1$ , the thickness will marginally diverge with time until the conversion is 100%. Only when  $n>1$ , the thickness will saturate to a finite thickness. Since currently there is no adequate information and satisfactory model to predict the kinetics of the structure change of the film, we will integrate Eq. (5.10) with selections of  $n=1$  and  $n=2$  and continue the analysis. Substituting Eq. (5.11) into Eq. (5.10) and integrating the equation give the polymer film thickness as follows:

$$\text{for } n=1, \quad L^2 = \frac{2M_w D_{B0} \Delta c}{\rho_p a^2} \ln(1 + a^2 t) \quad (5.12)$$

$$\text{for } n=2, \quad L^2 = \frac{2M_w D_{B0} \Delta c}{\rho_p a} \tan^{-1}(at) \quad (5.13)$$

Since  $M_p \approx \rho_p A L$  for small  $\varepsilon$ , Eq.(5.12) and (5.13) can be expressed as:

$$n=1, \quad M_p = \sqrt{K' \ln(1 + a^2 t)}, \quad \text{where } K' = \frac{2M_w D_{B0} \Delta c \rho_p A^2}{a^2} \quad (5.14)$$

$$n=2, \quad M_p = \sqrt{K \cdot \tan^{-1}(at)}, \quad \text{where } K = \frac{2M_w \rho_p A^2 D_{B0} \Delta c}{a} \quad (5.15)$$

These equations will be examined by the experimental data of nylon 610 produced at different time. The model parameters can be obtained by data fitting.

## 5.6.2 Experimental and Modeling Results

The kinetics study was conducted by measuring the mass of the product PA-HB8 at different time after the beginning of the polymerization. The controlled process parameters are the initial concentrations of the reactants. All reactors have the same cross-section area of

3.96cm<sup>2</sup>. Detailed data of the conversions and product mass of the nylon films against the reaction time are given in Appendix F and Appendix G, respectively.

Figure 5.38 depicts the conversion-time curves of PA-HB8 under a constant initial concentration (1.25M) of HDA but different initial concentrations of sebacoyl chloride (SC): 0.42M, 0.84M, and 1.25M. In the case of [HDA]/[SC]=1.25M:0.42M, the curve shows a rapid increase of conversion with time at the first three hours; the final conversion of the nylon is 27.48%. In the case of [HDA]/[SC]=1.25M:0.84M, the curve shows a higher slope at the first hour followed by a slow growth to level off. The final conversion of the nylon is 32.82%. In the case of [HDA]/[SC]=1.25M:1.25M, the curve exhibits a much steeper increase within the first 40 min; the final conversion of the nylon is 28.37%. An interesting observation is that despite the final products have different amounts, their conversions are similar (between 27-32%). Under the same concentration of HDA, the higher the concentration of sebacoyl chloride, the higher the reaction rate and the final mass of the product observed. As shown in Appendix D, the relation of the reactant concentration and the more the final product mass can be used to control the film thickness in the reaction.

All three curves above exhibit an initial rapid increase of the conversion followed by a level-off. The expected level-off is due to the fact that the precipitated polymer film becomes a barrier to the diffusion of the reactants, as explained in Sect. 5.6.1. These curves reveal how the final thickness of the film changes with the reaction conditions and how fast the final thickness is reached. One of the advantages of using interfacial polymerization for coating or microencapsulation is that there is no need for stoichiometric balance. Nevertheless, the maximum coating thickness and the characteristic time to reach such a thickness are important

parameters for process design. The characteristic time of the IP will be discussed in detail in the following section.

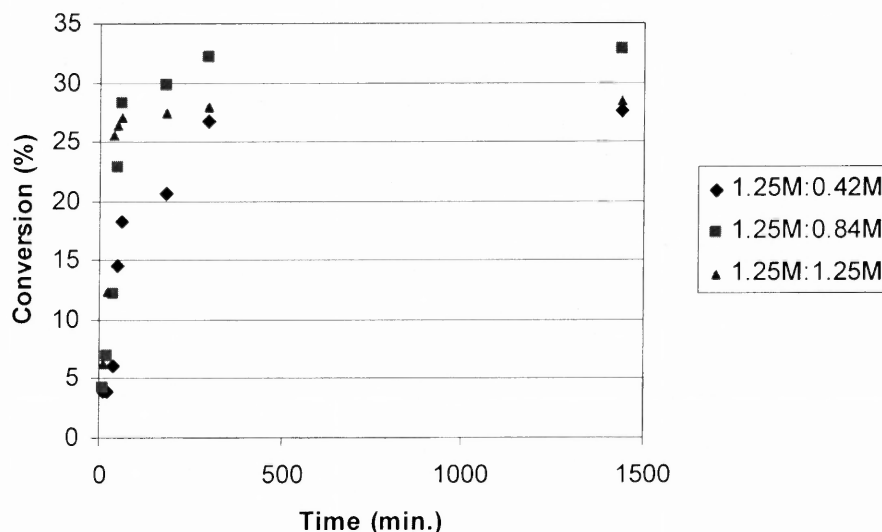


**Figure 5.38** Reaction conversion of polymer products vs. time of nylon 610 synthesized at the [omim][BF<sub>4</sub>]/n-hexane interface with a constant concentration of HDA (1.25M) but different concentrations of sebacyl chloride (0.42, 0.84, and 1.25M).

The conversion-time curves of the nylon synthesized under a constant concentration of SC (0.42M) but different concentrations of HDA (0.42M, 0.84M, 1.25M) are depicted in Figure 5.39. All three curves exhibit similar features as in Figure 5.38, i.e., the conversion increase rapidly in the beginning of the reaction and level off after a characteristic time. The final conversion depends on the reactant concentration. Unlike the cases in Figure 5.38, the conversions show a rather drastic decrease with the HDA concentration from 28% to 12%.

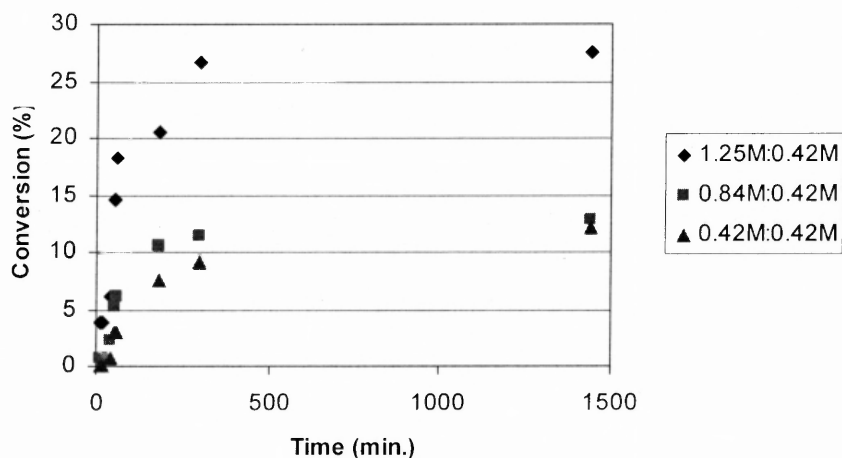


**Figure 5.39** Mass of polymer products vs. time of nylon 610 synthesized by IP at the [omim][BF<sub>4</sub>]/n-hexane interface with a constant concentration of SC (0.42M) but different concentrations of HDA (0.42, 0.84, and 1.25M).

### 5.6.3 Comparison of Theoretical Prediction and Experimental Data

The experimental data from Figures 5.38 and 5.39 were fitted with the theoretical model discussed in Sect. 5.6.1. Since the film thickness is proportional to the mass and if the effective densities of the films are the same, the conversion-time curves can be used for direct comparison with Eq. (5.14)  $M_p = \sqrt{K' \ln(1 + a^2 t)}$  and Eq. (5.15)  $M_p = \sqrt{K \cdot \tan^{-1}(at)}$ . The parameters used in these equations were obtained via data regression by mathematical software Polymath<sup>®</sup> 6.10. It was found that Eq. (5.15) gave better fitting results for all the curves compared to Eq. (5.14). Thus obtained model parameters for different initial reactant concentrations are listed in Table 5.5.

**Table 5.5** Parameters used in the model described by Eq.(5.15)

Sample	Reactant concentration ratio (HDA/sebacoyl chloride)	K	$\alpha$	R <sup>2</sup> value
A	1.25M:0.42M	0.00090	0.0072	0.90
B	1.25M:0.84M	0.0050	0.020	0.89
C	1.25M:1.25M	0.00775	0.0718	0.90
D	0.84M:0.42M	0.0002072	0.00515	0.90
E	0.42M:0.42M	0.0001943	0.002399	0.90
F	0.42M:1.25M	0.00075	0.00765	0.90

Note: Equation (5.15) gives  $M_p = \sqrt{K \cdot \tan^{-1}(at)}$ .

Figure 5.40 depicts the comparison of the experimental data with the calculation results from Eq. (5.15). It is found that the proposed model agrees satisfactorily with the experimental data, especially for the ones with high reactant concentration. However, slight deviations were found at the early stage of the reaction for cases of low reactant concentration; this is mainly due to a longer period of induction time needed to form a film. The progression of the time-dependent structures will be shown later. Note that the agreement of the model described by Eq. (5.15) and the experimental data also suggest that the effective diffusivity of the reactant in the film decays as  $t^{-2}$ . As discussed in section 5.6.1, the decrease of the diffusivity is originated from the continuing polymerization and the coarsening of the precipitated polymer.

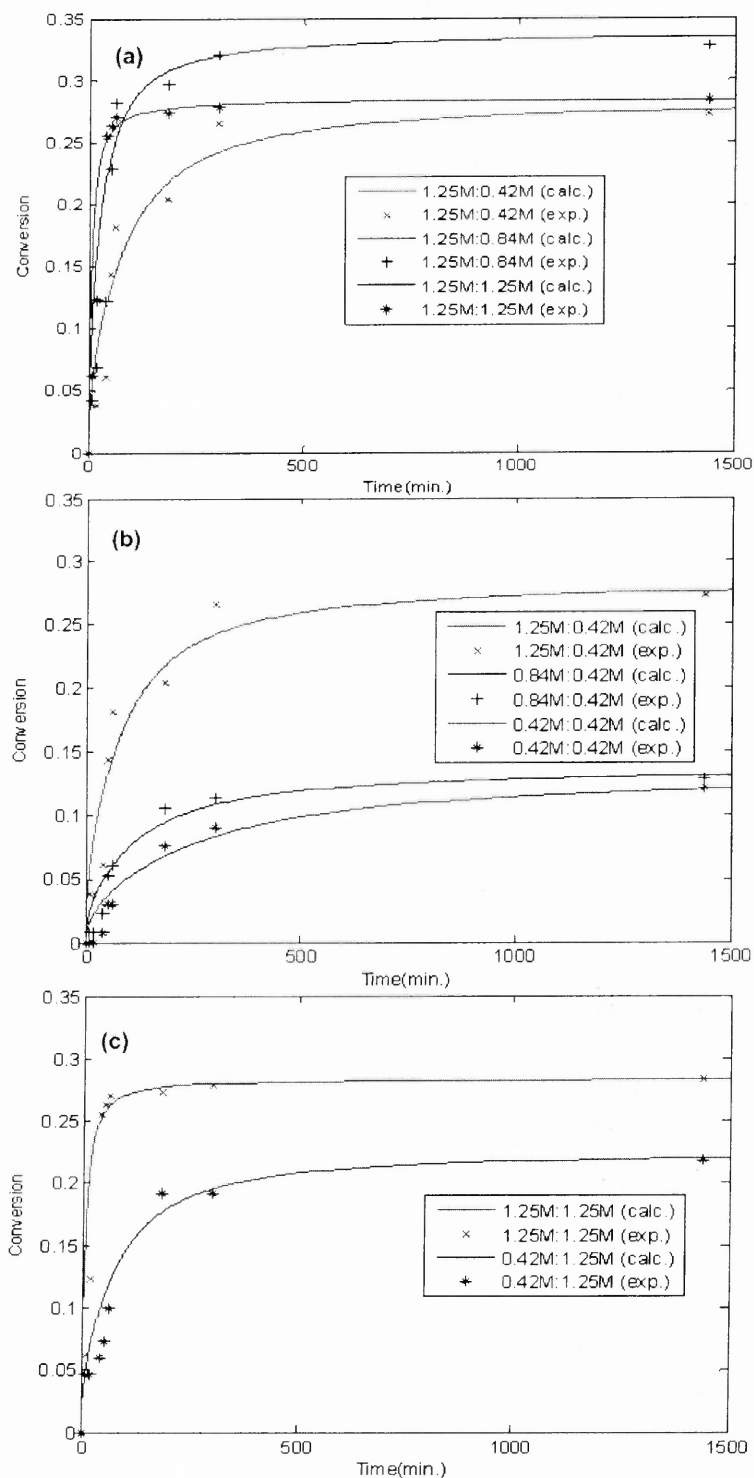


**Figure 5.40** Comparison of the prediction (solid line) and the experimental data (symbols) for the conversion of PA-HB8 as a function of reaction time at various [HDA]/[SC] concentrations: (a) Samples A, B, and C; (b) Samples A, D, and E; (c) Samples C and F.

**Table 5.6** Final conversions and product mass of Nylon 610 and the characteristic times for various reactant concentrations predicted by mathematical modeling.

Sample	Mole Concentration [HDA]/[Sebacoyl Chloride]	Final conversion (%)	Final Product Mass (mg)	Characteristic Time $\tau_c$ (min.)*
A	1.25:0.42	28.41	37.5	440
B	1.25:0.84	33.39	87.5	146
C	1.25:1.25	28.37	110	40
D	0.84:0.42	13.64	18	618
E	0.42:0.42	12.88	17	1087
F	0.42:1.25	22.51	34	389

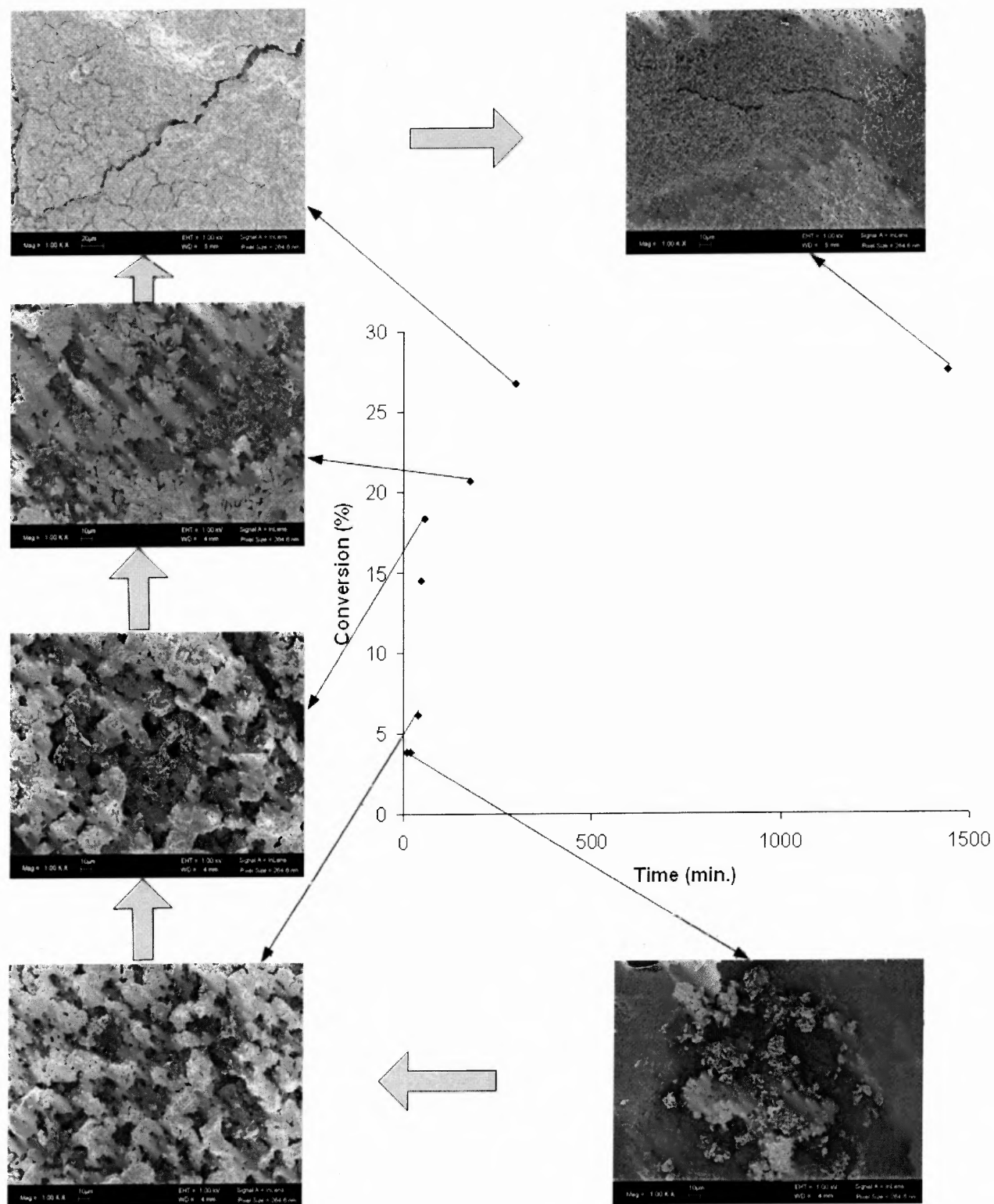
\*  $\tau_c$  is the characteristic time when the conversion reached 90% of the final conversion.

Table 5.6 depicts the predicted results of the final conversion, the mass of the products and the characteristic times under various reactant concentrations. The characteristic time  $\tau_c$  is defined as the time when the reaction conversion reached 90% of the final conversion, which is very useful in the the applications of IP such as coating and membrane fabrication. Comparing samples A, B, and C which have the same HDA concentration, the final mass increases linearly to 3-fold with the concentration of SC and the  $\tau_c$  decreases linearly to 11-fold. However, with a lower HDA concentration as in samples E and F, the changes become milder. Comparing samples F and C of the same SC concentration (1.25M), the final mass increased by 3-fold and  $\tau_c$  decreased by 10-fold. Similarly, if the SC concentration is lowered as in samples A, D, and E, the changes become milder again. From the table, it is concluded that the contributions from the concentrations of the two reactants to the final mass and the  $\tau_c$  are rather symmetric. The largest gradient to produce a designated film thickness within a shortest time is to follow



the path of equal concentrations of the reactants. On the other hand, comparing the final conversions of samples A, B and C, it is shown that the conversions of the three samples are quite consistent, within a narrow range between 28-33%. It indicated that at a high HDA concentration (1.25M), the variation of the TDI concentration has no significant effect on the final conversion. However, keeping TDI concentration at 0.42M, when the HDA concentration is lowered to 0.84M and 0.42M, as sample D and E shown, the conversions were drastically reduced from 28% to 12%.

Figure 5.41 shows the morphology change of the PA-HB8 films ([HDA]:[SC] = 1.25M:0.42M) with reaction time. Magnified SEM pictures were shown in Figure 5.42. As shown in Figure 5.41, at the very early stage of the polymerization (Figure 5.42 (a),  $t=20\text{min.}$ ), the reaction conversion is very low, and the product exhibits small random aggregates of polymer rather than a uniform film. In this “induction period”, the polymer does not have adequate mechanical strength to be a film; the molecular weight is also not large enough. As the reaction proceeds further, both the average molecular weight and the amount of the product increase; a porous film is formed, and the polymer film grows at a rapid rate in this period (Figure 5.42 (b)-(d)). At the late stage of the IP, the film becomes less porous and much denser, and the morphology is more uniform (Figure 5.42 (e) and (f)), thus hindering the diffusion and contact rate of the reactants, leading to a level-off of the conversion-time curve. The observation is consistent with the assumption made by Eq.(5.11) in the simplified model proposed in section 5.6.1, where the effective diffusivity  $D_B^{eff}$  was assumed to decay with the reaction time due to the change of the structures of the film.



**Figure 5.41** Illustration of the relationship between morphology change and film growth of the nylon 610 film prepared with [omim][BF<sub>4</sub>]. ([HDA]/[SC]=1.25M:0.42M)

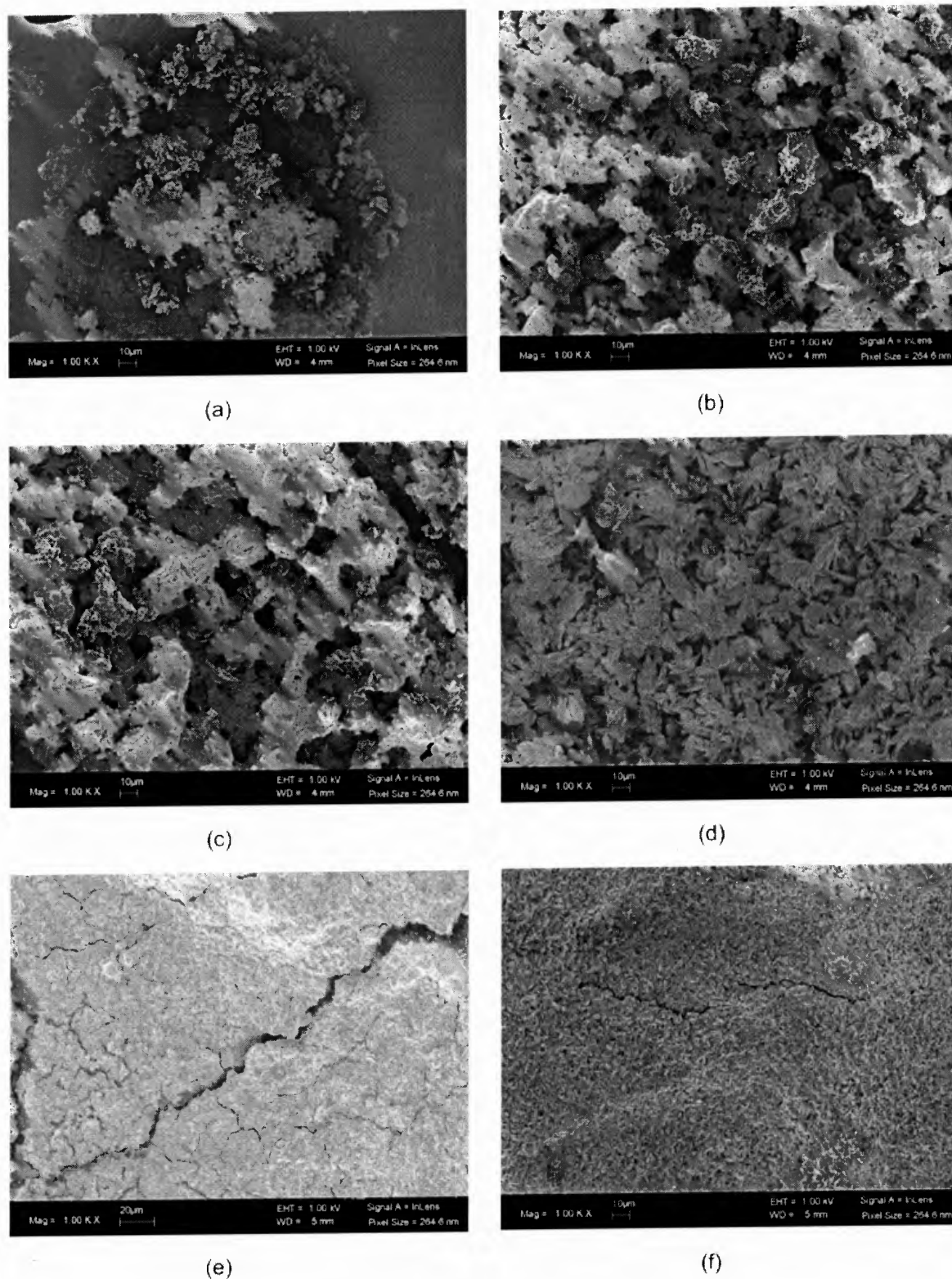


**Figure 5.42** SEM images of nylon 610 film prepared with [omim][BF<sub>4</sub>] at different reaction times ([HDA]/[SC]=1.25M:0.42M): (a) 20min; (b) 40min; (c) 60min; (d) 180min; (e) 300min; (f) 24 hours.

#### 5.6.4 Molecular Weight versus Reaction Time

The relationship between the polymer molecular weight and the polymerization time was investigated by measuring the intrinsic viscosity of the PA-HB8 ([HDA]:[SC]=1.25M:0.42M) samples collected at various reaction time. The intrinsic viscosity can be correlated to the molecular weight by Mark-Houwink equation. Though there are no available Mark-Houwink coefficients for the nylon 610/H<sub>2</sub>SO<sub>4</sub> system, the changes of intrinsic viscosity indicate the changes of the molecular weight against time. The results are listed in Table 5.7. As shown in Figure 5.43, the intrinsic viscosity curve increases drastically at the early stage of the polymerization, slows down after 40 min, and levels off at the late stage of the reaction. The characteristic time for the saturation of the intrinsic viscosity is about 40 min, which is much shorter than the characteristic time in the mass-time curve (440 min, sample A in Table 5.5). This suggests that after the early stage of polymerization ( $t > 40$  min.), the growth of longer polymer chains was suppressed due to the precipitation of the polymer. Had counter-diffusion of both reactants occurred in the film, i.e. the main reaction zone were at the middle of the film, longer chains would continue propagating and the average molecular weight would have increased constantly. The faster saturation of the molecular weight compared to the mass of the product supports the hypothetical model discussed in Section 5.6.1 in which the main reaction zone was proposed to occur at the liquid-solid interface.

**Table 5.7** Intrinsic viscosity ( $[\eta]$ ) of the synthesized PA-HB8 ([HDA]:[SC] = 1.25M:0.42M) as a function of reaction time

Reaction Time (min.)	$[\eta]$ (100ml/g) <sup>a</sup>
10	0.30
20	0.54
40	0.69
50	0.70
60	0.72
180	0.73
300	0.73
1440	0.73

<sup>a</sup>98% H<sub>2</sub>SO<sub>4</sub> is used as the solvent; polymer concentration is 0.1g/100ml.

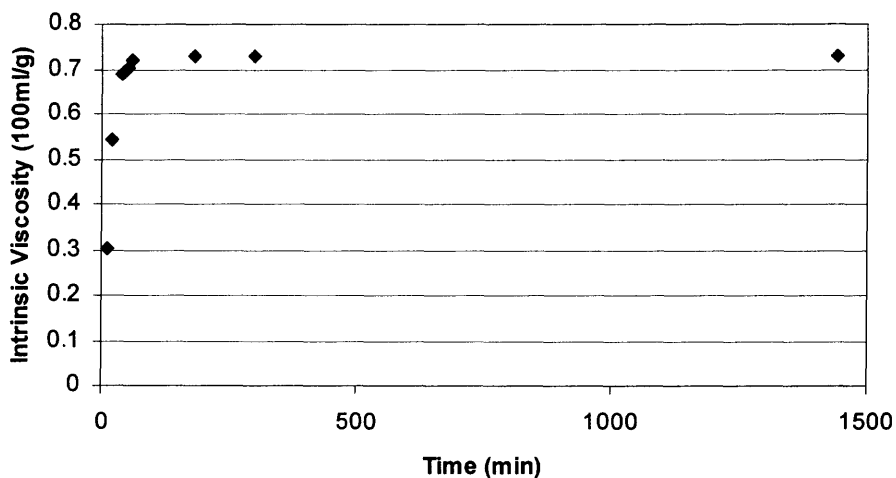


**Figure 5.43** Intrinsic viscosity ( $[\eta]$ ) of the synthesized PA-HB8 ([HDA]:[SC] = 1.25M:0.42M) versus the reaction time.

## CHAPTER 6

### CONCLUSIONS AND RECOMMENDATIONS FOR FUTURE WORK

#### 6.1 Conclusions

Low interfacial tensions between the 1-alkyl-3-methylimidazolium ILs and two organic solvents: n-hexane and toluene, were found to decrease with increased alkyl chain length attached to the IL cation, which could be ascribed to the descending polarity of the ILs as well as more exposure of the methyl group to the interface.

Self aggregations of ILs in aqueous solutions were studied by the measurement of interfacial tension between n-hexane and IL aqueous solutions at various concentrations. A critical aggregation concentration (CAC) of 0.75M and 0.9M was identified for [bmim][BF<sub>4</sub>] and [bmpm][BF<sub>4</sub>], respectively. Using the same method, the formation of inverse phase aggregates of ethanol in [hmim][BF<sub>4</sub>] and [omim][BF<sub>4</sub>] was found, with CAC of 1.2M and 0.8M for the two systems, respectively.

By applying IL as a reaction medium in interfacial polymerization, a series of polyureas with exotic nanoscale structures such as nanofibrils or nanoporous network with sizes ranging from 50~500nm, were synthesized at room temperature. FTIR spectra of the polyureas synthesized with water phase and those prepared with ILs showed no significant change of chemical compositions, implicating that the observed nanostructures originated from the kinetics of phase separation. XRD data show a suppression of the 3-D crystalline structure in the presence of ILs. Nanostructures of different shape and size were also found in the polyureas synthesized at the IL aqueous solution/n-hexane interfaces. FTIR results suggest the existence of rather significant intermolecular interactions between the IL molecules and the

polymer, which is hypothetically regarded as a major mechanism of the nanostructure formation. Typical factors affecting the polymeric surface nanostructures include: the reactant monomer, anions of the ILs, and alkyl chain length of cations.

Nylon films, synthesized with ILs, exhibit better thermal stability and higher molecular weight compared to the films synthesized at the water/n-hexane interface; the enhanced properties may be attributed to the elimination of the side reaction between TDI and water, and thus increase the polymer molecular weight. By using different ILs, rough surface morphologies, such as nanoparticle aggregates or porous structures, were observed on the film surface. No significant difference in surface morphology was found due to the difference in the alkyl chain lengths of the diamine.

Fine particulates coating process with IP has been studied. The effects of the stirring speed and the reactant concentration were studied through SEM examination, particle size analysis, and coating weight percentage. Increased stirring speed in the coating process leads to a decreased mean particle size and coating weight percentage, as well as a narrower particle size distribution. A porous coating layer was found on the surface of the core particles by incorporating IL in the coating process.

The kinetics study of nylon film growth with ILs confirmed the observation in previous studies that a diffusion barrier formed by the film results in a level-off of the conversion and the film ceases to grow. The characteristic reaction time marking the level-off largely depends on the initial monomer concentrations and varies from 1 hour to 3 hours as measured in this work. A simplified diffusion-controlled IP model, in which the effective diffusivity  $D^{eff}$  is assumed to be inversely proportional to the square of the reaction time  $t$ , i.e.  $D^{eff} \propto \frac{1}{t^2}$ , is found to fit the growth rate of the nylon film well. The calculated results agree quite well with

the experiment, though slight deviations were found at an early stage of the reaction for systems of low monomer concentrations. The relationship between the morphology change of the polymer film and time was examined by SEM. The porosity of the film is found to change with time.

## 6.2 Recommendations for Future Work

Future work is recommended in the following aspects:

### 1. Study of the self-aggregation behavior of ionic liquids in water and in other organic solvents

Small angle neutron scattering (SANS) is suggested for probing the size and shape of the IL self-aggregation in the aqueous solution under various IL concentrations. The effect of the IL molecular structure on aggregation can also be investigated by SANS and conductivity measurement. In addition, the inverse phase aggregates of organic solvents in ILs can be studied by using deuterated organic solvents, e.g. deuterated ethanol.

### 2. The mechanism of the morphology formation by IP with ILs

In this dissertation, polyureas with nanoporous or nanofibrous structures were synthesized by IP at the IL/n-hexane interface. Interactions between the IL molecules and polymer were found by the FTIR spectra. It is recommended that solid state NMR study can be employed, in order to probe the details of bonding connectivity and orientation, as well as to understand the origin of the polymeric nanostructure formation in ILs.

### 3. Exploration of IP in ILs in other polymer systems and their applications

The extension of IP in ILs to other polymers, as well as the optimization of various reaction parameters such as the reactant concentration and reaction media, is recommended to be studied in the future.



The porous polymer coating layer formed by the incorporation of ILs, as well as the polymeric surface nanostructures fabricated by IP in ILs, implied a potential application of this technique in those areas where nanoporous structures are desired. Typical examples include macroporous membrane architectures.

## APPENDIX A

### INTERFACIAL TENSION BETWEEN IONIC LIQUIDS AND ORGANIC SOLVENTS

Ionic Liquids	Interfacial Tension with n-Hexane (Dynes/cm)	Interfacial Tension with Toluene (Dynes/cm)
[emim] <sup>+</sup> [BF <sub>4</sub> ] <sup>-</sup>	23.0	8.5
[bmim] <sup>+</sup> [BF <sub>4</sub> ] <sup>-</sup>	15.0	4.6
[hmim] <sup>+</sup> [BF <sub>4</sub> ] <sup>-</sup>	9.1	2.2
[omim] <sup>+</sup> [BF <sub>4</sub> ] <sup>-</sup>	4.2	soluble
[bmim] <sup>+</sup> [PF <sub>6</sub> ] <sup>-</sup>	13.9	3.8
[hmim] <sup>+</sup> [PF <sub>6</sub> ] <sup>-</sup>	8.1	1.5
[bmpm] <sup>+</sup> [BF <sub>4</sub> ] <sup>-</sup>	12.7	3.5
Water	50.6	34.2

## APPENDIX B

### INTERFACIAL TENSION BETWEEN N-HEXANE AND IONIC LIQUID AQUEOUS SOLUTIONS\*

Conc. (Wt%)	0	5	10	15	20	25	30	50	80	100
[emim][BF <sub>4</sub> ]	50.6 (0.46)	37.8 (0.88)	35.1 (0.48)	33.7 (0.49)	30.5 (0.09)	29.9 (1.08)	29.3 (0.48)	26.6 (0.24)	23.0 (1.22)	23.0 (0.31)
[bmim][BF <sub>4</sub> ]	50.6 (0.46)	27.0 (0.32)	20.1 (0.38)	16.0 (0.66)	15.9 (0.35)	15.9 (0.68)	15.3 (0.26)	16.4 (0.26)	16.4 (0.37)	15.0 (0.72)
[bmpm][BF <sub>4</sub> ]	50.6 (0.46)	20.1 (0.70)	15.0 (0.46)	10.1 (0.47)	9.1 (0.46)	10.2 (0.08)	11.3 (0.67)	12.7 (0.08)	13.3 (0.25)	12.7 (0.64)

\*All the data in the above table are measured by ring method at room temperature, and the unit is dyne/cm. The numbers in the parentheses are standard deviation of the experiments.

## APPENDIX C

### PARTICLE MEAN SIZE OF POLYUREA-COATED DCR UNDER VARIOUS STIRRING CONDITIONS\*

Stirring Speed (rpm)	Particle mean size at 30% EDA volume concentration( $\mu\text{m}$ )	Particle mean size at 30% EDA volume concentration( $\mu\text{m}$ )
100	488.1	746.2
200	517.7	410.4
400	309.3	339.5
600	233.7	271.7
700	211.7	170.4
900	156.6	153.0

\* TDI/DCR=5g/2.5ml.

## APPENDIX D

### PARTICLE MEAN SIZES OF POLYUREA-COATED DCR UNDER VARIOUS DIAMINE CONCENTRATIONS (DCR/TDI=5g/2.5ml, 900 rpm)

EDA volume concentration (%)	Particle mean size ( $\mu\text{m}$ )
10	237.8
20	159.5
30	156.6
50	165.8

## APPENDIX E

### COATING WEIGHT PERCENTAGE OF POLYUREA-COATED DCR UNDER VARIOUS STIRRING SPEEDS (DCR/TDI=5g/2.5ml, VOLUME CONCENTRATION OF ETHYLENE DIAMINE IS 30%)

Stirring Speed (rpm)	Coating Weight Percentage (wt%)
100	41.98
200	30.99
400	33.97
600	26.42
700	23.98
900	32.39

## APPENDIX F

### REACTION CONVERSION OF NYLON 610 SYNTHESIZED BY IP IN ILS AS A FUNCTION OF TIME AT VARIOUS HDA/SEBACOYL CHLORIDE CONCENTRATION RATIOS

Reaction Time (min.)	Conversion at 1.25M:0.42M (%)	Conversion at 1.25M:0.84M (%)	Conversion at 1.25M:1.25M (%)
10	3.82	4.20	6.19
20	3.82	6.87	12.38
40	6.11	12.21	25.53
50	14.50	22.90	26.30
60	18.32	28.24	27.08
180	20.61	29.77	27.34
300	26.72	32.06	27.85
1440	27.48	32.82	28.37

Reaction Time (min.)	Conversion at 0.84M:0.42M (%)	Conversion at 0.42M:0.42M (%)	Conversion at 0.42M:1.25M (%)
10	0.76	0	4.64
20	0.76	0	4.64
40	2.27	0.76	5.96
50	5.30	3.03	7.28
60	6.06	3.03	9.93
180	10.61	7.58	19.21
300	11.36	9.09	19.21
1440	12.88	12.12	21.85

## APPENDIX G

### PRODUCT MASS OF NYLON 610 SYNTHESIZED BY IP IN ILS AS A FUNCTION OF TIME AT VARIOUS HDA/SEBACOYL CHLORIDE CONCENTRATION RATIOS

Reaction Time (min.)	Product Mass at 1.25M:0.42M (g)	Product Mass at 1.25M:0.84M (g)	Product Mass at 1.25M:1.25M (g)
10	0.005	0.011	0.024
20	0.005	0.018	0.048
40	0.008	0.032	0.099
50	0.019	0.060	0.102
60	0.024	0.074	0.105
180	0.027	0.078	0.106
300	0.035	0.084	0.108
1440	0.036	0.086	0.110

Reaction Time (min.)	Product Mass at 0.84M:0.42M (g)	Product Mass at 0.42M:0.42M (g)	Product Mass at 0.42M:1.25M (g)
10	0.001	0	0.007
20	0.001	0	0.007
40	0.003	0.001	0.009
50	0.007	0.004	0.011
60	0.008	0.004	0.015
180	0.014	0.010	0.029
300	0.015	0.012	0.029
1440	0.017	0.016	0.033



## REFERENCES

- Antonietti, M., Kuang, D., Smarsley, B. and Zhou, Y. (2004). Ionic Liquids for the Convenient Synthesis of Functional Nanoparticles and Other Inorganic Nanostructures. Angew. Chem. Int. Ed., 43, 4988-4992.
- Baker, R.W. (2000). Membrane Technology and Applications, McGraw-Hill, 114-119.
- Baldelli, S. (2003). Influence of Water on the Orientation at the Surface of a Room-Temperature Ionic Liquid: Sum Frequency Generation Vibrational Spectroscopic Study. Journal of Physical Chemistry B, 107(25), 6148-6152.
- Bartsch, R.A., Chun, S., Dzyuba, S.V. (2002). Ionic Liquids as Novel Diluents for Solvent Extraction of Metal Salts by Crown Ethers. ACS Symposium Series 818, 58-68.
- Baudequin, C., Baudoux, J., Levillain, J., Cahard, D., Gaumont, A-C. and Plaquevent, J-C. (2003). Ionic Liquids and Chirality: Opportunities and Challenges. Tetrahedron: Asymmetry, 14, 3081-3093.
- Biedron, T., Kubisa, P. (2004) Cationic Polymerization of Styrene in a Neutral Ionic Liquid. Journal of Polymer Science, Part A: Polymer Chemistry, 42(13), 3230-3235.
- Bowers, J. and Vergara-Gutierrez, M.C. (2004). Surface Ordering of Amphiphilic Ionic Liquids. Langmuir, 20, 309-312.
- Bowers, J., Butts, C.P., Martin, P.J., and Vergara-Gutierrez, M.C. (2004). Aggregation Behavior of Aqueous Solutions of Ionic Liquids. Langmuir, 20, 2191-2198.
- Brandrup, J., Immergut, E.H., Grulke, E.A. Eds. (1999) Polymer Handbook, 4<sup>th</sup> Edition, John Wiley & Sons, New York.
- Brennecke, J.F. and Maginn, E.J., (2001). Ionic Liquids: Innovative Fluids for Chemical Processing. AIChE Journal, 47(11), 2384-2389.
- Cadena, C., Maginn, E.J. (2005) Molecular Dynamics Study of Pyridinium- and Triazolium-Based Ionic Liquids. AIChE 2005 National Meeting Proceedings, Cincinnati, OH, 167f.
- Cammarata, L., Kazarian, S.G., Salter, P.A. and Welton, T. (2001). Molecular States of Water in Room Temperature Ionic Liquids. Physical Chemistry Chemical Physics, 3, 5192-5200.
- Cang, H., Li, J. and Fayer, M.D. (2003). Orientational Dynamics of the Ionic Organic Liquid 1-ethyl-3-methylimidazolium Nitrate. Journal of Chemical Physics, 119(24), 13017-13023.

- Carmichael, A.J., Haddleton, D.M., Bon, S.A.F., Seddon, K.R.(2000). Copper(I) Mediated Living Radical Polymerization in an Ionic Liquid. Chem. Commun.,14 , 1237-1238.
- Chiappe, C. and Pieraccini, D. (2005). Ionic Liquids: Solvent Properties and Organic Reactivity. Journal of Physical Organic Chemistry, 18, 275-297.
- Cullity, B.D. (1978) Elements of X-ray Diffraction, (2<sup>nd</sup> Ed.) Addison-Wesley Publishing Company, Inc., 3-143.
- Cussler, E.L. (1991) Diffusion, Cambridge University Press, New York, USA.
- Del Popolo, M.G. and Voth, G.A. (2004). On the Structures and Dynamics of Ionic Liquids. Journal of Physical Chemistry B, 108, 1744-1752.
- De Roche, J., Gordon, C.M., Imrie, C.T., Ingram, M.D., Kennedy, A.R., Celso, F.L. and Triolo, A. (2003) Application of Complementary Experimental Techniques to Characterization of the Phase Behavior of [C16mim][PF6] and [C14mim][PF6]. Chemistry of Materials, 15, 3089-3097.
- Dietz, M.L., Dzielawa, J.A., Jensen, M.P. and Firestone, M.A.(2003) Conventional Aspects of Unconventional Solvents: Room Temperature Ionic Liquids as Ion-Exchangers and Ionic Surfactants. ACS Symposium Series 856, Chapter 41, 526-543.
- Dupont, J. (2004). On the Solid, Liquid and Solution Structural Organization of Imidazolium Ionic Liquids. Journal of Brazilian Chemical Society. 15 (3), 341-350.
- Earle, M. J., Seddon, K.R., Adams, C.J., Roberts, G. (1998) Friedel - Crafts Reactions in Room Temperature Ionic Liquids. Chemical Communications (Cambridge), 19, 2097-2098.
- Earle, M.J., McCormac, P.B., Seddon, K.R. (1999). Diels-Alder Reactions in Ionic Liquids. Green Chemistry, 1, 23-25.
- Earle, M.J., McCormac, P.B., Seddon, K.R. (2000). The First High Yield Green Route to a Pharmaceutical in a Room Temperature Ionic Liquid. Green Chemistry, 2, 261-262.
- Fredlake, C.P., Crosthwaite, J.M., Hert, D.G., Aki, S.D.V.K. and Brennecke, J.F. (2004). Thermophysical Properties of Imidazolium-Based Ionic Liquids. Journal of Chemical Engineering Data, 49, 954-964.
- Fukushima, T., Kosaka, A., Ishimura, Y., Yamamoto, T., Takigawa, T., Ishii, N. and Aida, T. (2003). Molecular Ordering of Organic Molten Salts Triggered by Single-Walled Carbon Nanotubes. Science, 300, 2072-2074.
- Gao, H., Jiang, T., Han, B., Wang, Y., Du, J., Liu, Z. and Zhang, J.(2004). Aqueous/Ionic Liquid Interfacial Polymerization for Preparing Polyaniline Nanoparticles. Polymer, 45, 3017-3019.

- Gordon, C.M., Holbrey, J.D., Kennedy, A.R. and Seddon, K.R. (1998). Ionic Liquid Crystals: Hexafluorophosphate Salts. Journal of Materials Chemistry, 8, 2627-2636.
- Gordon, C.M., McLean, A.J., Muldoon, M.J. and Dunkin, I.R. (2002). Photochemistry in Ionic Liquids. ACS Symposium Series 818, 428-443.
- Grace, H.P. (1982) Dispersion Phenomena in High Viscosity Immiscible Fluid Systems and Application of Static Mixers as Dispersion Devices in Such Systems. Chemical Engineering Communications, 14(3-6), 225-227.
- Gunton, J.D., San Miguel, M., Sahni, P.S. (1983) Phase Transitions and Critical Phenomena, Vol.8, Chapter 3, Academic Press, London, pp321.
- Hanke, C.G., Johansson, A., Harper, J.B. and Lynden-Bell, R.M. (2003). Why Are Aromatic Compounds More Soluble than Aliphatic Compounds in Dimethylimidazolium Ionic Liquids? A Simulation Study. Chemical Physics Letters, 374, 85-90.
- Hardacre, C., Holbrey, J.D., Jane McMath, S.E., Bowron, D.T. and Soper, A.K. (2003). Structure of Molten 1,3-dimethylimidazolium chloride using neutron diffraction. Journal of Chemical Physics, 118(1), 273-278.
- Hirech, K., Payan, S., Carnelle, G., Brujes, L. and Legrand, J. (2003). Microencapsulation of an Insecticide by Interfacial Polymerization. Powder Technology, 130, 324-330.
- Holbrey, J.D. and Seddon, K.R. (1999). The Phase Behavior of 1-alkyl-3-methylimidazolium Tetrafluoroborates; Ionic Liquids and Ionic Liquid Crystals. Dalton Transaction, 2133-2139.
- Holbrey, J.D., Reichert, W.M., Reddy, R.G. and Rogers, R.D. (2003). Heat Capacities of Ionic Liquids and Their Applications as Thermal Fluids. Ionic Liquids as Green Solvents: ACS Symposium Series 856, 121-133.
- Hong, K. and Park, S. (2000). Preparation of Polyurea Microcapsules Containing Ovalbumin. Material Chemistry and Physics, 64, 20-24.
- Huddleston, J.G., Visser, A.E., Reichert W.M., Willauer, H.D., Broker, G.A. and Rogers, R.D. (2001) Characterization and Comparison of Hydrophilic and Hydrophobic Room Temperature Ionic Liquids Incorporating the Imidazolium Cation. Green Chemistry, 3, 156-164.
- Huddleston, J.G., Broker, G.A., Willauer, H.D., Rogers, R.D. (2002) Free-energy relationships and solvatochromatic properties of 1-alkyl-3-methylimidazolium ionic liquid. ACS Symposium 818, 270-288.
- Hunter, C.A., Sanders, J.K.M. (1990) The Nature of  $\pi$ - $\pi$  Interactions. Journal of American Chemical Society, 112, 5525-5534.

- Hurley, F. H., Wier, T.P., Jr. (1951) Electrodeposition of Metals from Fused Quaternary Ammonium Salts. Journal of the Electrochemical Society, 8 , 203-206.
- Iimori, T., Iwahashi, T., Ishii, H., Seki, K., Ouchi, Y., Ozawa, R., Hamaguchi, H-O. and Kim, D.(2004). Orientational Ordering of Alkyl Chain at the Air-Liquid Interface of Ionic Liquids Studied by Sum Frequency Vibrational Spectroscopy. Chemical Physics Letters, 389, 321-326.
- Ishihara, H., Kimura, I., Yoshihara, N.(1983-84) Studies on Segmented Polyurethane-urea Elastomers: Structure of Segmented Polyurethane-urea Based on Poly(tetramethyleneglycol), 4,4'-diphenylmethane diisocyanate, and 4,4'-diaminodiphenyl methane. Journal of Macromolecular Science, Physics, B22(5-6), 713-733.
- Ji, J., Dickson, J.M., Childs, R.F., and McCarry, B.E. (2000) Mathematical Model for the Formation of Thin-Film Composite Membranes by Interfacial Polymerization: Porous and Dense Films. Macromolecules, 33, 624-633.
- Johnson, E.D. (1985) A study of the Kinetics and Mechanism of Interfacial Polymerization. Ph.D. Dissertation, Carnegie-Mellon University, Pennsylvania.
- Karode, S.K., Kulkarni, S.S., Suresh, A.K. and Mashelkar, R.A. (1998). New Insights into Kinetics and Thermodynamics of Interfacial Polymerization. Chemical Engineering Science, 53(15), 2649-2663.
- Kim, H-W., Knowles, J.C., Kim, H-E. (2005). Hydroxypatite Porous Scaffold Engineered with Biopolymer Hybrid Coating for Antibiotic Vancomycin Release. Journal of Material Science: Materials in Medicine, 16, 189-195.
- Kubo, M., Harada, Y., Kawakatsu, T. and Yonemoto, T. (2001) Modeling of Formation Kinetics of Polyurea Microcapsules with Size Distribution by Interfacial Polycondensation. Journal of Chemical Engineering of Japan, 34 (12), 1506-1515.
- Kubisa, P.(2004). Application of Ionic Liquids as Solvents for Polymerization Processes. Progress in Polymer Science, 29, 3-12.
- Law, G. and Watson, P.R. (2001a). Surface Tension Measurement of N-Alkylimidazolium Ionic Liquids. Langmuir, 17, 6138-6141.
- Law, G. and Watson, P.R. (2001b) Surface Orientation in Ionic Liquids. Chemical Physics Letters, 345, 1-4.
- Lee, J-H. and Chopra, N.G. (2005) Nanostructure Augmentation of Surfaces for Enhanced Thermal Transfer with Increased Surface Area. United States Patent Application, 20050129928.

- Li, Z., Zhang, J., Du, J., Gao, H., Gao, Y., Mu, T. and Han, B.(2005). Synthesis of  $\text{LaCO}_3\text{OH}$  Nanowires via a Solvothermal Process in the Mixture of Water and Room-Temperature Ionic Liquid. Materials Letters, *59*, 963-965.
- Lozinskaya, E.I., Shaplov, A.S. and Vygodskii, Ya.S.(2004). Direct Polycondensation in Ionic Liquids. European Polymer Journal, *40*, 2065-2075.
- Lynden-Bell, R.M. (2003) Gas-Liquid Interfaces of Room Temperature Ionic Liquids. Molecular Physics, *101* (16), 2625-2633.
- Ma, J.C. and Dougherty, D.A. (1997). The Cation- $\pi$  Interaction. Chem. Rev., *97*, 1303-1324.
- Ma, H., Wan, X., Chen, X. and Zhou, Q-F. (2003). Reverse Atom Transfer Radical Polymerization of Methyl Methacrylate in Imidazolium Ionic Liquids. Polymer, *44*, 5311-5316.
- Mark, H.F., Bikales, N.M., Overburger, C.G. and Menges, G. Eds. (1985a) Encyclopedia of Polymer Science and Engineering, Volume 8, John Wiley & Sons, New York, 221-235.
- Mark, H.F., Bikales, N.M., Overburger, C.G. and Menges, G. Eds. (1985b) Encyclopedia of Polymer Science and Engineering, Volume 11, John Wiley & Sons, New York, 315-489.
- Mark, H.F., Bikales, N.M., Overburger, C.G. and Menges, G. Eds. (1985c) Encyclopedia of Polymer Science and Engineering, Volume 13, John Wiley & Sons, New York, 213-217.
- Mastrorilli, P., Nobile, C.F., Gallo, V., Suranna, G.P., Farinola, G. (2002). Rhodium(I) Catalyzed Polymerization of Phenylacetylene in Ionic Liquids. Journal of Molecular Catalysis A: Chemistry, *184*, 73-78.
- Mazurkiewicz, J.H., Innis, P.C., Wallace, G.G., MacFarlane, D.R. and Forsyth, M. (2003). Conducting Polymer Electrochemistry in Ionic Liquids. Synthetic Metals, *135-136*, 31-32.
- Morgan, P.W. and Kwolek, S.L. (1963) Interfacial Polycondensation. XIII. Viscosity-Molecular Weight Relationship and Some Molecular Characteristics of 6-10 Polyamide. Journal of Polymer Science: Part A, Volume 1, 1147-1162.
- Morgan, P.W. (1965) Condensation Polymers by Interfacial and Solution Methods. Interscience, New York, U.S.A.
- Morrow, T.I. and Maginn, E.J. (2002). Molecular dynamics study of the ionic liquid 1-n-butyl-3-methylimidazolium hexafluorophosphate. Journal of Physical Chemistry B, *106*(49), 12807-12813.

- Nakashima, T. and Kimizuka, N. (2003) Interfacial Synthesis of Hollow TiO<sub>2</sub> Microspheres in Ionic Liquids. Journal of the American Chemical Society, 125, 6386-6387.
- Ngo, H.L., LeCompte, K., Hargens, L., McEwen, A.B. (1998). Thermal Properties of Imidazolium Ionic Liquids. Thermochim. Acta, 97, 357-358.
- Odian, George. (2004). Principles of Polymerization (4<sup>th</sup> ed.): John Wiley and Sons, Inc., New York, 90-92.
- Ogihara, W., Sun, J., Forsyth, M., MacFarlane, D.R., Yoshizawa, M., Oho, H. (2003). Ionic Conductivity of Polymer Gels Deriving from Alkali Metal Ionic Liquids and Negatively Charged Polyelectrolytes. Electrochimica Acta, 49, 1797-1801.
- Okoturo, O.O. and VanderNoot, T.J. (2004). Temperature Dependence of Viscosity for Room Temperature Ionic Liquids. Journal of Electroanalytical Chemistry, 568, 167-181.
- Olivier, H. (1999). Recent Developments in the Use of Non-aqueous Ionic Liquids for Two-phase Catalysis. Journal of Molecular Catalysis A: Chemical, 146, 285-289.
- Olivier-Bourbigou, H. and Magna, Lionel (2002). Ionic Liquids: Perspective for Organic and Catalytic Reactions. Journal of Molecular Catalysis A: Chemical, 182-183, 419-437.
- Park, S. and Kazlauskas, R.J.(2003). Biocatalysis in Ionic Liquids-Advantages Beyond Green Technology. Current Opinion in Biotechnology, 14, 432-437.
- Pickup, P.G., Osteryoung, R.A. (1984).Electrochemical Polymerization of Pyrrole and Electrochemistry of Polypyrrole in Ambient Temperature Molten Salts. Journal of the American Chemical Society, 106, 2294-2299.
- Reid, R.C., Prausnitz, J.M., Poling, B.E. (1988) The Properties of Gases and Liquids. (4<sup>th</sup> Edition), McGraw-Hill, Singapore, pp606.
- Rogers, R.D., Seddon, K.R. Eds. (2002). Ionic Liquids: Industrial Applications to Green Chemistry, ACS Symposium 818.
- Scott, M.P., Rahman, M. and Brazel, C.S. (2003). Application of Ionic Liquids as Low-Volatility Plasticizers for PMMA. European Polymer Journal, 39, 1947-1953.
- Shin, J.H., Henderson, W.A., Passerini, S. (2003). Recent Development in the ENEA Lithium Metal Battery Project. Electrochemistry Communication, 5, 1016-1020.
- Snedden, P., Cooper, A.I. Scott, K. and Winterton, N. (2003). Cross-Linked Polymer-Ionic Liquid Composite Materials. Macromolecules, 36, 4549-4556.

- Solomon, O., Ciuta, I.Z. (1962) Determination of the Intrinsic Viscosity of Polymer Solutions by a Simple Determination of Viscosity. Journal of Applied Polymer Science, 6(24), 683-686.
- Sperling, L.H. (2001a) Introduction to Physical Polymer Science, 3<sup>rd</sup> Edition, John Wiley & Sons, New York, 130-147.
- Sperling, L.H. (2001b) Introduction to Physical Polymer Science, 3<sup>rd</sup> Edition, John Wiley & Sons, New York, 173-176.
- Sperling, L.H. (2001c) Introduction to Physical Polymer Science, 3<sup>rd</sup> Edition, John Wiley & Sons, New York, 100-101.
- Strobl, G. (1997) The Physics of Polymers: Concepts for Understanding Their Structures and Behavior, 2<sup>nd</sup> Edition, Springer, Berlin.
- Szymanski, Herman A. and Erickson, Ronald E. (1970) Infrared Band Handbook. Volume 1, IFI/Plenum.
- Urahata, S.M. and Ribeiro, M-C.C. (2004). Structure of Ionic Liquids of 1-alkyl-3-methylimidazolium Cations: A Systematic Computer Simulation Study. Journal of Chemical Physics, 120 (4), 1855-1863.
- Uyama, H., Takamoto, T., Kobayashi, S. (2002). Enzymatic Synthesis of Polyesters in Ionic Liquids. Polymer Journal, 24 , 94-96.
- Visser, A. E. and Rogers, R.D. (2003) Room-Temperature Ionic Liquids: New Solvents for f-element Separations and Associated Solution Chemistry. Journal of Solid State Chemistry, 171(1-2), 109-113.
- Vygodskii, Y.S., Lozinskaya, E.I., Shaplov, A.S. (2002). Ionic Liquids as Novel Reaction Media for the Synthesis of Condensation Polymers. Macromolecular Rapid Communication, 23 , 676-680.
- Walden, P. (1914) Molecular Weights and Electrical Conductivity of Several Fused Salts. Bull. Acad. Sci. St. Petersburg , 405-422.
- Walheim, S., Schaffer, E., Mlynek, J., Steiner, U. (1999) Nanophase-Separated Polymer Films as High-Performance Antireflection Coatings. Science, 283 , 520-522.
- Wang, J., Gao, J., Fang, B., Lu, P., Deng, S. and Wang, H. (2005). Synthesis and Characterization of Multipod, Flower-like, and Shuttle-like ZnO Frameworks in Ionic Liquids. Materials Letters, 59, 1405-1408.
- Wasserscheid, P., Welton., T. (Eds.) (2002). Ionic Liquids in Synthesis, WILEY-VCH.

- Watanabe, M., Mizumura, T. (1996). Conductivity Study on Ionic Liquid/Polymer Complexes. Solid State Ionics, 86-88 , 353-356.
- Weast, R.C., Astle, M.J., Beyer, W.H. (Eds.) (1983) CRC Handbook of Chemistry and Physics, 64<sup>th</sup> Edition, CRC Press, Inc., Boca Riton, Fl, F-33.
- Welton, T. (1999) Room-Temperature Ionic Liquids. Solvents for Synthesis and Catalysis. Chem. Rev., 99 , 2071-2083.
- Wilkes, J. S., Levisky, J. A., Pflug, J. L., Hussey, C.L., Scheffler, Towner B. (1982). Composition Determinations of Liquid Chloroaluminate Molten Salts by Nuclear Magnetic Resonance Spectrometry. Analytical Chemistry, 54(13), 2378-2379.
- Winston Ho, W.S. and Sirkar, K.K. (Eds.) (2001). Membrane Handbook, Kluwer Academic Publishers, Norwell, MA, USA.
- Xiao, Y., Malhotra, S.V. (2004). Diels-Alder Reactions in Pyridinium Based Ionic Liquids. Tetrahedron Letters, 45(45), 8339-8342.
- Yadav, S.K., Suresh, A.K. and Khilar, K.C. (1993). Microencapsulation in Polyurea Shell by Interfacial Polycondensation. AICHE Journal, 36(3), 431-437.
- Yadav, S.K., Khilar, K.C. and Suresh A.K. (1996). Microencapsulation in Polyurea Shell: Kinetics and Film Structure. AICHE Journal, 42(9), 2616-2626.
- Yadav, J.S., Reddy, B.V.S., Basak, A.K. and Narsaiah, A.V.(2003). [Bmim]PF<sub>6</sub> and BF<sub>4</sub> Ionic Liquids as Novel and Recyclable Reaction Media for Aromatic Amination. Tetrahedron Letters, 44, 2217-2220.
- Yashin, V.V. and Balazs, A.C. (2004). Theoretical Model of Interfacial Polymerization. Journal of Chemical Physics, 121(22), 11440-11454.
- Zhang, H., Bu, L., Li, M., Hong, K., Visser, A.E., Rogers, R.D. and Mays, J.W. (2002). Homopolymerization and Block Copolymer Formation in Room-Temperature Ionic Liquids. ACS Symposium Series 818 , 114-124.
- Zhao, D., Wu, M., Kou, Y. and Min, E. (2002). Ionic Liquids: Applications in Catalysis. Catalysis Today, 74, 157-189.
- Zhao, H., Malhotra, S.V. (2002). Applications of Ionic Liquids in Organic Synthesis. Aldrichimica, 35(3), 75-83.
- Zhou, D., Spinks, G.M., Wallace, G.G., Tiyapiboonchaiya, C., MacFarlane, D.R., Forsyth, M, Sun, J. (2003). Solid State Actuators Based on Polypyrrole and Polymer-in-Ionic Liquid. Electrochimica Acta, 48 , 2355-2359.



- Zhou, Y. and Antonietti, M.(2003). Synthesis of Very Small TiO<sub>2</sub> Nanocrystals in a Room-Temperature Ionic Liquids and Their Self-Assembly toward Mesoporous Spherical Aggregates. Journal of the American Chemical Society, 125, 14960-14961.
- Zhou, Y., Schattka, J.H. and Antonietti, M. (2004). Room-Temperature Ionic Liquids as Template to Monolithic Mesoporous Silica with Wormlike Pores via a Sol-Gel Nanocasting Technique. NanoLetters, 4(3), 477-481.
- Zuidema, H.H., Waters, G.W. (1941). Ring Method for the Determination of Interfacial Tension. Industrial and Engineering Chemistry, Analytical Edition, 13 , 312-313.